

1-1-2005

# Using rheometry for prediction the pumping characteristics of highly concentrated W/O emulsion explosives

Sithethi Espin Nkomo  
*Cape Peninsula University of Technology*

---

## Recommended Citation

Nkomo, Sithethi Espin, "Using rheometry for prediction the pumping characteristics of highly concentrated W/O emulsion explosives" (2005). *CPUT Theses & Dissertations*. Paper 184.  
[http://dk.cput.ac.za/td\\_cput/184](http://dk.cput.ac.za/td_cput/184)

This Text is brought to you for free and open access by the Theses & Dissertations at Digital Knowledge. It has been accepted for inclusion in CPUT Theses & Dissertations by an authorized administrator of Digital Knowledge. For more information, please contact [barendsc@cput.ac.za](mailto:barendsc@cput.ac.za).

**USING RHEOMETRY FOR PREDICTION THE PUMPING  
CHARACTERISTICS OF HIGHLY CONCENTRATED W/O  
EMULSION EXPLOSIVES**

By

**SITHETHI ESPIN NKOMO**

B.Tech. (Chemical Engineering) (Cape Technikon)

Dissertation submitted in fulfilment of the requirements for the Masters Degree in  
Technology: Chemical Engineering in the Department of Chemical Engineering of  
Cape Peninsula University of Technology.

**Supervisor: Prof. Irina Masalova**

**Co-supervisor: Prof. P. T. Slatter**

**Cape Town, South Africa**

**April 2005.**

## ABSTRACT

### USING RHEOMETRY FOR PREDICTING THE PUMPING CHARACTERISTICS OF HIGHLY CONCENTRATED W/O EXPLOSIVE EMULSIONS

The emulsion used for this study is a new thermodynamically unstable multi-component water-in-oil (w/o) explosive type with an internal phase ratio of approximately 94%, i.e. far beyond the close packing limit of spherical droplets of 74%. Economic considerations and the ongoing need for continuous drilling, loading and blasting in the mining industry, has made long-distance pipeline transportation of these emulsion explosive systems a viable economic option. Presently, rheological characterization of emulsion explosives is well documented (Bampfield & Cooper, 1988, Utracki, 1980). However, very little or none has been done for this system, pertaining to the use of rheometry for prediction of pumping characteristics of these systems in long-distance pipeline transport. This Master's dissertation is devoted to develop rheological methods of testing, characterization and correlation in order to develop a basis for predicting the pumping characteristics of highly concentrated w/o emulsion explosives from rheometry.

The literature and theory pertinent to the pipeline flow of high internal phase ratio emulsion explosives are presented, as well as the fundamentals of both concentric cylinder rheometry and pipe viscometry. The most relevant is the work of Bampfield and Cooper (1988), Utracki (1980) and Pal (1990).

Two experimental test facilities were used for data collection. Pipeline experiments were done using an experimental test facility at African Explosives Limited (AEL), and rheometry was conducted at the Rheology Laboratory of the Cape Peninsula University of Technology Flow Process Research Centre. The AEL experimental test facility consisted of a four-stage Orbit progressive cavity pump, two fluid reservoirs, (a mixing tank and a discharge reservoir), five 45m HDPE (high density polyethylene) pipes of internal diameters of 35.9 mm, 48.1 mm, 55.9 mm, 65.9 mm and 77.6 mm pipes. The test work was done over a wide range of laminar flow rates ranging from 3 kg.min<sup>-1</sup> to 53 kg.min<sup>-1</sup>. Rheometry was done using a PaarPhysica MCR300 rheometer, and only standard rotational tests (i.e. flow curve) at 30 °C in controlled rate mode were done.

Rheological characterisation was done using three rheological models, i.e. the Herschel-Bulkley, the Power Law and the Simplified Cross models. The coefficients obtained from these models were then used to predict pumping characteristics. The performances of these models were then evaluated by comparing the pipeline flow prediction to the actual pipeline data obtained from pipeline test experiments. It was found that the flow behaviour depicted by this explosive emulsion system was strongly non-Newtonian, and was characterized by two distinct regions of deformation behaviour, a lower Newtonian region of deformation behaviour in the shear rate region lower than 0.001 s<sup>-1</sup> and a strong shear thinning region in the shear rate range greater than 0.001 s<sup>-1</sup>.

For all the models used for this study, it was evident that rheometry predicts the pumping characteristics of this high internal phase ratio emulsion reasonably well, irrespective of the choice of the model used for the predictions. It was also seen that the major difference between these models was in the lower shear rate domain. However, the Simplified Cross model was

preferred over the other two models, since its parameter (the zero shear viscosity denoted by  $\eta_0$ ) can in general be correlated to the structure of the emulsion systems (i.e. mean droplet size, bulk modulus, etc.). Thus, structural changes induced by shearing (either inside the pump or when flowing inside a pipe) can be detected from changes in the value of the  $\eta_0$ . The above statement implies that  $\eta_0$  can be used as a quality control measure. Different pumping speeds were found to cause different degrees of shear-induced structural changes which were manifested by two opposing processes. These two opposing processes were the simultaneous coalescence and flocculation of droplets encountered at low rates of shear, and the simultaneous refinement and deflocculation of droplets encountered at high rates of shear. These two droplet phenomena were associated with a decrease or an increase in viscous effects, leading to both lower and higher viscous stresses and pumping pressures during pump start-up respectively.

## DECLARATION

I, Sithethi Espin Nkomo, hereby declare that, to the best of my knowledge, this Master's dissertation represents my own work and has not been submitted previously for examination toward any degree or diploma qualification at any other University. Further more it represents my own opinions and not necessarily those of the Cape Peninsula University of Technology.



.....  
Sithethi Espin Nkomo

April 2005

## DEDICATION

This Master's dissertation is dedicated to the following important persons:

My mother, Nontobeko Ngxukuma, the pillar of my strength, encouragement and a beacon of light to me,

My father, Phakamile Joba, for his fatherly advice, motivation and support,

My stepfather, John Ngxukuma, who made me whom I am today

My daughter, Portia, the source of my inspiration,

My two brothers (Siyolo and Lubabalo), close relatives, and friends for their support, encouragement and advice,

My two grandmothers (father and mother family side), who passed away while I was still studying toward this degree,

My ancestors (the Sukwinis, the Nkomos and the Tshawes) for their protection,

And finally to my Lord, my saviour, my guide and spiritual teacher, from whom I derived all my strength, perseverance, motivation and health,

*"God is our refuge and strength, a very present help in time of trouble".*

PSALMS 46:1

*"We are each of us angels with only one wing; and we can fly, only by embracing one another".*

Luciano de Crescenzo

## ACKNOWLEDGEMENTS

I hereby wish to pass my sincere gratitude to the following people and organisations for their contribution towards completion of this Master's dissertation:

Prof. Slatter, head of the Cape Peninsula University of Technology Flow Process Research Centre who gave me the opportunity to pursue my goal, and allowed me to research in his research unit, his constant motivational speeches and in-depth knowledge in this field,

Prof. Irina Masalova, for her guidance, insight in the field, encouragement, moral and technical support, and motherly advice,

African Explosive Limited, the company that provided all the research material, and permission to use their Experimental Test Facility, as well as to make known results of this study,

The National Research Foundation and the Cape Peninsula University of Technology Research Development Department for their financial assistance,

The Cape Peninsula University of Technology Flow Process Research Centre staff and students, for their assistance and support,

Caroline Thandiwe Ngamlana, for editing this Master's dissertation,

My family and friends for their moral support, love and prayers.

## TABLE OF CONTENTS

<b>PREAMBLE</b>	
<b>ABSTRACT</b> .....	<b>ii</b>
<b>DECLARATION</b> .....	<b>iv</b>
<b>DEDICATION</b> .....	<b>v</b>
<b>ACKNOWLEDGEMENTS</b> .....	<b>vi</b>
<b>CONTENTS</b> .....	<b>vii</b>
<b>GLOSSARY</b> .....	<b>xv</b>
<b>NOMENCLATURE</b> .....	<b>xviii</b>
<b>CHAPTER 1</b> .....	<b>1.1</b>
<b>INTRODUCTION</b> .....	<b>1.1</b>
<b>CHAPTER 2</b> .....	<b>2.1</b>
<b>THEORY AND LITERATURE REVIEW</b> .....	<b>2.1</b>
2.1 <b>INTRODUCTION</b> .....	<b>2.1</b>
2.2 <b>RHEOLOGY</b> .....	<b>2.2</b>
2.3 <b>CLASSIFICATION OF FLUID FLOW BEHAVIOUR</b> .....	<b>2.4</b>
2.3.1 <b>Newtonian fluid behaviour</b> .....	<b>2.5</b>
2.3.2 <b>Non-Newtonian fluid behaviour</b> .....	<b>2.7</b>
2.3.2.1 <b>Time independent flow behaviour</b> .....	<b>2.8</b>
2.3.2.2 <b>Time dependent fluid behaviour</b> .....	<b>2.10</b>
2.3.2.3 <b>Viscoelastic flow behaviour</b> .....	<b>2.13</b>
2.4 <b>RHEOLOGICAL OR FLOW MODELS OF NON-NEWTONIAN FLUIDS</b> .....	<b>2.14</b>
2.4.1 <b>Herschel-bulkley / Yield-Pseudoplastic model</b> .....	<b>2.16</b>
2.4.2 <b>Power Law / Pseudoplastic/ Ostwald- de-Waele Model</b> .....	<b>2.18</b>
2.4.3 <b>Bird-Carreau / Cross Structural Viscosity Model</b> .....	<b>2.18</b>

2.5	THEORY AND RHEOLOGY OF EMULSIONS .....	2.20
2.5.1	Internal Phase Ratio, $\phi$ .....	2.23
2.5.2	Viscosity of the Internal Phase, $\eta_i$ or Viscosity Ratio, $\frac{\eta_i}{\eta_{out}}$ .....	2.26
2.5.3	Droplet Size and Size Distribution .....	2.28
2.5.4	Rheology of Highly Concentrated Emulsions .....	2.30
2.5.5	Rheology of Emulsion Explosives .....	2.36
2.5.5.1	Summary .....	2.41
2.6	RHEOMETRY OF NON-NEWTONIAN FLUIDS .....	2.42
2.6.1	Pipe viscometry .....	2.43
2.6.1.1	Entrance and end effects and their correction .....	2.45
2.6.1.2	Pipe end kinetic energy and viscous effects and their correction .....	2.48
2.6.1.3	Viscous heating effect and correction .....	2.49
2.6.1.4	Hole pressure effect and correction .....	2.51
2.6.2	The concentric cylinder geometry .....	2.51
2.6.2.1	End effects corrections .....	2.54
2.6.2.2	Wall Slip .....	2.56
2.6.2.3	Viscous heating .....	2.60
2.6.2.4	Cavitation .....	2.61
2.6.2.5	Inertia and secondary flow .....	2.61
2.7	PREDICTION OF FLOW RATE AND PRESSURE DROP FROM RHEOMETRY .....	2.63
2.8	FLOW IN PIPES OF CIRCULAR CROSS-SECTION .....	2.66
2.8.1	Laminar Pipe Flow .....	2.67
2.8.1.1	Simplified Cross or Modified Bird-Carreau Model .....	2.69
2.8.2	Investigation and Correction of pipe wall slip .....	2.71
2.9	CONCLUSION .....	2.74
<b>CHAPTER 3.....</b>		<b>3.1</b>
<b>EXPERIMENTATION.....</b>		<b>3.1</b>
3.1	INTRODUCTION .....	3.1
3.2	OBJECTIVES OF THE EXPERIMENTAL INVESTIGATIONS: .....	3.2

3.3	SAMPLES .....	3.2
3.4	EXPERIMENTAL APPARATUS .....	3.4
3.5	EXPERIMENTAL ERRORS .....	3.4
3.5.1	Statistical analysis of experimental data.....	3.6
3.5.1.1	Precision of the measurements .....	3.7
3.5.1.1.1	Propagation of errors .....	3.10
3.5.1.2	Accuracy of measurements.....	3.11
3.5.1.2.1	Propagation of errors .....	3.12
3.6	PIPE VISCOMETRY .....	3.15
3.6.1	Layout of experimental test facility and Basic principles of operation.....	3.15
3.6.2	Experimental Procedure .....	3.17
3.6.3	Pipeline experimental test results and data correction.....	3.20
3.6.3.1	Entrance effects and their correction .....	3.25
3.6.3.2	Pipe end kinetic energy effects and correction.....	3.26
3.6.3.3	Hole pressure effect and correction.....	3.26
3.6.3.4	Viscous heating effect and correction .....	3.27
3.6.3.5	Construction of pseudo-shear rate diagram and slip evaluation.....	3.28
3.7	RHEOMETRY .....	3.31
3.7.1	Concentric Cylinder Measuring system, CC 27 .....	3.32
3.7.2	Experimental Procedure .....	3.33
3.8	SUMMARY .....	3.34
<b>CHAPTER 4.....</b>		<b>4.1</b>
<b>RESULTS AND DISCUSSIONS.....</b>		<b>4.1</b>
4.1	INTRODUCTION .....	4.1
4.2	FLOW CURVES.....	4.2
4.2.1	Rheological Models.....	4.6
4.2.2	Effect of Pumping on the Rheological Properties of Emulsion Explosives.....	4.16
4.3	PREDICTION OF FLOW RATE AND PRESSURE DROP FROM RHEOMETRY.....	4.30
4.4	SUMMARY .....	4.36

<b>CHAPTER 5.....</b>	<b>5.1</b>
<b>SUMMARY AND CONCLUSION.....</b>	<b>5.1</b>
5.1 INTRODUCTION.....	5.1
5.2 SUMMARY.....	5.1
5.3 CONCLUSION.....	5.4
5.4 FUTURE RESEARCH RECOMMENDATIONS.....	5.6
5.5 FINAL CONCLUSION.....	5.7
<b>REFERENCES.....</b>	<b>R1-R10</b>
<b>APPENDIX A.....</b>	<b>A1</b>
Hydrophile-Lipophile balance scales.....	A1
<b>APPENDIX B.....</b>	<b>B1</b>
Derivation of an equation for calculating the cone angle for concentric cylinder geometry... ..	B1
<b>APPENDIX C.....</b>	<b>C1</b>
Normal frequency distribution curve.....	C1
<b>APPENDIX D.....</b>	<b>D1</b>
Statistical table for t-frequency distribution.....	D1
<b>APPENDIX E.....</b>	<b>E1</b>
Skewness of a frequency distribution.....	E1
<b>APPENDIX F.....</b>	<b>F1</b>
Kurtosis or peakedness of a frequency distribution.....	F1
<b>APPENDIX G.....</b>	<b>G1</b>
Summary statistics for the Cross model.....	G1
<b>APPENDIX H.....</b>	<b>H1</b>
<b>AVERAGED RHEOMETRY DATA.....</b>	<b>H1</b>
<b>APPENDIX H1.....</b>	<b>H1</b>

H1: Pipe diameter of 35.9 mm.....	H1
<b>APPENDIX H2 .....</b>	<b>H2</b>
H2: Pipe diameter of 48.1 mm.....	H2
<b>APPENDIX H3 .....</b>	<b>H3</b>
H3: Pipe diameter of 55.9 mm.....	H3
<b>APPENDIX H4 .....</b>	<b>H4</b>
H4: Pipe diameter of 65.9 mm.....	H4
<b>APPENDIX H5 .....</b>	<b>H5</b>
H5: Pipe diameter of 77.6 mm.....	H5
<b>APPENDIX I.....</b>	<b>I1-I2</b>
<b>TYPICAL APPROXIMATION OF SYSTEM CURVE FOR 48.1mm PIPE</b>	
I1: $\Delta P$ -Q relation from Herschel-Bulkley model.....	I1
I1: $\Delta P$ -Q relation from Power Law model.....	I1
I2: List of possible error using Herschel-Bulkley and Power Law models.....	I2
<b>APPENDIX J.....</b>	<b>J1-J2</b>
<b>Re<sub>MR</sub> FOR ALL FLOW CONDITIONS.....</b>	
<b>APPENDIX J1.....</b>	<b>J1</b>
J1: Pipe diameter of 35.9 mm.....	J1
<b>APPENDIX J2.....</b>	<b>J1</b>
J2: Pipe diameter of 48.1 mm.....	J1
<b>APPENDIX J3.....</b>	<b>J1</b>
J3: Pipe diameter of 55.9 mm.....	J1
<b>APPENDIX J4.....</b>	<b>J2</b>
J4: Pipe diameter of 65.9 mm.....	J2
<b>APPENDIX J5.....</b>	<b>J2</b>
J5: Pipe diameter of 77.6 mm.....	J2
<b>APPENDIX K.....</b>	<b>K1</b>
Graphical representation of the effect of pump speed.....	K1

## LIST OF FIGURES

FIGURE 2. 1 TWO-PLATE MODEL .....	2.5
FIGURE 2. 2 TYPES OF TIME-INDEPENDENT FLOW BEHAVIOUR .....	2.8
FIGURE 2. 3 THIXOTROPIC AND RHEOPECTIC BEHAVIOUR OF NON-NEWTONIAN FLUIDS. ....	2.12
FIGURE 2. 4 THIXOTROPIC AND RHEOPECTIC BEHAVIOUR OF NON-NEWTONIAN FLUIDS. ....	2.13
FIGURE 2. 5 INFLUENCE OF $D_M$ ON $\eta_\infty$ .....	2.30
FIGURE 2. 6 COMMON RHEOLOGICAL INSTRUMENTS . ....	2.42
FIGURE 2. 7 PIPE VISCOMETRY. ....	2.44
FIGURE 2. 8 MEASURING PRINCIPLE FOR CONCENTRIC CYLINDER GEOMETRY. ....	2.53
FIGURE 2. 9 PLUG FLOW OF YIELD STRESS FLUIDS IN CONCENTRIC CYLINDER GEOMETRY. ....	2.58
FIGURE 2. 10 TYPICAL $\left(\tau_w - \frac{8V}{D}\right)$ RELATION IN DIFFERENT PIPE DIAMETERS. ....	2.71
FIGURE 2. 11 EFFECT OF SLIP IN PIPE OF DIFFERENT DIAMETERS. ....	2.72
FIGURE 2. 12 APPARENT FLUIDITY VS. $\frac{1}{D^m}$ FOR $m \geq 1$ .....	2.74
FIGURE 3. 1 RECEIVING TANKER ACTING AS A DISCHARGE RESERVOIR. ....	3.16
FIGURE 3. 2 SCHEMATIC LAYOUT OF AEL EXPERIMENTAL TEST FACILITY. ....	3.16
FIGURE 3. 3 SAMPLING PROCEDURE. ....	3.20
FIGURE 3. 4 SYSTEM CURVE: PRESSURE DROP ( $\Delta P$ ) VS. FLOW RATE ( $Q$ ). ....	3.22
FIGURE 3. 5 $\tau_w$ VS. $\frac{8V}{D}$ DIAGRAMS OF ALL PIPE DIAMETERS. ....	3.299
FIGURE 3. 6 AVERAGED $\tau_w$ VS. $\frac{8V}{D}$ DIAGRAMS OF ALL DIAMETERS. ....	3.3130
FIGURE 3. 7 AVERAGED $\tau_w$ VS. $\frac{8V}{D}$ DIAGRAMS OF ALL DIAMETERS. ....	3.3131
FIGURE 3. 8 RHEOMETER MCR 300 FROM PAARPHYSICA. ....	3.322
FIGURE 3. 9 CONCENTRIC CYLINDER GEOMETRY, CC27. ....	3.333
FIGURE 4.1 TYPICAL VISCOSITY CURVE IN LOGARITHMIC SCALE. ....	4.3
FIGURE 4.2 TYPICAL FLOW CURVE IN LOGARITHMIC SCALE. ....	4.3

FIGURE 4.3 TYPICAL THEORITICAL FLOW BEHAVIOUR.....	4.35
FIGURE 4.4 HERSCHEL-BULKLEY APPROXIMATION OF THE EXPERIMENTAL DATA.....	4.13
FIGURE 4.5 POWER LAW APPROXIMATION OF THE EXPERIMENTAL DATA.....	4.14
FIGURE 4.6 CROSS MODEL APPROXIMATION OF THE EXPERIMENTAL DATA.....	4.15
FIGURE 4.7 EFFECT OF FLOW RATE FOR PIPE DIAMETER OF 35.9MM.....	4.17
FIGURE 4.8 EFFECT OF FLOW RATE FOR PIPE DIAMETER OF 35.9MM.....	4.18
FIGURE 4.9 EFFECT OF FLOW RATE FOR PIPE DIAMETER OF 48.1MM.....	4.21
FIGURE 4.10 EFFECT OF FLOW RATE FOR PIPE DIAMETER OF 48.1MM.....	4.21
FIGURE 4.11 E-FFFECT OF FLOW RATE FOR PIPE DIAMETER OF 65.9MM.....	4.23
FIGURE 4.12 EFFECT OF FLOW RATE FOR PIPE DIAMETER OF 65.9MM.....	4.24
FIGURE 4.13 PSEUDO-SHEAR RATE DIAGRAM CONSTRUCTED FROM THE CROSS MODEL.....	4.31
FIGURE 4.14 $\Delta P$ vs. $Q$ FOR $D = 35.9$ MM.....	4.32
FIGURE 4.15 $\Delta P$ vs. $Q$ FOR $D = 48.1$ MM.....	4.33
FIGURE 4.16 $\Delta P$ vs. $Q$ FOR $D = 55.9$ MM.....	4.34
FIGURE 4.17 $\Delta P$ vs. $Q$ FOR $D = 65.9$ MM.....	4.35
FIGURE 4.18 $\Delta P$ vs. $Q$ FOR $D = 77.6$ MM.....	4.35

## LIST OF TABLES

TABLE 3.1 DATA FOR PIPE DIAMETER OF 35.9 MM:.....	3.21
TABLE 3.2 DATA FOR PIPE DIAMETER OF 48.1 MM:.....	3.21
TABLE 3.3 DATA FOR PIPE DIAMETER OF 55.9 MM:.....	3.21
TABLE 3.4 DATA FOR PIPE DIAMETER OF 65.9 MM:.....	3.22
TABLE 3.5 DATA FOR PIPE DIAMETER OF 77.6MM:.....	3.22
TABLE 3.6 RESULTS OF QUALITY CONTROL TESTS.....	3.23
TABLE 3.7 ENTRANCE LENGTHS $L_E$ OF THE DIFFERENT TEST PIPES.....	3.266
TABLE 3.8 LIST OF AVERAGE TEMPERATURE AND VISCOSITY VARIATIONS.....	3.267
TABLE 4.1 COEFFICIENTS OF THE HERSCHEL-BULKLEY MODEL FOR UNPUMPED SAMPLES.....	4.111
TABLE 4.2 COEFFICIENTS OF THE POWER LAW MODEL FOR UNPUMPED SAMPLES.....	4.11

---

TABLE 4.3 COEFFICIENTS OF THE CROSS MODEL FOR UNPUMPED SAMPLES.....	4.12
TABLE 4.4 CROSS COEFFICIENTS AT DIFFERENT PUMPING SPEEDS FOR D = 35.9 MM.....	4.18
TABLE 4.5 CROSS COEFFICIENTS AT DIFFERENT PUMPING SPEEDS FOR D = 48.1MM.....	4.22
TABLE 4.6 CROSS COEFFICIENTS AT DIFFERENT PUMPING SPEEDS FOR D = 54.9, 65.9 .....	4.25
TABLE 4.7 AVERAGED RHEOLOGICAL COEFFICIENT OF THE CROSS MODEL FOR ALL D. ....	4.28
TABLE 4.8 WEIGHTED AVERAGED RHEOLOGICAL CONSTANTS . ....	4.30
TABLE 4.9 LIST OF POSSIBLE ERRORS . ....	4.31

## GLOSSARY

<b>Term</b>	<b>Definition</b>
<b>Coalescence</b>	Spontaneous joining together of smaller droplets in an emulsion system to form larger ones, (it may eventually lead to breaking of the emulsion system into two separate phases in the absence of a surfactant).
<b>Complex fluids</b>	All single phase fluids that are non-Newtonian and all multiphase fluids involving two or more fluids, a mixture of fluids and solids etc., which are capable of flowing in a pipe.
<b>Congelation</b>	Phase conversion of a thin waxy liquid into a thick congealed waxy material often effected by cooling.
<b>Deflocculation</b>	Reverse process of flocculation, i.e. breaking of three-dimensional clusters into smaller droplets and smaller clusters usually by mechanical action, as in vigorous agitation.
<b>Emulsion explosive</b>	High internal phase water-in-oil emulsion of a concentrated solution of nitrate salts in water emulsified into an oil base.
<b>Flocculation</b>	Cohesion of droplets in the formation of three-dimensional clusters without coalescence.
<b>Flow curve/Rheogram</b>	Curve relating shear stress to the true rate of shear.
<b>Laminar flow</b>	Laminar flow is when the fluid elements move in an orderly streamline fashion without intermixing with adjacent fluid elements.

---

<b>Newtonian Fluids</b>	Fluids depicting a flow behaviour in which the shear viscosity of the fluid remains constant irrespective of the amount of stress or shear is applied. Mathematically, shear stress is linearly related to the rate of shear.
<b>Non-Newtonian Fluids</b>	Fluids whose flow behaviour does not obey Newton's Law, i.e. shear stress is not linearly related to strain or viscosity is stress or shear rate dependent.
<b>Peclet number</b>	Dimensionless group which relates forced convection of a system to its heat conduction
<b>Relaxation time</b>	The time (in seconds) it takes for a macromolecule to be stretched out when deformed.
<b>Reynolds number</b>	Ratio of inertial forces to viscous forces, indicative of the various flow regions, i.e. Laminar, Laminar-Turbulent transition, and Turbulent flow regions
<b>Rheology</b>	Science of the deformation and flow of matter, it deals with the deformation of materials as a result of applied stress.
<b>Rheological Model</b>	An idealised relationship of rheological behaviour expressable in mathematical terms.
<b>Rheometer</b>	An instrument for measuring rheological properties.
<b>Rheopexy</b>	Fluid flow behaviour characterised by a gradually increasing viscosity when the fluid is subjected to a given stress.
<b>Sauter mean diameter</b>	The ratio of volume to surface area of the dispersed phase droplets.

---

<b>Shear rate</b>	Rate of shear deformation, change of shear deformation per unit time.
<b>Shear stress</b>	Component of stress parallel or tangential to the direction of flow.
<b>Shear thinning</b>	A reduction of the viscosity with increasing rate of shear in steady flow.
<b>Thixotropy</b>	Fluid flow behaviour characterised by a gradually decreasing viscosity when the fluid is subjected to a given stress.
<b>Viscosity</b>	The property of a material to resist deformation increasingly with increasing shear rate, a measure of this property is defined as the quotient of shear stress divided by shear rate in steady flow.
<b>Viscoelastic materials</b>	Materials exhibiting both viscous and elastic effects under the action of outside stresses, in the absence of time dependency.
<b>Viscoplastic materials</b>	Materials exhibiting irreversible deformation when a certain amount of stress (i.e. the yield stress) is exceeded, in the absence of time dependency.
<b>Yield point</b>	The point on the stress-strain or stress-shear rate curve corresponding to the transition from elastic to plastic deformation.
<b>Yield stress</b>	Stress corresponding to a yield point.

## NOMENCLATURE

Symbol	Description	Unit
A	Cross-sectional area of pipe	m <sup>2</sup>
A <sub>T</sub>	Empirical constant	....
A	Empirical constant with a value of 2.5	....
B <sub>T</sub>	Empirical constant	....
B	Empirical constant	....
C	Correction term for kinetic and viscous friction losses	....
C <sub>L</sub>	End effect correction factor	....
C <sub>p</sub>	Heat capacity of a fluid	J/kg. <sup>0</sup> C
C <sub>s</sub>	Slip coefficient	....
c	Empirical constants	....
D	Internal pipe diameter	m
d	Droplet size	m
d <sub>m</sub>	Mean droplet size	m
d <sub>s</sub>	Mean solids size	m
d <sub>saut</sub>	Sauter mean diameter of droplets	m
E	Energy dissipated by viscous flow	J
F	Force	N
f <sub>A</sub>	Weight fraction of component A	....
G	Complex shear modulus or Young's modulus	Pa
g	Gravitation acceleration	m.s <sup>-2</sup>
HLB	Hydrophile-Lipophile balance	....
h	Gap length	m
h <sub>0</sub>	Effective height	m
j	Mechanical equivalent of heat	....
K	Fluid consistency coefficient	Pa.s <sup>n</sup>
k <sub>0</sub> and k <sub>1</sub>	Kinetic constants	....
L	Pipe length	m
L <sub>E</sub>	Entrance length	m
m	Any coefficient of a rheological model	....
M	Viscosity ratio	....
N <sub>a</sub>	Namhe number	....
N <sub>pe</sub>	Peclet number	....
n	Fluid behaviour index for Herschel-Bulkley and Power Law models, or Cross index for Cross model	....
P	Probability	....
P <sub>atm</sub>	Atmospheric pressure	Pa
P <sub>vap</sub>	Vapour pressure	Pa
ΔP	Pressure drop in the pipe	Pa
ΔP <sub>cor.</sub>	Corrected pressure drop in the pipe	Pa
ΔP <sub>entr.</sub>	Entrance pressure losses	Pa
ΔP <sub>meas.</sub>	Measured pressure drop	Pa
Q	Mean mass flowrate	kg.min <sup>-1</sup>

$Q_v$	Mean volumetric flowrate	$m^3.s^{-1}$
$Q_c$	Corrected mean volumetric flowrate	$m^3.s^{-1}$
$Q_s$	Slip mean volumetric flowrate	$m^3.s^{-1}$
$R$	Pipe radius	m
$R_b$	Bob radius	m
$R_c$	Inner radius of measuring cylinder	m
$\Delta R$	Measuring gap radius	m
$r$	Mean droplets radius	m
$r^2$	Multiple regression correlation coefficient	....
$Re$	Reynolds number	....
$Re'_{e,BP}$	Bingham Plastic Reynolds number	....
$Re_{crit}$	Critical Reynolds number	....
$Re'_{e,pl}$	Power Law Reynolds number	....
$s$	Standard deviation	....
$SS_{reg}$	Regression sum of squares	....
$SS_{res}$	Residual sum of squares	....
$T$	Temperature	$^{\circ}C$
$Ta_c$	Critical Taylor number	....
$T_c$	Congelation temperature	$^{\circ}C$
$T_d$	Crystallisation temperature or Fudge Point	$^{\circ}C$
$T_i$	Initial temperature of sample at pipe inlet	$^{\circ}C$
$T_f$	Final temperature of sample at pipe outlet	$^{\circ}C$
$T_{hn}$	Homogenous nucleation temperature	$^{\circ}C$
$T$	Torque	N.m
$\Delta T_{vb}$	Temperature change due to viscous heating	$^{\circ}C$
$\Delta T_{visc}$	Temperature change necessary to change viscosity	$^{\circ}C$
$V$	Mean velocity in the pipe	$m.s^{-1}$
$V_b$	Linear velocity of bob	$m.s^{-1}$
$V_c$	Corrected mean velocity	$m.s^{-1}$
$V_s$	Slip velocity	$m.s^{-1}$
$(V_s)_{bob}$	Slip velocity of bob	$m.s^{-1}$
$(V_s)_{cup}$	Slip velocity of cup	$m.s^{-1}$
$X_S$	Parameter for steady temperature profile approximation	....
<b>Greek symbols</b>		
$\alpha_k$	Kinetic energy correction factor	....
$\gamma$	Deformation	....
$\dot{\gamma}$	True shear rate	$s^{-1}$
$\dot{\gamma}_{ch}$	Measure of the characteristic shear rate	$s^{-1}$
$\lambda$	Cross relaxation time	s
$\eta$	Shear viscosity	Pa.s
$\ell$	Entrance effect correction factor	....
$\eta_0$	Zero shear viscosity	Pa.s
$\eta_i$	Viscosity of inner phase	Pa.s

$\eta_{out}$	Viscosity of outer phase	Pa.s
$\eta_{\infty}$	Infinite shear viscosity	Pa.s
$\eta_{\beta}$	Surface viscosity of interfacial film	Pa.s
$\eta_s$	Shear viscosity of interfacial film	Pa.s
$\eta_{int}$	Intrinsic viscosity	....
$\eta_{pl}$	Bingham Plastic viscosity	Pa.s
$\eta_{sp}$	Specific increase in viscosity	....
$\eta_{rel}$	Relative viscosity	....
$(\eta_{rel})_0$	Zero-shear rate relative viscosity	....
$\tau$	Shear stress	Pa
$\tau_w$	Wall shear stress	Pa
$\tau_y$	Yield stress	Pa
$\phi$	Internal phase ratio or volume fraction	....
$\phi_{eff}$	Effective volume fraction	....
$\phi_m$	Maximum volume fraction	....
$\phi_s$	Volume fraction of solids	....
$\sigma$	Logarithmic standard deviation	....
$\epsilon$	Dielectric constant of continuous phase	....
$\kappa$	Specific conductivity of continuous phase	$W/m^2 \cdot ^\circ C.kg$
$\kappa$	Thermal conductivity of the fluid	$W/m^2 \cdot ^\circ C$
$\zeta$	Zeta potential	V
$\rho$	Density	$Kg.m^{-3}$
$\omega$ and $\Omega$	Angular velocity	$rad.s^{-1}$
$\delta$	Radius ratio	....
$\theta$	Cone angle	$rad$ or $^\circ$
$\Gamma$	Surface tension of the droplets	$N.m^{-1}$
$\chi_s$	Distance required to approach a limiting temperature profile in tube flow	m

# **CHAPTER 1**

## CHAPTER 1

### INTRODUCTION

Bulk emulsion explosives are progressively penetrating the underground mining market and are replacing packaged explosives for reasons of improved safety, more efficient logistics, high rates of detonation and reduced overall blasting costs (Bampffield & Cooper, 1988). Developments over the past decade concentrated on obtaining suitably stable emulsion formulations, prevention of crystallisation and the use of correctly specified delivery systems for transferring the emulsion. This is normally achieved by pumping emulsions over relatively short distances in reasonable practical time frames. Existing technology is able to deliver the product over long distances, but the quality of the emulsion is not always constant and specification of the delivery systems may be over or under systems requirements from the context of delivered product quality.

The emulsion explosive used for this study is a new colloid, multi-component, water-in oil (w/o) explosive type with internal phase ratio of approximately 94 %, which is far beyond the close packing limit of spherical droplets of 74 %. This system is thermodynamically unstable due to its colloid nature, non-equilibrium and metastable state of its droplets, which consists of supercooled aqueous solutions of inorganic salts.

Inherent problems associated with transport-induced structural decomposition is normally caused by high speed pumping as well as by ageing of the emulsion. In order to prevent such problems during application, large-scale pipeline trial experiments are usually performed. These trial experiments require approximately 50 tons of emulsions, and are time and cost consuming. Thus, prediction of pumping characteristics of explosive emulsions for long distance pipeline

transportation from rheometry is required in order to replace the existing large-scale pipeline trial experiments. The reasons for this is that rheometry has important economic advantages associated with it as it minimises the effort (time and labour) and cost (test material and test equipment) associated with pipeline trial experiments.

The main objective of the study is to develop a method of using rheometry in prediction of pumping characteristics for emulsion explosives. In order to achieve this objective, the following methodology is proposed:

- Review the relevant literature pertaining to the research study.
- Find a suitable rheological model that describes the flow behaviour of explosive emulsions.
- Determine the effect of high speed pumping on the rheological properties of emulsion explosive systems.
- Calculate the pressure drops ( $\Delta P$ ) - flow rates ( $Q$ ) relation from rheometry data and to compare the results with data obtained from pipeline trial experiments.

This research study will provide a better understanding of the rheological properties of highly concentrated w/o emulsions explosives, and will serve as a basis for the prediction of pumping characteristics of this emulsion system from rheometry, which is a prerequisite for efficient delivery systems.

This Master's dissertation is subdivided to the following chapters:

- Chapter 1 serves as an introduction to this Master's dissertation.
  
- Chapter 2 is a presentation of the relevant literature review pertaining to the study. It covers relevant literature on pipeline flow of non-Newtonian materials. This includes theoretical rheological fundamentals of high internal phase ratio emulsion explosives. The most relevant is the work of Utracki (1980), Bampfield and Cooper (1988), Pal (1990) and Masalova *et al.* (2003).
  
- Chapter 3 provides a comprehensive description of the methods of experimentation, procedures used in the analysis of experimental errors, and the inherent discussions pertaining to their corrections. It is subdivided into two sections:
  - Part I deals with pipe viscometry (or pipeline trial experiments).
  
  - Part II deals with rheometry.
  
- Chapter 4 deals with the analysis of results and the inherent discussions pertaining to the experimental findings. It also presents the inherent comparison between rheometry predictions and pipeline data.

- Chapter 5 presents the summary of the Master's dissertation. It describes the background, the objectives and an overview of the research dissertation. Conclusions drawn from experimental results are also presented, including possible future research studies.

# **CHAPTER 2**

## CHAPTER 2

### THEORY AND LITERATURE REVIEW

#### 2.1 INTRODUCTION

This chapter is a presentation of the relevant fundamental rheological theory and literature review pertaining to the pipeline flow of high internal phase ratio emulsion explosives. The relevant rheological fundamentals are discussed, with more emphasis on the most generally used and applicable flow models for pseudoplastics, namely the Herschel-Bulkley, the Power Law and the Cross models. The theory on concentric cylinder rotational rheometry and pipe viscometry is also presented, which includes the basic equations governing the flow of materials in these two measuring systems. The application of rheometry in prediction of the pumping characteristics is also discussed in detail; including the inherent problems associated with experimental tests, as well as their corrections.

The following topics are presented: (a) definition of rheology, (b) general classification of fluid flow behaviour, (c) rheological models for non-Newtonian fluid flow behaviour and rheological characterisation, with specific emphasis on the Herschel-Bulkley flow; the Power Law and the Cross models, (d) a comprehensive theory and literature review of emulsions, with emphasis on high internal phase ratio emulsions, and particularly, high internal phase ratio emulsions explosives, (e) rheometry (with emphasis on concentric cylinder rotational rheometry) and pipe viscometry, as well as the inherent problems associated with experimental testing and their corrections, (f) application of rheometry in the prediction of pumping characteristics ( $\Delta P - Q$  data), and finally (g) flow in circular pipes, and correction of slip effect.

## 2.2 RHEOLOGY

The name is a term that comes from a Greek word: “rheos” meaning river, flowing or streaming. The first use of the word “rheology” is accredited to Eugene C. Bingham who also describe the motto of the subject as πανταρει (“panta rhei” from the works of the Greek philosopher, Heraclitus, in about 500 B.C) meaning “everything flows.”. Rheology is now a well-developed independent branch of natural sciences that deals with the deformation and flow of matter: It is a study of the manner in which materials respond to applied stress or strain (Steffe, 1996: 1). According to Malkin (1994), rheology considers real materials with changing structure, and pretends to deal with reality by means of phenomenological models that reflect the most important characteristics of an object.

The ideas of liquids and solids are also classified as models. The formal mathematical representation of ideal liquids and solids originated from the works of Isaac Newton and Robert Hook respectively. Newton ‘s ideas on liquid resistance were converted by Stokes to the general law governing ideal liquid-like behaviour, now known as the Newton-Stokes law:

$$\tau = \eta \cdot \dot{\gamma} \quad (2.1)$$

Where  $\eta$  is the coefficient of proportionality, referred to as coefficient of viscosity or simply shear viscosity,  $\tau$  is the applied shear stress, and  $\dot{\gamma}$  the resulting rate of deformation or shearing. This law assumes a proportional relation between the applied force (or resistance or stress) and resulting velocity of movement (or rate of deformation).

Bernoulli translated a similar proposal by Hooke to the general law governing ideal solid-like behaviour, i.e. the Hooke's Law:

$$\tau = G.\gamma \quad (2.2)$$

Where  $G$  is the coefficient of proportionality, referred to as complex shear modulus or Young's modulus,  $\tau$  is the applied shear stress, and  $\gamma$  the resulting deformation.

This law assumes a proportional relation between the applied shear stress and resulting shear deformation. The exact meaning of the terms in equations 2.1 and 2.2 are discussed below in section 2.3. However, the response of real materials to applied shear stress quite often deviate from the point of view of classical concepts of liquids and solids. Such materials are commonly referred to as rheological materials, and include many real materials that are encountered everyday, e.g. foams, emulsions, slurries and other complex mixtures. Rheology can also be defined as a science dealing with materials having properties that are not described by the models of Newton-Stokes and Hooke.

All materials have rheological properties, and are relevant in many fields of study, namely, mining and geology; concrete technology; polymers and composites; paint flow and pigment dispersion; emulsion technology; cosmetics and toiletries; tribology (which is the study of lubrication; friction and wear); and other fields of study not mentioned. Rheologists are mainly concerned with rheometry (which is defined as a study dealing with the methods and devices

used to measure rheological data); characterisation; interpretation and application of the flow and deformation behaviour of materials (Steffe, 1996: 1).

In general, rheology is critical in the formulation; storage; quality control and long distance pipeline transportation of the highly concentrated w/o emulsion explosives.

### 2.3 CLASSIFICATION OF FLUID FLOW BEHAVIOUR

Fluids are classified in two different ways: firstly, according to their response to externally applied pressure as compressible or as incompressible fluids. This classification is based on whether or not the volume of the fluid element is influenced by pressure and temperature. If the volume of an element of fluid is independent of its pressure and temperature, then the fluid is said to be incompressible. However, if its volume is affected by changes in pressure and temperature, it is said to be compressible). Secondly, fluids are classified according to the effects produced under the action of a shear stress (Coulson & Richardson, 1990: 51-52, Chhabra & Richardson, 1999: 5). The latter mode of classification is termed rheological classification, and it is based on the observation of the flow behaviour of the fluid under a range of measuring conditions. A fluid can be classified as exhibiting one type of fluid flow behaviour based on its predominant rheological behaviour over the shear rate range of interest, and may also exhibit certain minor rheological properties of another type of fluid flow behaviour measured at certain rates of shear (Huang, 1988).

### 2.3.1 Newtonian fluid behaviour

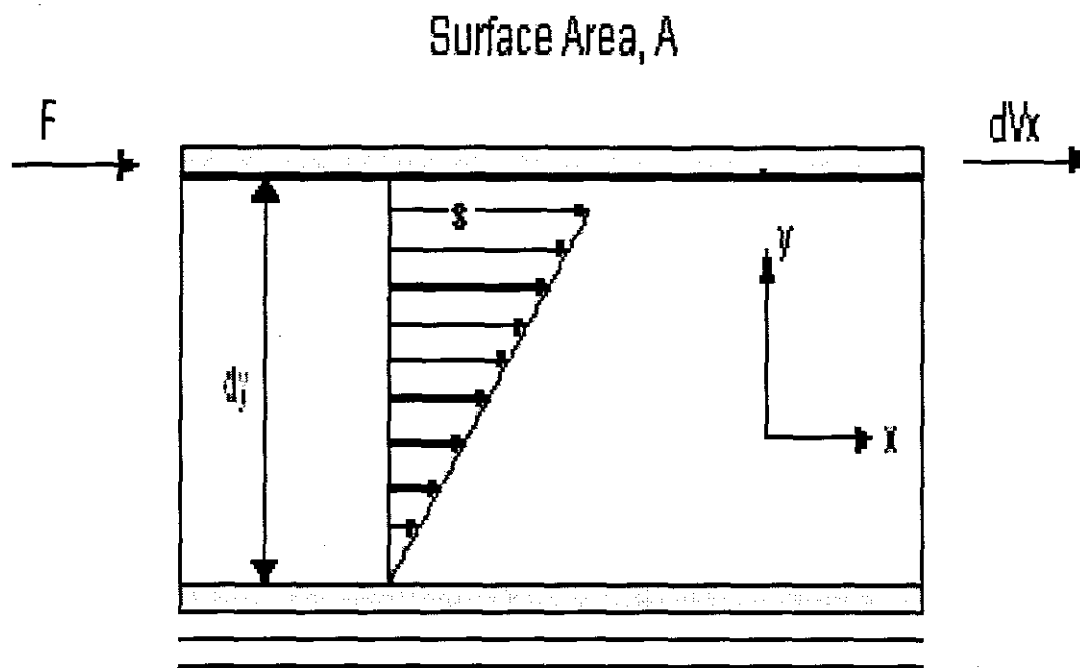


FIGURE 2. 1 Two-plate model (Chhabra & Richardson, 1999)

The two-plate model represents the simplest case wherein the velocity vector has only one component in the x-direction, and varies only in the y-direction. Consider a thin layer of a fluid contained between two parallel plates a distance  $dy$  apart, as shown in Figure 2.1. Now, if under steady state, the fluid is subjected to a shear by the application of a force  $F$  as shown, this force will be balanced by an equal and opposite internal frictional force in the fluid. The shearing force  $F$  moves the upper plate with a shearing area  $A$  to a deflection with the amount  $s$ . The measuring sample is assumed to have adhesion to both surfaces, and that the bottom plate is fixed and stationary.

For an incompressible Newtonian fluid in laminar flow, the following equations are valid:

$$(a) \text{ shear stress (in Pascals, denoted by Pa), } \tau = \frac{F}{A}, \quad (2.3)$$

$$(b) \text{ shear deformation, } \gamma = \frac{s}{dy}, \quad (2.4)$$

$$(c) \text{ rate of shear deformation or shear rate } \dot{\gamma} = \frac{d\gamma}{dt} = \frac{dV_x}{dy}, \quad (2.5)$$

Sir Isaac Newton postulated the following relationship between the shear stress  $\tau$  and shear rate  $\dot{\gamma}$  in a fluid as follows.

*“The resistance which arises from lack of slipperiness originating in a fluid, other things being equal, is proportional to the velocity by which the parts of the fluid are being separated from each other.”*

Mathematically, this can be expressed as follows:

$$\tau_{yx} = \frac{F}{A} \propto \frac{dV_x}{dy} \text{ or } \tau_{yx} = \eta \left( -\frac{dV_x}{dy} \right) = \eta \dot{\gamma}_{yx} \quad (2.6)$$

This means that the resulting shear stress is equal to the product of the shear rate,  $\dot{\gamma}$  and the viscosity of the fluid medium,  $\eta$ . In this case the shear rate may be expressed as the velocity gradient normal to the direction of the shear force,  $F$ . Note that the first subscript on both  $\tau$  and  $\dot{\gamma}$  indicates the direction normal to that of the shear force ( $F$ ) while the second subscript indicates the direction of the force and the flow. The constant of proportionality  $\eta$  (which is defined as the ratio of the shear stress to the rate of shear.) is called the Newtonian viscosity.

The Newtonian viscosity is independent of shear stress ( $\tau_{yx}$ ) or shear rate ( $\dot{\gamma}_{yx}$ ), but depends only on the material properties, its pressure and its temperature. The plot of shear stress ( $\tau_{yx}$ ) against shear rate ( $\dot{\gamma}_{yx}$ ), the so-called 'flow curve' or 'rheogram' is therefore a straight line of slope  $\eta$ , and passing through the origin on a linear scale. However, on a logarithmic scale, the flow curve is a straight line inclined at  $45^\circ$  to both axes and the  $\tau$ -intercept (or the ordinate offset) being the logarithm of the Newtonian viscosity. The single constant  $\eta$  completely characterises the flow behaviour of a Newtonian fluids at a fixed temperature and pressure (Chhabra & Richardson, 1999: 1-2, Malkin, 1992: 62, Slatter & Chhabra 2002: 5).

### 2.3.2 Non-Newtonian fluid behaviour

By definition, non-Newtonian fluids are fluids that deviate from the flow behaviour described by the Newton-Stokes law, (i.e. equation 2.1). In general their rheograms or flow curves (the shear stress-shear rate relation) are characterised by non-linearity of the shear stress-shear rate relation. In fact, the apparent shear viscosity, denoted as  $\eta$  is not constant at a given temperature, but is dependent on the flow conditions such as shear rate,  $\dot{\gamma}$  or shear stress,  $\tau$  and the flow geometry. Sometimes it also depends on the kinematic history of the fluid element under consideration. Non-Newtonian materials are grouped into three general classes:

- a) Time independent, pure viscous, inelastic fluids or simply Generalised Newtonian fluids.
- b) Time dependent fluids.
- c) Visco-elastic fluids.

### 2.3.2.1 Time independent flow behaviour

For this class of fluids, the apparent shear viscosity and the corresponding rate of shear are determined only by the value of the shear stress at that point. In other words, the apparent shear viscosity is shear rate or shear stress dependent at a given temperature of the system. These fluids are subdivided into three types:

- a) Shear-thinning or Pseudoplastic
- b) Viscoplastic
- c) Shear-thickening or dilatant.

Typical rheograms for this class of fluids, as well as for Newtonian fluids are given below in Figure 2.2.

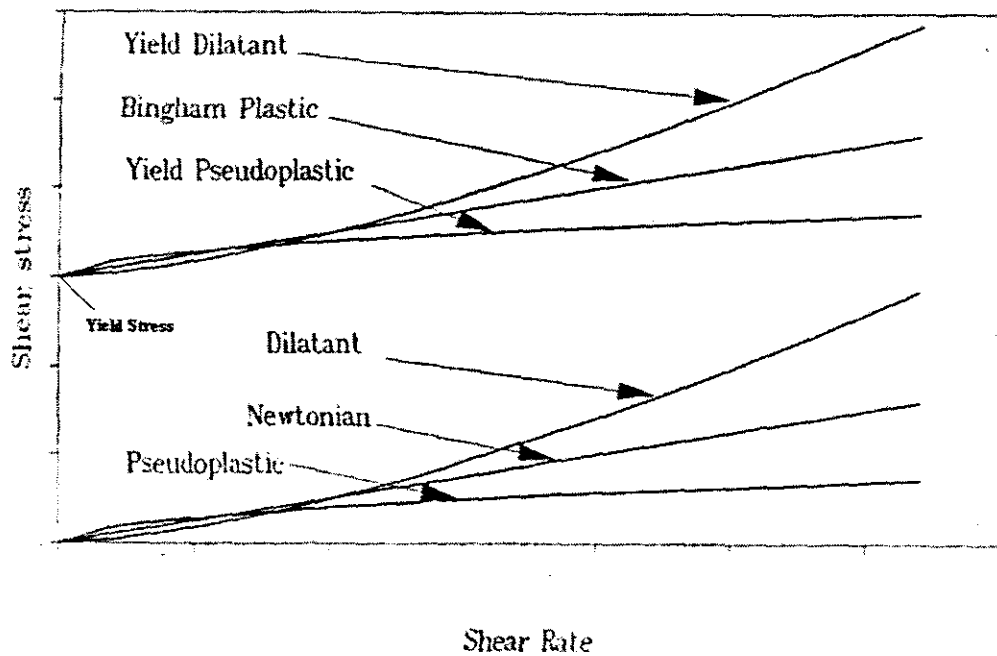


FIGURE 2. 2 Types of time-independent flow behaviour (Slatter & Chhabra, 2002)

Shear-thinning fluid flow behaviour or Pseudoplasticity is characterised by the absence of yield behaviour, as well as by a decreasing apparent viscosity as the shear rate or shear stress increases. However, most Pseudoplastics exhibit Newtonian viscosity at very low and at very high rates of shear. These Newtonian limits are referred to as zero shear rate Newtonian viscosity, and the infinite shear rate Newtonian viscosity, denoted by  $\eta_0$  and  $\eta_\infty$  respectively. Thus, the apparent shear viscosity decreases from  $\eta_0$  to  $\eta_\infty$  with increasing rate of shear. Shear-thickening fluid flow behaviour or dilatancy is also characterised by the absence of a yielding behaviour, but in this case, the apparent shear viscosity increases with increasing rates of shearing or increasing shear stress. (Chhabra & Richardson, 1999, 1: 6-7, 14).

Some fluids exhibit flow properties intermediate between those of solids and those of liquids, with a sharp transition from solid-like to liquid-like behaviour. When the applied stress is below a certain critical stress (i.e. the yield stress, denoted by  $\tau_y$ ), such fluids do not flow, but deform plastically like solids with definite strain recovery upon the removal of stress. However, when the yield stress is exceeded, the applied external stress is greater than the internal structural forces within the fluid, and consequently, these fluids will flow like truly viscous materials with finite viscosity. Such fluids, which are known for their viscoplastic behaviour, are termed yield pseudoplastics (Nguyen & Boger, 1992, Malkin, 1994, 4: 66).

Yield stress fluids are characterised by the existence of a dynamic yield stress ( $\tau_y$ ), which must be exceeded before they deform plastically or flow. Below the yield stress, these fluids behave as elastic solids, and above the yield stress, ( $\tau > \tau_y$ ), their rheograms may be linear or non-linear, but will not pass through the origin. If the flow behaviour is characterised by a yielding behaviour,

followed by non-linear shear-thinning region, such fluid behaviour is termed as Yield-Pseudoplastic. However, if the yielding behaviour is followed by a non-linear shear-thickening region, the flow behaviour is said to be yield-dilatant. If the yielding behaviour is followed by a linear Newtonian region, such behaviour is termed Bingham-plastic (Chhabra & Richardson, 1999,1: 11-13).

### 2.3.2.2 Time dependent fluid behaviour

In time-dependent fluids, the apparent shear viscosities depend upon the shear history of the fluid. Time dependent fluid flow phenomenon is associated with structural changes occurring within the material during shearing. It involves a decreasing or an increasing resistance with the time of shear to some shear-dependent limiting value. This shear dependent limit can be described in terms of rupturing or formation of internal structural linkages, until the rate of breakage or of formation equals the rate of reformation or of breakage respectively. On cessation of shear, random motion allows gradual recovery of structure, implying that the process is completely reversible (Usher *et al*, 1998, Coulson & Richardson, 1990, 3: 100-101, Chhabra & Richardson, 1999, 1: 17).

Fluid flow behaviour that is characterised by a gradual decrease or increase in an apparent shear viscosity (and shear rate) with time, when subjected to a given stress, are sub-divided into two categories, namely: thixotropy, negative thixotropy and rheopexy. The current accepted definition of thixotropy (which also holds for rheopexy) is based on Freundlich's definition (1928) as

outlined below, and was a result of experimental measurements done with thixotropic fluid. The definition includes the following characteristics:

- (a) Thixotropic (or rheopectic) materials are inelastic fluids, and have a shear rate and time dependent viscosity.
- (b) Thixotropy or rheopecty accompanies an isothermal structural change, which is induced by mechanical disturbance to the fluids. When the mechanical disturbance is removed, these fluids recover their equilibrium structures.
- (c) The flow curves of both thixotropic and rheopectic fluids exhibit a hysteresis loop and a stress decay (or stress build-up in the case of rheopectic materials) under a constant rate of shearing. These fluids exhibit a yield stress, because of the dual gel and sol (or dual sol and gel structure in the case of rheopectic materials) structure of the fluids (Huang, 1988).

The time of structural breakdown and recovery is the primary difference between thixotropy and pseudo-plasticity, and the time scale is finite and measurable for thixotropy, but rapid and undetectable for pseudo-plasticity (Usher *et al.*, 1998). Time-dependency flow behaviour can be illustrated graphically in three ways:

- a) As a linear plot of shear stress against shear rate. In this case the shear stress or shear rate is steadily increased from zero, and subsequently decreased again. A typical hysteresis loop is obtained for both types of time-dependent fluid flow behaviour as illustrated below in Figure 2.3.

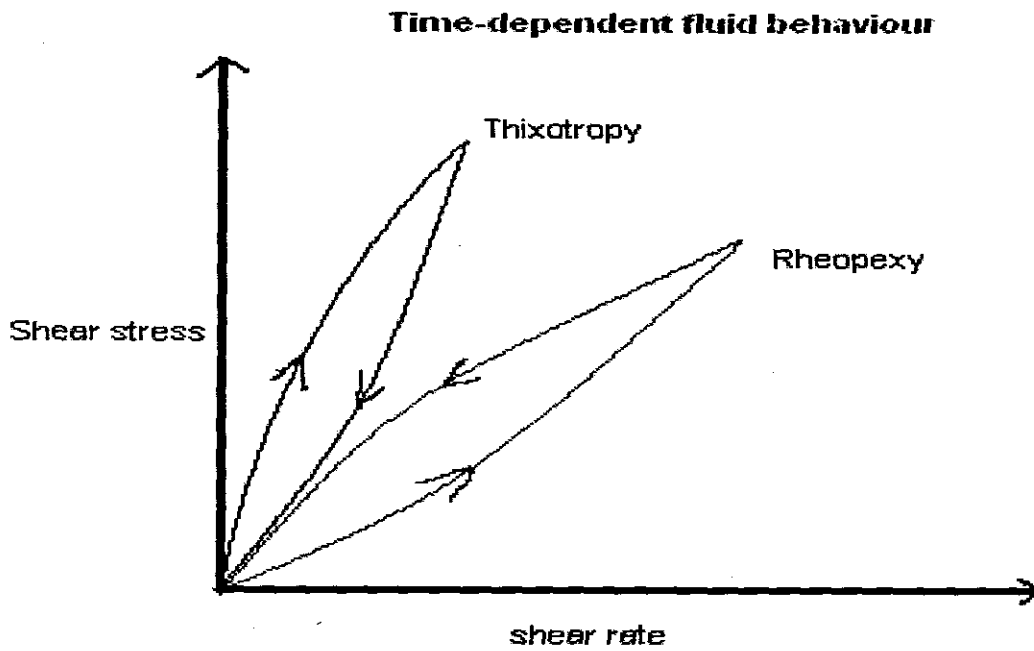


FIGURE 2.3 Thixotropic and rheopectic behaviour of non-Newtonian fluids.

- b) As a linear plot of shear stresses or shear rates against time. In this case a constant shear stress or shear rate is maintained for specific time duration, and the resulting deformations or shear stresses are measured. Typical stress-time and deformation-time curves obtained for both types of time-dependency are illustrated below in Figure 2.4.

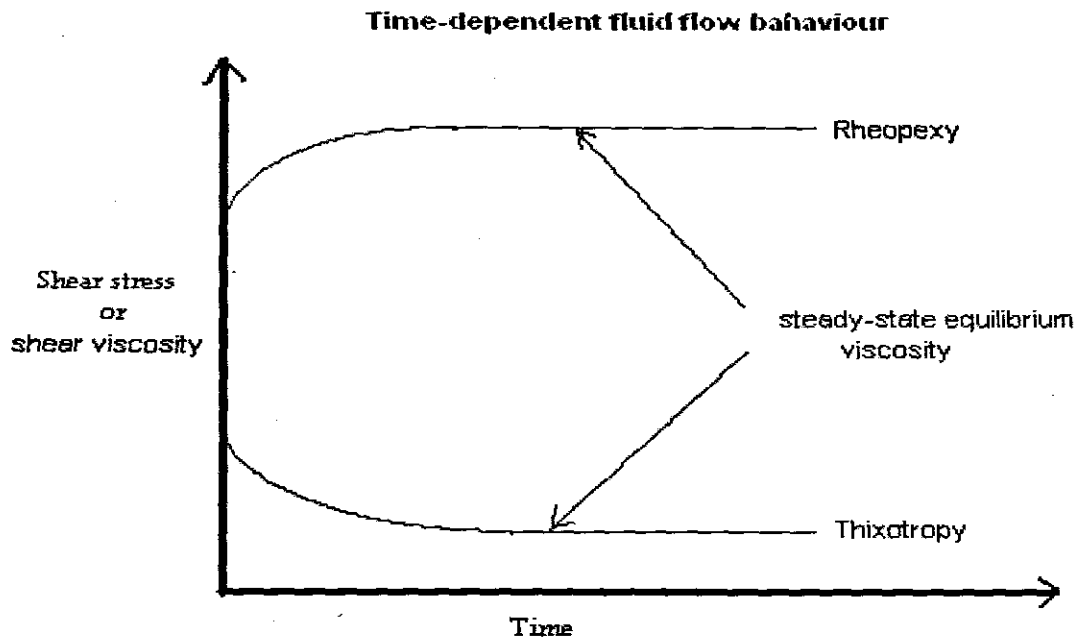


FIGURE 2.4 Thixotropic and rheopectic behaviour of non-Newtonian fluids.

- c) As a logarithmic plot of the apparent viscosities against time, As in (b) above, a constant shear stress or shear rate is maintained for specific time duration, the resulting apparent viscosities are measured. The viscosity-time curves obtained for both types of time-dependency will have the same form as the curves illustrated above in Figure 2.4.

### 2.3.2.3 Viscoelastic flow behaviour

When an ideal solid is deformed elastically, it regains its original state on removal of the stress. However, if the applied stress exceeds the characteristic yield stress of the material, complete recovery will not occur and 'creep' will take place: i.e. the 'solid' will have flowed. At the other extreme, an ideal fluid flows when subjected to stress, and the motion stops as soon as the stress

is removed. Many materials show both elastic and viscous effects under appropriate circumstances, and in the absence of time-dependent behaviour, they are said to be viscoelastic. Such materials have some ability to store and recover shear energy (Coulson & Richardson, 1990, 3: 101-102, Chhabra, 1999, 1: 19-20).

Viscoelastic effects are of practical importance in unsteady state shear flow, and where there are rapid changes in the pressure to which the fluid is subjected. They can give rise to very complex behaviour and mechanical analogues have sometimes been found useful for calculating viscoelastic behaviour. The classical concepts of both liquids and solids as described by the Newton-Stokes and Hooke laws (as mentioned previously in section 2.2 by equations 2.1 and 2.2) respectively, depict the limiting cases of viscoelastic behaviour.

## 2.4 RHEOLOGICAL OR FLOW MODELS OF NON-NEWTONIAN FLUIDS

In order to understand both qualitatively and quantitatively the relationship between the stresses acting on a body, and the resulting deformations occurring as a result of their action, rheologists make use of rheological models. The model that best represents the material depends not only on the nature of the behaviour of that material, but also on the quality and range of viscosity data available for that material, as well as on the intended application (Malkin, 1994: 1 - 3). The selection of a suitable rheological model which accurately describes the flow behaviour of the material, is called rheological characterisation. The choice of model is extremely important, not only for characterisation in laminar flow, but even more important for turbulent predictions. The reasons for this is that data is usually extrapolated to much higher shear stresses for turbulent

flow predictions than can be measured in laminar flow, even in small diameter tubes (Slatter, 1999).

As a practical basis for rheological characterisation, and for a fundamental understanding of non-Newtonian flow behaviour, an ideal constitutive rheological model should meet the following essential requirements:

- (a) It should give an accurate fit of experimental data over a wide range of shear.
- (b) It should involve a minimum number of independent rheological constants (i.e. emphasis is on the simplicity of the constitutive equation), which have real physical significance.
- (c) These coefficients should be readily evaluated, and finally.
- (d) The best model should meet the intended application.

On the other hand, over a wider range of shear rate, it is possible that no single model adequately describes the observed flow behaviour. It is thus recommended that whatever model used, great care should be exercised, if the resulting empirical equation is to be used beyond the range of experimental data obtained. (Cross, 1965, Nguyen and Boger, 1992)

Numerous flow and structural viscosity models have been proposed by various authors (Cross 1965, Utracki 1980, Pal 1990, Slatter 1999 & Masalova *et al.* 2003) for characterising non-Newtonian flow behaviour. The distinction between flow and structural viscosity models, is that the latter have a distinctly expressed range of zero shear viscosity only or a distinctly expressed range of both the zero and infinite shear viscosities. A common feature with structural viscosity models is that they all have limits when  $\dot{\gamma} \rightarrow 0$  and when  $\dot{\gamma} \rightarrow \infty$  equal to  $\eta_0$  and  $\eta_\infty$  respectively,

and that they all transit to the so-called Power law (given below by equation 2.5) at sufficiently high values of shear rate. The the most widely used models for pumping predictions are:

a) Herschel-Bulkley or Yield-Pseudoplastic Flow Model:  $\tau = \tau_y + K \cdot \dot{\gamma}^n$  (2.4)

b) Power Law or Pseudoplastic Flow Model:  $\tau = K \cdot \dot{\gamma}^n$  (2.5)

c) Bingham Plastic Model:  $\tau = \tau_y + \eta_{pl} \cdot \dot{\gamma}$  (2.6)

d) Cross Structural Viscosity Model:  $\eta(\dot{\gamma}) = \eta_{\infty} + \frac{\eta_0 - \eta_{\infty}}{1 + (\lambda \cdot \dot{\gamma})^n}$  (2.7)

e) Carreau Structural Viscosity Model:  $\eta(\dot{\gamma}) = \eta_{\infty} + \frac{\eta_0 - \eta_{\infty}}{[1 + (\lambda \cdot \dot{\gamma})^2]^p}$  (2.8)

$\tau$  is the shear stress (Pa);  $\dot{\gamma}$  is the shear rate ( $s^{-1}$ );  $\eta_0$  is the zero shear Newtonian viscosity (Pa.s);  $\eta_{\infty}$  is the infinite shear Newtonian viscosity (Pa.s), and all the other symbols are empirical or semi-empirical parameters.

Only the three flow models will be described in detail: the Herschel-Bulkley Flow Model, the Power Law Flow Model and the Cross Structural Viscosity Model.

#### 2.4.1 Herschel-bulkley / Yield-Pseudoplastic model

This three-parameter constitutive rheological model is given above by equation 2.4. The Herschel-Bulkley model accommodates both the yield stress ( $\tau_y$ ) and the shear-thinning behaviour of the overall fluid flow behaviour. It describes the behaviour of yield pseudoplastics with reasonable accuracy, except at low and high rates of shear. The shear thinning behaviour shows non-linearity of the flow behaviour, and can be seen clearly in Figure 2.2 from the

convexity of the rheogram curvature. The flow consistency coefficient (K) and the flow behaviour index (n) describe the rheogram curvature. All the flow model constants are empirical, which means that they are not related to the structure of the material, in fact, the  $\tau_y$  value obtained often differ from the value of the 'true' dynamic and static yield stresses (Larson 1999: 270).

The advantage of the Herschel-Bulkley is that, it incorporates the features of the pseudoplastic model (rheogram curvature) and the Bingham plastic model (yield stress), (Slatter, 1999). In fact, this model can be used to characterise all time-independent flow behaviour illustrated in Figure 2.2 above, including Newtonian fluids. The major disadvantage of this flow model is that, it is in direct opposition to the notion that there exist Newtonian asymptotes at both low and high rate of shear (Cross, 1965, Kozicki and Kuang, 1993, Slatter, 1999, Utracki, 1980). Referring to Figure 2.2, the following rheological relationships can be accommodated in the Yield Pseudoplastic model:

- Yield dilatant  $\{\tau_y > 0, n > 1\}$
- Bingham Plastic  $\{\tau_y > 0, n = 1\}$
- Yield Pseudoplastic  $\{\tau_y > 0, n < 1\}$
- Dilatant  $\{\tau_y = 0, n > 1\}$
- Pseudoplastic  $\{\tau_y = 0, n < 1\}$
- Newtonian  $\{\tau_y = 0, n = 1\}$

#### 2.4.2 Power Law / Pseudoplastic/ Ostwald- de-Waele Model

This two-parameter constitutive rheological model is given above by equation 2.5. The Pseudoplastic or Power Law model accommodates only the shear-thinning behaviour, and is described by the flow consistency coefficient ( $K$ ) and flow behaviour index ( $n$ ). The flow behaviour index ( $n$ ) is determined as the slope of the logarithmic plot of the wall shear stress against the shear rate. Chhabra and Richardson (1999) listed the following shortcomings for this model:

- a) It is applied over a limited range of shear rates (i.e. only over the shear thinning shear rate region), and that the value of  $K$  and  $n$  depend on the range selected.
- b) It depicts the absence of the dynamic yield stress,  $\tau_y$  and the two limiting Newtonian viscosities,  $\eta_0$  and  $\eta_\infty$ , that usually exists at very low and at very high rates of shearing respectively in highly concentrated dispersion systems.
- c) The dimensions of  $K$  depend on the value of the flow behaviour,  $n$ .
- d) The value of the flow consistency coefficient,  $K$ , can be viewed as the value of the apparent viscosity,  $\eta$ , when the shear rate,  $\dot{\gamma}$ , is unity and will therefore depend on the time unit employed.

#### 2.4.3 Bird-Carreau / Cross Structural Viscosity Model

Cross (1965) postulated the four-parameter, semi-theoretical, structural viscosity model given above by equation 2.7 based on the assumption that pseudoplasticity in flow is associated with the formation and rupture of structural linkages of a material. According to Utracki (1980) and Cross (1965), the value of the Cross index ( $n$ ) varies with polydispersity (when applied to

polymer melts). The Cross coefficient ( $\lambda$ ) is associated with the rupture of structural linkages, and it is the measure of the characteristic rate of shear ( $\dot{\gamma}_{ch}$ ). The characteristic rate of shear is the shear rate, at which the value of the shear viscosity of the system is the mean of the two limiting Newtonian viscosities,  $\eta_0$  and  $\eta_\infty$  :-

$$\eta = \frac{\eta_0 + \eta_\infty}{2}, \dot{\gamma}_{ch} = \lambda^{-1} \quad (2.9)$$

Substituting equation (2.9) in equation (2.7), the Cross model can be re-written as a four-parameter model of the form: -

$$\eta(\dot{\gamma}) = \eta_\infty + \frac{\eta_0 - \eta_\infty}{1 + \left( \frac{\dot{\gamma}}{\dot{\gamma}_{ch}} \right)^n} \quad (2.10)$$

The Cross constant,  $\lambda$  is derived from theory which assumes that the rupture of a material structure is solely attributed to shearing action with additional contribution from Brownian motion. The effective rate constant for rupture can be written as  $k_0 + k_1 \dot{\gamma}^n$ , and  $\lambda = \frac{k_1}{k_0}$ , i.e. ratio

of the kinetic constants, one for link rupture due to  $\dot{\gamma}(k_1)$  and one for the Brownian motion,  $k_0$ .

A substantial body of knowledge is available pertaining to the evaluation of zero and infinite Newtonian shear viscosities (denoted by  $\eta_0$  and  $\eta_\infty$  respectively), although  $\eta_\infty$  for concentrated solutions and melts is not usually measurable due to the occurrence of polymer degradation, viscous heating effects and other problems which are associated with high rates of shear. The

value of  $\eta_\infty$  is usually much less than  $\eta_0$  (Kozicki and Kaung, 1993). The value of the infinite shear viscosity is usually very small, and approximately equal to zero, and setting  $\eta_\infty = 0$ , equation (2.7) reduces to a simple three-parameter model of the form:

$$\eta(\dot{\gamma}) = \left( \frac{\eta_0}{1 + (\lambda\dot{\gamma})^n} \right) \quad (2.11)$$

Equation 2.11 is referred as the Simplified Cross Model.

## 2.5 THEORY AND RHEOLOGY OF EMULSIONS

Emulsions are one of the most intriguing subjects for rheological investigations, due to combination of various properties, such as non-Newtonian behaviour, viscoelastic and time-dependent flow properties. The term “emulsions” formally describes a great number of blends of immiscible liquids, including polymeric substances, and thus emulsions are generally defined as mixtures of two partially miscible or immiscible liquids, with one of the phases dispersed in the form of droplets in the other. However, as a general rule for emulsions, one refers to mixtures of low-molecular weight components (such as water and oil) in which one phase (the “outer” phase) is continuous, and the other (the “inner”) phase is dispersed. Emulsions of common types are widely spread in different branches of technology, including food processing, pharmaceuticals, enhanced oil recovery, and are frequently encountered in biological systems.

Emulsions are classified according to their constituent liquids as either water-in-oil (w/o) or oil-in-water (o/w) emulsions, although intermediate cases can also be found. The term oil generally

refers to water insoluble organic fluid. Apart from chemical composition, an important variable in the description of emulsions is the ratio of the volume of the inner dispersed phase to that of the outer continuous phase. This ratio is usually referred to as the volume fraction of the dispersed phase or internal phase ratio (and is denoted by  $\phi$ ). A natural value for  $\phi$  of 74% represents the close packing limit of spheres, and surface tension criterion indicates that a stable emulsions should not exist with an internal phase ratio exceeding 74% (Adamson, 1990: 528). However, it has been shown that w/o emulsions can be produced with a much higher water phase content, up to 99% (Pons, 1992). Two possible explanations are as follows: the emulsion droplet size distribution is polydispersed (i.e. the emulsion is very heterogeneous in particle size), with smaller droplets occupying spaces between larger ones (i.e. the well-known Farris Effect for polydispersed suspension of spheres) and that the thin films separating droplets have lower surface tension than that of the bulk interfacial tension, and, as a consequence, spontaneous droplets deformation leads to polyhedral shape of the droplets. (Adamson, 1990: 528-529, Larson, 1999, 6: 267).

Emulsion systems and emulsions rheology are classified into two broad categories namely dilute emulsions (and the rheology of dilute emulsions) and highly concentrated emulsions (and rheology of highly concentrated emulsions) according to this maximum packing limit,  $\phi$  of 74%. Dilute emulsions and the rheology of dilute emulsions exist for  $\phi < 74\%$ . While highly concentrated emulsions (and rheology of highly concentrated emulsions) exist for  $\phi > 74\%$ . Rheological studies of emulsion systems are not restricted to measuring the viscosity, but can yield other rheological parameters (e.g. storage and loss moduli, denoted by  $G'$  and  $G''$  respectively), which are characteristic properties of the emulsion system like viscoelasticity; time

dependency, etc. Most emulsions, apart from very dilute ones ( $\phi < 0.05$ ), show viscoelastic behaviour at low shear due to droplets flocculation, i.e. they behave like solids in the initial stages of shear and subsequently exhibit shear-thinning fluid flow behaviour “in the sense that the work of shearing deformation is not conserved, as in solids, nor is it completely dissipated as in fluids” (Sherman, 1968: 237).

This study was devoted to the rheology and long-distance pipeline transportation of highly concentrated w/o type emulsions with an internal phase ratio far greater than 74%, i.e. approximately 95%. Such emulsions consist of droplets of the water-containing phase dispersed in a continuous organic liquid phase. Three types of ageing processes occur for emulsions: the inner phase may undergo flocculation (i.e. clustering of droplets without losing their identity). The flocs undergo gravity separation if they are part of or subsequent to flocculation. The entire process is known as creaming. However, if coalescence occurs, the eventual breaking of the emulsion follows, giving two liquid layers (Adamson, 199: 534 - 537). Emulsion systems are thermodynamically unstable, and can only be stabilized if the water droplets are covered with a surfactant (or an emulsifier), and thus w/o emulsions are complex multi-component and multi-phase systems.

The effect of the emulsifier in the emulsion systems is twofold: since emulsions present large interfacial areas, it assists in the formation of emulsions by lowering the interfacial tension (this is a simple thermodynamic basis for the role of an emulsifying agent), and it also inhibits coalescence of water droplets as they collide as a result of shear which accompanies flow. Griffin (1954) developed a numerical rating scheme to correlate the chemical structure of surfactants to

their effectiveness as emulsifiers in order to predict the type and stability of emulsion that a given set of constituents will produce. This rating scheme is known as the hydrophile-lipophile balance, or simply HLB number (see Appendix A). In this scheme, numbers are assigned on a one-dimensional scale of surfactant action from 0 to 20. The resulting correlation is then checked with Bancroft's rule (1915), which states that the type of emulsion formed (w/o or o/w) depends on the solubility of the surfactant, with the continuous phase the phase in which the surfactant is more readily soluble. Each surfactant is then rated according to this scale. At the high end of the scale lies hydrophilic or lyophobic surfactants; while at the lower end lies the lyophilic or hydrophobic surfactants. It is assumed that surfactant mixtures can be assigned an HLB number on a weight-proportioned basis which is expressed as follows:  $HLB_{\text{mix}} = (f_A \times HLB_A) + (1 - f_A)HLB_B$ ,  $f_A$  is the weight fraction of A in the surfactant mixture (Adamson, 1990: 525-538, Myers, 1992: 232-241, Randall *et al*, 2000).

Various factors exert some effect on the rheological behaviour of emulsion systems, and all these factors are influenced by the chemical nature and other properties of the ingredients used in preparing the emulsion. To summarise some of the most important factors:

### 2.5.1 Internal Phase Ratio, $\phi$

Very dilute emulsions with an internal phase ratio,  $\phi < 0.05$ , containing non-deformable spherical droplets exhibit Newtonian behaviour. Their viscosity (denoted by  $\eta$ ) is given below by Einstein's limiting law (1906, 1911):

$$\eta_{\text{rel}} = \frac{\eta}{\eta_0} = 1 + a\phi \quad (2.12.)$$

Where  $a$  is an empirical constant with a value of 2.5,  $\eta_0$  is the zero-shear viscosity of the continuous phase,  $\phi$  is the internal phase ratio,  $\eta_{rel}$  is the relative viscosity which is the ratio of the viscosity of the emulsion to that of the continuous phase. Equation 2.12 assumes that there is no hydrodynamic interaction between the droplets, the separation distance between the droplets greatly exceeds their mean diameter, and that the viscosity,  $\eta$  arises from dissipation of energy or viscous drag produced by modifications to fluid flow near the droplet surfaces.

Equation 2.12 can be written as:

$$\eta_{rel} - 1 = \frac{\eta}{\eta_0} - 1 = \eta_{sp} = a\phi \quad (2.13)$$

$\eta_{sp}$  denotes the specific increase in viscosity, and a linear plot of  $\eta_{sp}$  against  $\phi$  results in a straight line of slope  $a = 2.5$ .

Dividing equation 2.13 by  $\phi$  and taking the limit as  $\phi$  approaches zero yields:

$$\left[ \frac{\eta_{rel} - 1}{\phi} \right]_{\phi \rightarrow 0} = \left[ \frac{\eta_{sp}}{\phi} \right]_{\phi \rightarrow 0} = \eta_{int} = [\eta] = a = 2.5 \quad (2.14)$$

$\eta_{int}$  is the intrinsic viscosity, which is the dilution limit of the viscosity increment per unit droplet volume fraction divided by the continuous phase viscosity.

Equations 2.12, 2.13 and 2.14 are valid for  $\phi < 0.05$ , but the limiting value for  $\phi$  depends on the droplet size, as it will be discussed later in this section.

However, the hydrodynamic interaction between the droplets or aggregates of droplets increases with an increase in  $\phi$  due to closer approach of the droplets and subsequent overlapping of the associated flow patterns in the continuous phase and other related factors (which include droplets collisions; slight aggression and the effective volume occupied by droplets).

The hydrodynamic interaction between two spheres leads to a contribution to viscosity that is proportional to  $\phi^2$ , and amongst three spheres, the contribution is proportional to  $\phi^3$ . In general, the hydrodynamic interactions between  $n$  spheres leads to a contribution to viscosity that is proportional to  $\phi^n$ , and to account for all these hydrodynamic interactions, Einstein limiting law (equation 2.12) is modified into a polynomial function in  $\phi$  of the form (Sherman, 1968: 287 – 292, Adamson, 1990: 527):

$$\eta_{\text{rel}} - 1 = \frac{\eta}{\eta_0} - 1 = \eta_{\text{sp}} = a\phi + b\phi^2 + c\phi^3 + \dots \quad (2.15)$$

$b, c, \dots$  are additional empirical constants, with  $a = 2.5$  and  $0 < b < 11$

To account for the probability of a droplet to be transferred from one plane of shear to another (Thomas, 1965) at infinitely high rates of shear, i.e. where aggregation of droplets is absent, Equation 2.15 is modified to include an exponential term:

$$\eta_{\text{rel}} - 1 = \frac{\eta}{\eta_0} - 1 = \eta_{\text{sp}} = a\phi + b\phi^2 + c\phi^3 + \dots + A_T e^{B_T \phi} \quad (2.16)$$

For  $A_T$  and  $B_T$  are empirical constants, with  $a = 2.5$ .

### 2.5.2 Viscosity of the Internal Phase, $\eta_i$ or Viscosity Ratio, $\frac{\eta_i}{\eta_{\text{out}}}$ .

Taylor (1932) extended Einstein hydrodynamic treatment for dilute suspension of hard sphere (equation 2.12) to dilute suspension of droplets in liquid media. His hydrodynamic treatment of dilute suspension of droplets in liquid media is based on the assumption that any emulsifier film around the droplets would not prevent the transmission of tangential and normal stresses from the continuous to the dispersed phase in the absence of slippage at the oil-water interface. These stresses produce fluid circulation within the droplets, which result in subsequent reduction in the distortion of flow patterns around the droplets. The precise effect depends primarily on the viscosity ratio, denoted by  $\frac{\eta_i}{\eta_{\text{out}}}$  or by simply M:

$$\eta_{\text{rel}} - 1 = \eta_{\text{sp}} = a \left[ \frac{\eta_i + 0.4\eta_{\text{out}}}{\eta_i + \eta_{\text{out}}} \right] \phi = \left[ \frac{1 + 2.5M}{1 + M} \right] \phi \quad (2.17)$$

Where M is the viscosity ratio, i.e. the ratio of the viscosity of the dispersed phase to that of the continuous phase, and  $\left[ \frac{1 + 2.5M}{1 + M} \right]$  or  $a \left[ \frac{\eta_i + 0.4\eta_{\text{out}}}{\eta_i + \eta_{\text{out}}} \right]$  account for the internal currents within the droplets.

Leviton and Leighton (1936) modified equation 2.17 to extend its validity to more concentrated emulsions with  $\phi < 0.4$ :

$$\eta_{\text{rel}} - 1 = \eta_{\text{sp}} = a \left[ \frac{\eta_i + 0.4\eta_{\text{out}}}{\eta_i + \eta_{\text{out}}} \right] \left( \phi + \phi^{\frac{5}{3}} + \phi^{\frac{11}{3}} \right) = \left[ \frac{1 + 2.5M}{1 + M} \right] \left( \phi + \phi^{\frac{5}{3}} + \phi^{\frac{11}{3}} \right) \quad (2.18)$$

For emulsions obeying equation 2.18,  $\left[ \frac{1 + 2.5M}{1 + M} \right]$  increases as the viscosity ratio,  $M$  increases.

For higher concentrations, outside of the dilute region, Pal (1992) proposed the following empirical equation for the zero-shear viscosity of an emulsion:

$$\frac{\ln(\eta_{\text{rel}})_0}{K} = \frac{2.5\phi}{1 + \frac{\phi}{\phi_m}} \quad \text{for } K = \frac{0.4 + M}{1 + M} \quad (2.19)$$

Where  $(\eta_{\text{rel}})_0 = \frac{\eta}{\eta_0}$  is the zero-shear rate relative viscosity, and  $\phi_m$  is the maximum packing volume fraction, which for emulsions is 0.74.

The effect of shear viscosity of the interfacial film ( $\eta_s$ ) and its area viscosity ( $\eta_\beta$ ), which is a two dimensional equivalent of bulk viscosity, on  $\eta_{\text{rel}}$  as measured in slow steady-state experiments is given by:

$$\eta_{\text{rel}} - 1 = \eta_{\text{sp}} = \frac{a \left[ \eta_i + 0.4\eta_0 + 0.4(2\eta_s + 3\eta_\beta) / r \right] \phi}{\eta_i + \eta_0 + \frac{0.4(2\eta_s + 3\eta_\beta)}{r}} \quad (2.20)$$

Where  $r$  is the mean droplet radius, thus a viscous film has an effect, which is equivalent to increasing  $\eta_i$  by  $\frac{0.4(2\eta_s + 3\eta_\beta)}{r}$ , and Nawab and Mason (1958) found that the quantity  $(2\eta_s + 3\eta_\beta)$  for several dilute emulsions lie within the range  $0.014 \times 10^{-4}$  to  $0.92 \times 10^{-4}$  g.sec<sup>-1</sup>. Any effect exerted by  $\eta_i$  is more difficult to analyse because of superimposed effects due to droplets interactions and aggregation, and possibly, also due to droplet deformation.

### 2.5.3 Droplet Size and Size Distribution

Leviton and Leighton (1936) observed that the viscosity of dilute o/w emulsion did not change when the diameter,  $d_m$  was reduced from  $3.0\mu\text{m}$  to  $0.7\mu\text{m}$ . They then suggested that the droplet size exerted little effect on the viscosity of dilute emulsions where the droplets were not closely packed. However, Richardson (1950, 1953) in his study of concentrated o/w emulsions ( $\phi = 0.75$ ), observed that the emulsion systems were very viscous, and that their flow behaviour was strongly non-Newtonian. He also observed that the infinite shear viscosity,  $\eta_\infty$ , was proportional to the reciprocal of mean droplet size (i.e.  $\frac{1}{d_m}$ ), with the product  $\eta_\infty \cdot d_m$  constant, provided that the spread of the sizes around  $d_m$  was narrow. Rajagopal (1960) proposed the following equation for the effect of droplet size,  $d_m$ , on relative viscosity,  $\eta_{rel}$  for very dilute emulsions:

$$\eta_{rel} - 1 = \eta_{sp} = \frac{2.5 \left[ \eta_i + 0.4\eta_0 + \frac{4\eta_0\eta_i}{S_c} \left( \frac{1}{d_m} \right) \right] \phi}{\eta_i + \eta_0} \quad (2.21)$$

$S_c$  is the slip coefficient between droplets and the continuous phase.

When  $\eta_1 \rightarrow \infty$  :

$$\eta_{rel} - 1 = \eta_{sp} = \left[ 2.5 + \frac{10\eta_0}{S_c} \left( \frac{1}{d_m} \right) \right] \phi \quad (2.22)$$

The size of droplets for emulsions with very narrow distribution exerts a pronounced influence on the viscosity of pseudoplastic w/o and o/w emulsions stabilised by non-ionic surfactant over a wide range of  $\phi$  (Sherman, 1968). It could be seen from Figures 2.5 (a) and (b), that when  $d_m < 2\mu\text{m}$ , w/o showed a large curvilinear increase in  $\eta_\infty$  with decreasing  $d_m$  at all values of  $\phi$ , but the effect was less pronounced in o/w emulsions, and it only appeared when  $\phi > 0.5$ . This difference is related to the rheology of the respective emulsifier films around the droplets, with the w/o emulsifiers giving a film with high surface rigidity, whereas the o/w emulsifiers gave a film of low viscosity.

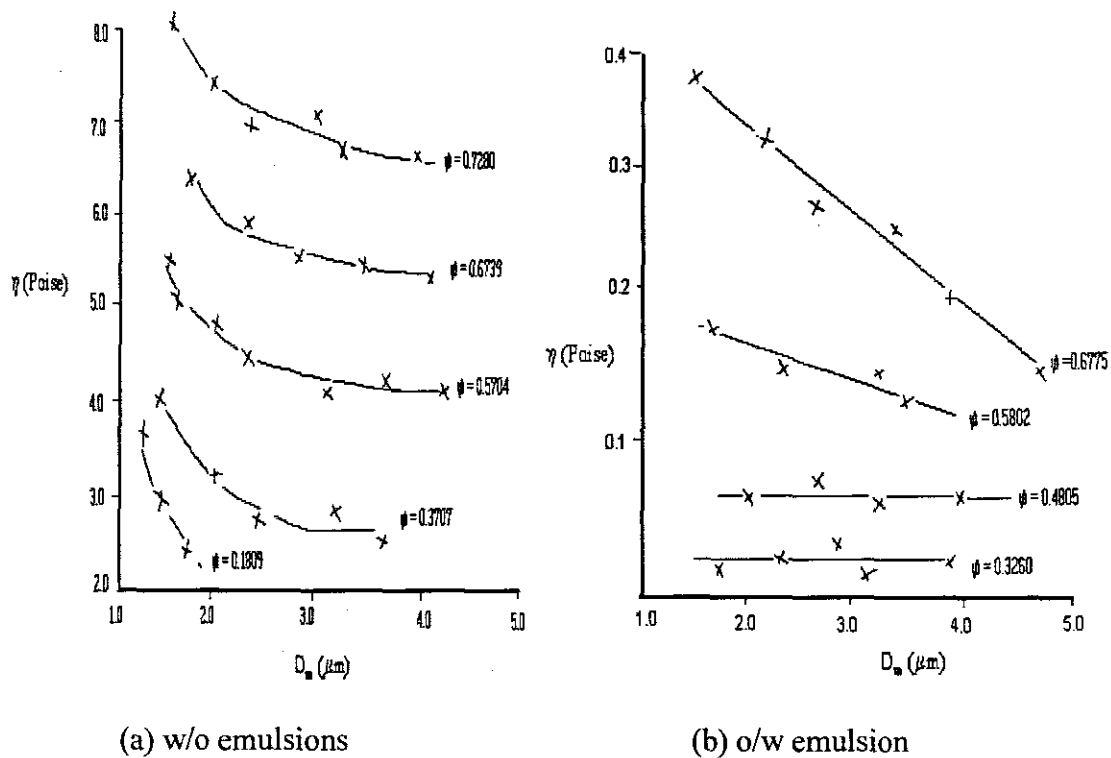


FIGURE 2.5 Influence of  $d_m$  on  $\eta_\infty$  (Sherman, 1968: 302-303).

The droplet size distribution of emulsion systems is often log normal in type, i.e. the following equation is obeyed (Adamson, 1990:527):

$$P = \frac{1}{\sigma\sqrt{2\pi}} e^{-\left[\frac{(\ln d - \ln d_m)^2}{2\sigma^2}\right]} \quad (2.23)$$

$P$  is the probability of finding an emulsion drop of size  $d$  if  $d_m$  is the mean size and  $\sigma$  is the logarithmic standard deviation.

## 2.5.4 Rheology of Highly Concentrated Emulsions

Highly concentrated emulsions are classified as high internal phase ratio emulsions (or simply HIPRE emulsions) with internal phase volume fractions of approximately 94%, which is far

beyond the close packing limit of spherical droplets of 74%. At these volume fractions, the dispersed phase droplets are deformed and thus arranged in a closely packed configuration, assuming hexagonal shapes. This closely packed configuration and the profound hydrodynamic interaction between neighbouring droplets, induce mechanical interference between the droplets, and thus, prohibiting their free movement. In such systems, extensive aggregation or flocculation of the dispersed phase droplets occur, which results in a stable weak gel-like particulate network, (Jager-Lézer *et al.*, 1998, Partal *et al.*, 1997).

High internal phase ratio emulsion systems tend to exhibit a strong non-Newtonian behaviour, which is characterised by both shear thinning and elastic effects. The flow properties of these highly concentrated emulsion systems are governed by the different interaction forces that occur within them. These forces are dependent on the volume fraction of the dispersed phase, the concentration and nature of the emulsifier, the chemical composition of the continuous phase and the interfacial properties. Other structural parameters which also exert some effect include the droplet size and shape, the polydispersity of the droplet size distribution and the rheological properties of the continuous phase (Partal *et al.*, 1997, Princen, 1983, 1985, Princen and Kiss, 1986a, 1986b).

The non-Newtonian behaviour is characterised by the existence of a yielding behaviour and a strong shear-thinning region, in which the apparent shear viscosity is dependent on the rate of shear or shear stress. The yielding behaviour in highly concentrated emulsions can be explained as follows: the dispersed phase droplets exist as overcrowded flocculated hexagonal droplets (i.e. agglomerates of hexagonal droplets). When the applied shear stress exceeds the dynamic yield

stress ( $\tau_y$ ), these flocs undergo deformations in the direction of flow as well as in the direction of the flow gradient. They then disintegrate into spheres with increase in the rate of shear or shear stress. During this process the droplet-droplet interaction forces decreases, thus lowering the emulsion viscosity (Mezger, 2002, Pal, 1999).

Below the dynamic yield stress, the deformations of the droplets are insufficient to allow flow in a global movement, and consequently, the material exhibits elastic behavior (Jager-Lézer *et al.*, 1998, Mezger, 2002: 29). At low rates of shear, highly concentrated emulsion systems exhibit a lower limiting Newtonian shear viscosity, (which is also referred to as the zero-shear viscosity,  $\eta_0$ ), and thus, behave as elastic solids at this low shear rate region (Cross 1965; Utracki 1980; Kozicki and Kuang 1993). The zero-shear viscosity ( $\eta_0$ ) may be considered as a metastable equilibrium between the restructural kinetics and the shear rate decrease. The zero shear rate region is depicted by the horizontal plateau of a logarithmic plot of the viscosity curve or by the lower linear region of the rheogram. This zone of constant response (plateau region) defines the elastic domain, and it indicates an unaltered structure, which is not disturbed by shear. In this linear region, the applied deformation is very low to allow the overcrowded dispersed phase droplets to move freely past one another, (Jager-Lézer *et al.*, 1998).

The existence and evaluation of both the zero and infinite Newtonian shear viscosities ( $\eta_0$  and  $\eta_\infty$  respectively) is widely established. A mathematical justification of their existence was given in a paper by Kozicki and Kuang (1993). The value of  $\eta_\infty$  for concentrated solutions and melts is not usually measurable, due to the occurrence of polymer degradation, viscous heating effects and other problems associated with high rates of shear, (Cross, 1965). The value of the infinite

shear viscosity is usually very small compared to  $\eta_0$ , and approximately equal to zero (Kozicki and Kaung, 1993).

Shearing causes the emulsion droplets to deform in the direction of flow, and that of the flow gradient, inducing droplets deflocculation with increase in shear stress or in the rate of shear, and subsequently, resulting in a slacker configuration, which is associated with decrease in flow resistance (Jager-Lézer, 1998, Pal, 1996 and 1999, Partal, *et. al.*, 1997, Mezger, 2002: 29). It was also found that, with decrease in droplet size, the yield stress; shear viscosity; elastic modulus etc., increase significantly (Pal, 1996). It is widely established that intense shearing causes refinement of droplets, and this implies that the refinement of the emulsion droplets induces an increase in rheological properties (especially, viscosity, elastic modulus, yield stress, etc.).

Numerous authors (Mason 1996, Pal 1996, Bower 1999, Pal *et al.*, 2001, Malkin *et al.*, 2004) have shown the dependence of the zero-shear viscosity on the structural properties of highly concentrated emulsions, and such structural properties include droplet size and shape, polydispersity and rheological properties of the continuous phase. The structure and properties of emulsions were studied in many papers from different points of view. Pioneering works published by Princen (1983, 1985) and Princen and Kiss (1986a, b) demonstrated the role of concentration of the dispersed phase and showed that their rheological properties are characterised by elasticity at low shear stresses and the existence of yielding behavior. Concentration dependency of viscosity for emulsions of two immiscible liquids was successfully described by a new model by Pal (2001).

The influence of droplet size on viscous properties of w/o emulsions was studied by Otsubo and Prud'homme (1994a), and they found that viscosity (especially at high concentration of a dispersed phase) strongly depends not only on average droplet size but also on the width of droplets size distribution. However, for relatively narrow distributions, this effect can be neglected (Barnes, 1999, Lacroix *et al.*, 1997). The influence of droplet size and the internal phase ratio on the viscosity of emulsions was also demonstrated, among others, by Pal (1996). Previous experimental studies proved that water-in-oil (or simply w/o) emulsion systems age faster than oil-in-water (or o/w) type emulsions.

Many authors (Utracki, 1980, Pal, 1990 & 1996, Mason *et al.*, 1996, Masalova *et al.*, 2003, Malkin *et al.*, 2004) described the flow curves of emulsions, and the general feature from experimental observations is the existence of strong shear-thinning behaviour for all emulsions described in literature. However the domain of very low shear rates (and stresses) is under discussion. Barnes and Walters (1985) and Barnes (1994, 1999) showed that zero-shear-rate-limiting viscosity exists at shear rates less than approximately  $10^{-4}\text{s}^{-1}$ . The complete flow curves of emulsions in many cases can be described by the Cross (1965) equation with two (low and upper) limiting values of Newtonian viscosity. However, experiments rarely reach the domain of the upper limiting viscosity (Bampffield & Cooper 1958, Manca *et al.*, 2001, Utracki 1980, Pal 2000, Masalova *et al.*, 2003). A physical model explaining the main rheological parameters of emulsions in structure terms was proposed by Pal and co-workers (1997), and Jansen *et al.*, (2001) recently developed a new approach.

The systematic rheological study of w/o emulsions (exemplified by mayonnaise samples) covering both, linear and non-linear domains of viscoelastic behaviour was carried out by Bower et al. (1999). These authors observed several phenomena typical for such systems: non-Newtonian flow curves, strong amplitude dependence of dynamic modules, possibility of slip at a solid surface, and structure rearrangement induced by shearing. Very clear non-linear effects (in the form of amplitude dependence of complex dynamic modules) were also observed for concentrated w/o emulsions of cosmetic application (Jager-Lézer *et al.*, 1998). It is interesting to mention that rheological behavior of concentrated emulsions in this respect is similar to properties of wet foams: the latter also demonstrate elasticity at high concentration of disperse phase and strong non-linearity in loss modules.

It was shown that w/o emulsions could be formulated with much higher water phase content, up to 99% (Pons *et al.*, 1992). Meanwhile the rheological studies of such emulsions are very rare. One of the interesting exceptions is the publication of Langenfield *et al.* (1999) devoted to measuring of viscoelastic properties of highly concentrated w/o type emulsions. Although the authors did not specify the real concentration of disperse phase, they mentioned that the close packing of 74% was widely overtaken. They showed that such emulsions behave as elastic solids, however the viscous properties of the emulsions were not measured.

It is worth mentioning that few or no experimental rheological studies of emulsions touched with pipeline flow of highly concentrated emulsion explosives, as well as correlating their steady state properties (as measured by rotational instruments) for predicting pumping characteristics of these systems for long-distance transport. Meanwhile, such correlation might not be trivial due to time

effects and deformation-induced structure rearrangement in flow. The study of these problems is the goal of this work. Besides, the object of this study is a very highly concentrated w/o emulsion of rather special formulation used in explosive technique. Published results of rheological investigation of such explosive emulsions were not found.

### 2.5.5 Rheology of Emulsion Explosives

Traditionally, the commercial explosives industry consisted of three types of explosives, namely: nitroglycerine dynamite, dry blasting agents and slurries or water gels. In general, commercial explosives consist of an intimate mixture of condensed oxidisers, almost regularly the nitrate salts of ammonia, sodium, and calcium, which are mixed with a hydrocarbon fuel oil or wax and other additives. These additives are used to control the rheology, and to provide the correct reactivity, physical form, and density to ensure reliable detonation. Such mixtures are used in three physical forms for three different modes of loading into drilled holes: (a) as prilled solids which are poured or augured into boreholes, (b) as pumpable liquids which are loaded from a truck in bulk into the ground, and (pipe flow c) in the form of stiff paste or gels which are packaged into paper or plastic tubes.

The term *emulsion explosive* refers to high internal phase w/o emulsion of a concentrated solution of nitrate salts in water emulsified (as supercooled, supersaturated droplets) into a hydrocarbon oil or oil-wax base. Current developments are aimed at resolving inherent problems associated with stability, crystallisation, as well as attaining product design specifications relating to cost, rheology, and detonation parameters. Their detonation capabilities depend on maintaining a very intimate all-liquid mixture. In practice, this requires a droplet size of the order of 1 $\mu$ m. The

aqueous dispersed phase comprises 90% or more of the emulsion formulation, and conventionally consists of a melt of ammonium, sodium and calcium nitrates with a little water to lower the melting point. These melts have a crystallisation point (more properly a Fudge point),  $T_d \cong 65 - 70$  °C, and therefore must be heated before inclusion into the emulsion. Surfactants in emulsion explosives are used to form and stabilise the high internal phase w/o emulsions, and to prevent bulk crystallisation of the emulsion.

There is a large amount of literature dealing with the rheology of emulsions; notably the review by Sherman (1968), on the rheological properties of high internal phase w/o emulsions. However, little work has been reported on the rheology of high internal phase w/o emulsion explosives, pertaining to application in long-distance pipeline transport of these systems. Explosive emulsions are complex systems with properties related not only to composition and method of preparation, but also to the temperature range. The two critical temperatures, which significantly affect their rheology, are: (a) the crystallisation point “ or the Fudge point”,  $T_d$  of the aqueous phase, and (b) the “congelation temperature”,  $T_c$  of the oil phase, when waxes are employed as part of the continuous phase. At temperatures,  $T \leq T_d$ , shearing imparts bulk crystallisation of the aqueous dispersed phase, and at  $T \leq T_c$ , partial crystallisation of the wax in the oil phase occurs, resulting in the formation of a slurry (i.e. suspension-emulsion or simply suspo-emulsion system where the emulsion system acts as the continuous phase, and the crystals the dispersed phase). The following physical states of explosive emulsions exist: (a) true emulsion at  $T > T_d > T_c$ , (b) suspension-emulsion at  $T_d > T > T_c$ , and (c) solid froth at  $T < T_c < T_d$ . True emulsion explosive exhibit many of the same features as those of more conversional w/o emulsions.

There are two factors influencing emulsion viscosity, and these are the total effective volume fraction of the dispersed phase,  $\phi_{\text{eff}}$  (the higher the value of  $\phi_{\text{eff}}$ , the higher the viscosity,  $\eta$ ), and the deformability of the droplets (the larger the size of the droplets, the higher is their deformability, and the lower is the viscosity). Their internal pressure, or the Laplace pressure ( $\frac{\Gamma}{r}$ , for  $\Gamma$  is the surface tension of the droplets and  $r$  is the radius) controls both the elasticity and the deformability of the droplets (Mason *et al.*, 1996). By virtue of deformable interface, Hand and King (1980) demonstrated that all emulsions at high enough concentrations show viscoelastic behaviour. The semi-theoretical, four-parameter model of Cross (1965) was recommended by numerous authors (Bampffield *et al.*, 1988, Utracki, 1980) for characterising the flow of emulsion explosive systems, i.e. equation 2.7 in section 2.4, which deals with rheological characterisation.

Findings from studies done by Utracki (1980) on the droplet size distribution of these high internal phase emulsion explosive systems revealed that:

(a) The aqueous phase was a blend of three generations of log-normal distributions [ $\phi(1)$ ,  $\phi(2)$  and  $\phi(3)$ ] in the following proportions 22%, 58% and 20% respectively (note that log-normal distribution is given by equation 2.23 in section 2.5.3)

(b) The mean droplet sizes and standard deviations for these generations were as follows  $\overline{d}_m(1) : \overline{d}_m(2) : \overline{d}_m(3) = 1 : 0.69 : 0.37$  and  $\sigma(1) : \sigma(2) : \sigma(3) = 1 : 1.3 : 3.5$ .

(c) The generation with the largest  $\overline{d}_m$  is the most homogenous, while the one with the smallest  $\overline{d}_m$  is the most polydispersed.

(d)  $0.1 \mu\text{m}$  was the limiting size for these systems.

Emulsion explosive are considered as supercooled, aqueous-phase dispersion (with volume fraction of about 0.90 or more) in a partially crystallised oil phase. Due to a high degree of supercooling, partial crystallisation of the aqueous phase by a heterogeneous nucleation mechanism at a temperature,  $T_d \cong 65 - 70 \text{ }^\circ\text{C}$  occurs. Consequently, the system changes to a suspension-emulsion system, whose properties are intermediate between those of suspensions, and those of emulsions. In such system, the emulsion system acts as the continuous phase, while the solid crystals act as the dispersed phase. On storage, slow morphological changes of these crystals take place, from multi-crystalline form of a drop toward a poly-crystalline material. The remaining droplets in the absence of the heterogeneous nuclei can be supercooled down to the homogenous nucleation temperature,  $T_{hn}$  ( $^\circ\text{K}$ ):

$$T_{hn} = k(T_d + 273) \quad (2.24)$$

Where  $k = 0.82 \pm 0.02$ , and  $T_{hn} = -3 \text{ }^\circ\text{C}$  to  $11 \text{ }^\circ\text{C}$ .

The rate of this crystallisation process is directly proportional to the size of the droplets, and it decreases with temperature at  $T \leq T_{hn}$ . Two different situations must be distinguished, that is the shear crystallisation of the continuous phase or surfactant and the crystallisation of a component of the continuous phase. The former is due to lowering of the temperature below its congelation point  $T_c$ . If the suspo-emulsion system undergoes high rate of shearing, the crystallisation will be very pronounced, and suspension rheology will govern the flow, e.g. if the effective volume fraction of the crystallised phase  $\phi_{eff} \rightarrow \phi_m$ , then  $\eta \rightarrow \infty$  and the flow will stop. However, if the emulsion explosive system is carefully cooled to  $T_{hn} < T < T_c$ , then the system can be described in terms of the rheology of partially crystallised oil phase, which primarily depend on the rigidity of

the matrix, the wax content in the oil phase, but not on the size and / or concentration of the dispersed water droplets. If the material is sheared, the aqueous phase will crystallise, which will eventually lead to solidification of the emulsion explosive.

Little work has been reported on the rheology of high internal phase suspo-emulsion. However, from studies conducted by Pal and colleagues (1991), the following conclusions can be drawn pertaining to the rheology of suspension-emulsions:

- a) At lower volume fraction of the solids, i.e.  $\phi_s < 0.1$ , the size of the solid particles exerts little effect on the rheology of emulsion systems. However, at  $\phi_s > 0.1$ , the solid particle size effect is more pronounced, and the smaller the size the larger is the size effect.
- b) Addition of solids to emulsion systems leads to bimodal size suspo-emulsion systems with higher viscosities than the parent monomodal emulsion systems.
- c) The emulsions system act as a continuous phase towards the solids, when the solids are much larger than the emulsion droplets, i.e. when the size ratio of solids to droplets  $\frac{\bar{d}_s}{d} > 3$ . In such systems, the Barnea and Mizrahi (1973) equation can be used to describe the viscosity of the suspension-emulsions relative to that of solid-free emulsions provided the shape of the solid particles is spherical and  $\phi_s \leq 0.04$ .
- d) In general, suspension-emulsions always have higher viscosities than solid-free emulsions at the same total concentration of the dispersed phase.
- e) The effect of solid shape on the viscosity decreases as the shear stress increases, and that the more the solid shape deviates from that of sphere, the higher is the viscosity of the suspensions (Utracki, 1980, Bampfield and Cooper, 1988: 282-300, Pal *et al.*, 1991).

### 2.5.5.1 Summary

The following summary can be drawn from literature review of high internal phase ratio w/o emulsion explosives (Utracki, 1980):

- a) W/O emulsion explosives are purely viscous, true emulsions at  $T > T_d > T_c$  with their droplet size determined by the surfactant concentration.
- b) Their flow curve is described by the four-parameter Cross model for pseudoplastic fluids.
- c) Above the Fudge point, i.e.  $T > T_d$  of the aqueous dispersed phase, they flow as true pseudoplastic liquids with a yield stress.
- d) Below the Fudge point, i.e.  $T < T_d$ , shearing induces crystallisation of the dispersed phase.
- e) Below the congelation temperature of the oil/wax phase,  $T_d > T_c > T$ , the yield stress and rheopectic behaviour are observed, and their rheology depends on the composition and structure of the oil/wax phase. The zero-shear rate viscosities,  $\eta_0$  are inversely proportional to the average droplet diameter.
- f) The infinite-shear rate viscosities,  $\eta_\infty$  seems to be proportional to the average droplet diameter.
- g) Their structure (i.e. droplet size distribution) changes on handling e.g. pumping, with time.
- h) The effect of temperature on the flow properties of coarse emulsions is very pronounced, than that on fine emulsions, virtually nil for  $\dot{\gamma} < 100 \text{ s}^{-1}$ , and relatively small at higher shear rates.
- i) The viscosity depends on a different higher-order average droplet size (called Sauter mean diameter, denoted by  $d_{\text{saut}}$ ) from the surface average,  $D_s$ , which is determined by the surfactant concentration.

- a) The initial droplet size (at  $T > T_d$ ) changes with time and  $\dot{\gamma}$  toward an equilibrium value.

## 2.6 RHEOMETRY OF NON-NEWTONIAN FLUIDS

Rheometry is defined as a study dealing with the methods and devices used to measure the fundamental rheological properties of materials, and the devices used to measure these rheological properties are called rheometers, whereas viscometers are limited to only measure the viscous properties of materials, i.e. simply the viscosity of materials. Rheometers may be placed into two broad categories: rotational type and tube type as shown in Figure 2.6. All these instruments are “volume loaded” devices with container dimensions critical in the determination of rheological properties (Steffe, 1996, 1: 2-4).

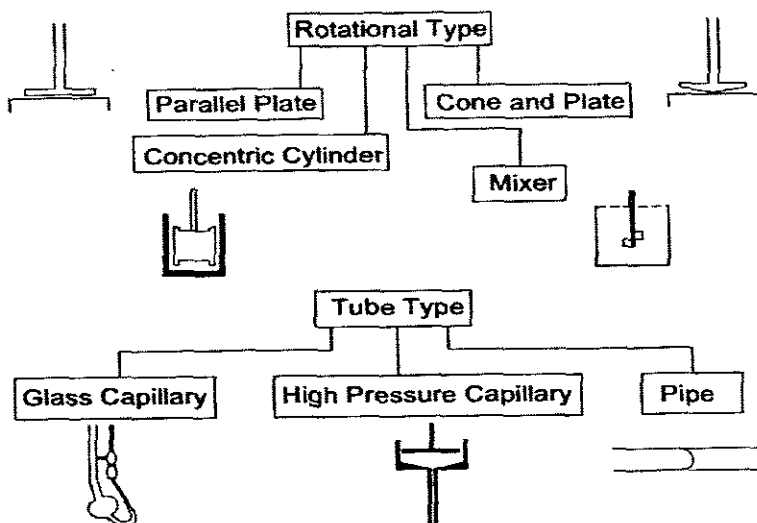


FIGURE 2. 6 Common rheological instruments (Steffe, 1996, 1: 3).

Rotational instruments may be operated in the steady shear (constant angular velocity) or oscillatory mode. Some rotational instruments function in the controlled stress mode (or simply CSS mode) facilitating the collection of creep data; the analysis of materials at very low shear rates and the investigation of the yield stress. Such information is vital for understanding the internal structure of materials. The chief advantage of rotational rheometers (and rotational viscometers) is that, continuous measurements may be made for extended periods of time, and other measurements may be made in the same sample using the same instrument. Thus, time-dependent effects are generally determined from measurements obtained from rotational instruments. The controlled rate mode (or simply CSR mode) is most useful to collect data required for process engineering calculations. Only the concentric cylinder rotational type rheometry and the pipe viscometry will be discussed in this section.

### 2.6.1 Pipe viscometry

Tube viscometers of rheological importance are classified into three types (as shown in Figure. 2.6), namely: glass capillaries, high pressure capillaries and pipe viscometers (Figure. 2.7), and their mode of operation is by creating a pressure difference in order to create flow. The primary difference between a capillary and pipe viscometer is the size of the tube. Capillary viscometers have very small diameters while pipe viscometers have bigger diameters of various sizes. This sub-section mainly deals with pipe viscometers, especially, inherent problems associated with time-independent rheological measurements, using this measuring system.

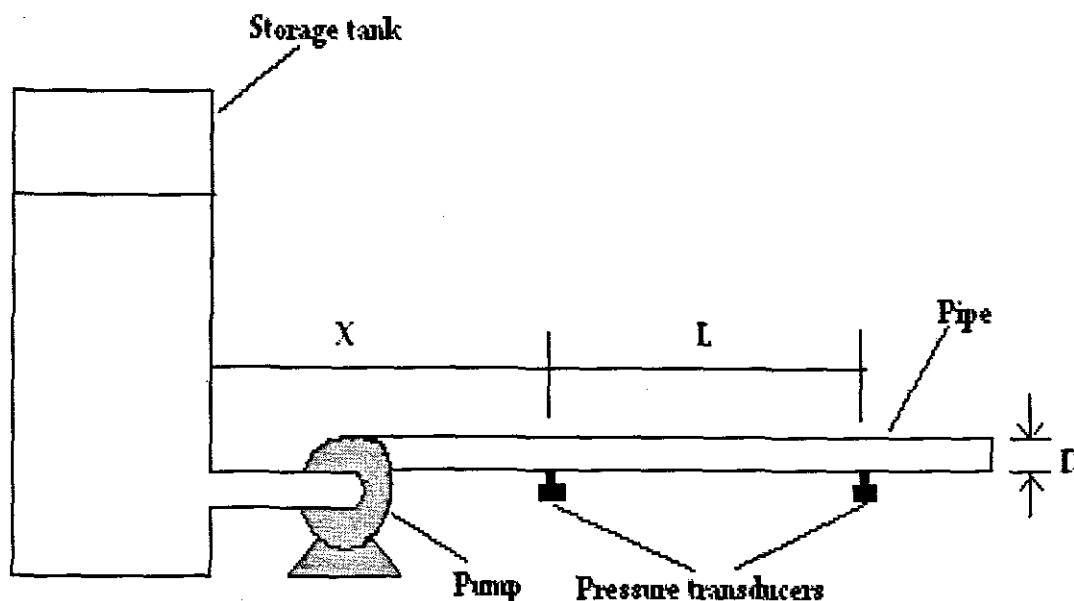


FIGURE 2. 7 Pipe viscometry.

Pipe viscometers make use of pump systems to transport fluids through the pipe. The fluid viscosity is determined from the measured volumetric flow rate, pressure drop and the pipe dimensions (i.e. pipe diameter,  $D$ , and pipe length,  $L$ ). A complete pipe viscometer consists of the following: (1) fluid reservoir, (2) pipe of known dimensions (i.e.  $L$  and  $D$  are known), (3) a unit for controlling and measuring the applied pressure (i.e. pump and differential pressure cells or pressure transducers, respectively), (4) a unit for measuring flow rate (i.e. mass flow meters or weight tank), and (5) a unit for controlling the temperature (Steffe, 1996: 94 - 97, Van Wazer *et al.*, 1966: 188-191). The derivation of the basic equations for pipe and capillary viscometers is discussed in detail in sections 2.7 and 2.8.1.

Serious errors in rheological data obtained from pipe viscometers are due to various factors, and these factors include entrance and end effects, kinetic energy losses, entrance length, wall slip (this effect is discussed separately in section 2.8.2), viscous heating and hole pressure effects.

### 2.6.1.1 Entrance and end effects and their correction

Entrance and end effects are energy losses due to viscous or elastic behaviour. These effects occur when the fluid converges on entering the pipe from a large reservoir, and when it diverges on leaving the pipe. The internal frictional losses due to both sudden contraction (at the pipe inlet) and sudden enlargement (at pipe outlet), are functions of the area ratios (area of reservoir to pipe cross-sectional area), the kinetic energy of the fluid in the pipe, the shape of the pipe ends, and the nature of the fluid. Entrance effect can be evaluated experimentally from plots of the pressure drop,  $\Delta P$  versus  $\frac{L}{D}$  ratio at various flow rates (Bagley, 1957).

The combined effects of the pipe inlet kinetic energy loss and entrance viscous friction due to sudden contraction in geometry, for laminar flow of non-elastic, non-Newtonian fluids, is given by the expression developed by Bogue (1959) as:

$$\frac{2\Delta P}{\rho V^2} = 64 \left[ \frac{L}{D} \right] Re + C \quad (2.25)$$

$\rho$  is the density of the fluid,  $\Delta P$  is the pressure drop,  $V$  is the mean bulk velocity,  $C$  is the correction term for the combined effects of kinetic energy and viscous friction,  $Re$  is the generalised Reynolds number,  $Re = \frac{\rho V D}{\eta}$  which for power law fluids is given as:

$$Re_{PL} = \frac{\rho V^{(2-n)} D^n g^{(1-n)}}{K \left[ \frac{3n+1}{4n} \right]^n} \quad (2.26)$$

The correct pressure drop ( $\Delta P_{cor}$ ) is found by subtracting the entrance pressure drop loss ( $\Delta P_{entr.}$ ) from the measured pressure drop ( $\Delta P_{meas}$ ), and the result is used to calculate the wall shear stress:

$$\tau_w = \frac{D \Delta P_{cor}}{4L} \text{ or entrance effects can also be corrected by using the effective pipe length } (l + \ell R),$$

resulting in:

$$\tau_w = \frac{D \Delta P_{meas}}{4(L + \ell R)} \text{ for } \ell = \left[ \frac{2 \Delta P_{entr}}{\Delta P_{meas} - \Delta P_{entr}} \right] \left[ \frac{L}{D} \right] \quad (2.27)$$

Boger (1982) developed the following expression for estimating the entrance length ( $L_E$ ), (which is defined as the distance at which the centreline velocity of the velocity profile is 99% of fully developed laminar flow) for Newtonian fluids:

$$\frac{L_E}{D} = 0.55 + 0.055 Re \quad (2.28)$$

The constant, 0.55 accounts for the entrance effect at very low values of Re.

For pseudoplastic fluids, Collins and Schowalter (1963) developed an expression for  $L_E$ , based

on a modified power law Reynolds number,  $Re'_{PL} = \frac{\rho V^{(2-n)} D^n}{K}$ :

$$\frac{L_E}{D Re'_{PL}} = (-0.125n + 0.175) \left( 8^{n-1} \left[ \frac{3n+1}{4n} \right]^n \right) \quad (2.29)$$

For Bingham plastic fluids, Michiyosi *et al.*, (1966) developed the following expression for  $L_E$ :

$$\frac{L_E}{D Re'_{BP}} = 0.0476 e^{\left( -5.125 \frac{\tau_y}{\tau_w} \right)} \quad (2.30)$$

Entrance effects are minimised if  $\frac{L_E}{L}$  is of the order of 0.01. Current literature (Chabbra &

Richardson, 1999: 145) recommends an entrance length of the order of forty pipe diameters for inelastic fluids, and about 110D for visco-elastic fluids is sufficient to minimise entrance effects.

However, Dervisoglu and Kokini (1982), from their studies with various food materials found that an entrance length of 90D was sufficient to minimise entrance effects. These effects can also

be alleviated by making use of long pipes with  $\frac{L}{D} \geq 100$ , and having trumpet-shaped or rounded

pipe entrances, coupled by strategically located pressure transducers or differential pressure cells,

so that the entrance region does not influence experimental data (Steffe, 1996: 112-116, Van Wazer *et al.*, 1966: 205-206)

### 2.6.1.2 Pipe end kinetic energy and viscous effects and their correction

Pipe end kinetic energy effects are energy losses due to viscous or elastic behaviour when the fluid stream diverges on discharge at the pipe outlet into air. The stream usually discharges with high velocity and this kinetic energy loss may account for a sizable proportion of the total applied pressure for some viscometers under certain operating conditions. Viscometry equations are usually employed in correcting these energy losses, and the measured or observed pressure ( $\Delta P_{\text{meas}}$ ) is corrected for kinetic energy loss as follows:

$$\Delta P_{\text{cor}} = \Delta P_{\text{meas}} - \frac{\rho V^2}{\alpha_k} = \Delta P_{\text{meas}} - \frac{\rho Q^2}{\alpha_k \pi^2 R^4} \quad (2.31)$$

$\alpha_k$  is the kinetic energy correction factor, and this factor is a function of the velocity-distribution pattern in the pipe.

The velocity distribution is parabolic for Newtonian fluids in laminar flow, and  $\alpha_k = 1$ . The correction factor ( $\alpha$ ), for pseudoplastic fluids, is given by:

$$\alpha_k = \frac{(4n+2)(5n+3)}{[3(3n+1)^2]} \quad (2.32)$$

$n$  is the power law exponent.

End effects are eliminated when long capillaries (or pipes) with  $\frac{L}{D} \geq 400$  are used, so that the end effects are negligible compared with the pressure drop due to laminar flow within the capillary or pipe (Van Wazer *et al.*, 1966: 200-205).

### 2.6.1.3 Viscous heating effect and correction

Isothermal conditions are usually assumed in the derivation of the basic flow equations for fluids. As a consequence of viscosity-induced frictional heat dissipation, when a fluid is caused to flow through a pipe at high levels of stress, substantial radial and axial temperature distributions may develop. Thus, viscous heating effects are defined as effects due to frictional heat dissipation arising from flow of any viscous fluid. These effects may incur serious experimental errors in rheological data (especially for very viscous fluids). For pipe viscometers, viscous heating effects depend on the temperature of the pipe system boundaries, the pipe geometry (i.e. pipe size and length), the applied pressure and fluid properties.

Toor (1956, 1957) developed the following expression for estimating the distance ( $\chi_s$ ) required to closely approach a limiting temperature distribution (i.e. when all the temperature distributions within the fluid are constant) for power law fluids:

$$\chi_s = \left[ \frac{3n+1}{2(n+1)} \right] X_s R N_{pe} = 0.5 \left[ \frac{3n+1}{2(n+1)} \right] X_s D N_{pe} \quad (2.33)$$

With

$$N_{pe} = \frac{4QC_p\rho}{\pi D\kappa} = \frac{VDC_p\rho}{\kappa} \text{ and } (0.5 \leq X_s \leq 1) \quad (2.34)$$

$n$  is the power law coefficient,  $X_s$  is a parameter concerned with the closeness of approach to the steady temperature distribution,  $C_p$  is the heat capacity of the fluid,  $Q$  and  $V$  are the bulk volumetric flowrate and velocity respectively,  $\kappa$  is the thermal conductivity of the fluid, and  $N_{pe}$  is the Peclet number (a dimensionless number relating the forced convection of a system to its heat conduction).

Gee and Lyon (1957) showed that the radial position corresponding to the average flow temperature ( $T$ ) was about  $\frac{r}{R} = 0.64$ . Whorlow (1992) developed a simple expression for evaluating the extent of viscous heating:

$$\Delta T_{vh} = \frac{\Delta P}{\rho C_p} \quad (2.35)$$

The Nahme number ( $N_a$ ) may also be used to evaluate the effects of viscous heating, and it is given by the following equation:

$$N_a = \frac{\Delta T_{vh}}{\Delta T_{visc}} \quad (2.36)$$

$\Delta T_{vh}$  is the temperature change due to viscous heating, and  $\Delta T_{visc}$  is the temperature change necessary to significantly change viscosity (Steffe, 1996:118-119, Van Wazer *et al*, 1966: 211-213).

#### 2.6.1.4 Hole pressure effect and correction

Sometimes the pressure in the pipe is measured by a transducer communicating with the fluid in the pipe through a fluid well connected to the pipe. This practise causes curvature in the flow streamlines, which may cause serious errors in the pressure measurements. Hole pressure effect in pipe viscometers is alleviated by the use of identical pressure transducers at each sensing location, and this effect cancels out when  $\Delta P$  is calculated (Steffe, 1996:118-120, Van Wazer *et al.*, 1966: 211-213).

#### 2.6.2 The concentric cylinder geometry

The measuring systems of the concentric cylinder rheometry (and concentric cylinder viscometry) consist of a fixed part and a rotating part, and the word “concentric” implies that the cup and the bob are arranged on the same rotational axis. Two measurement principles are applied; see diagram on page 2.57 (PaarPhysica, 1995):

- a) Searle’s principle: consist of a rotating bob and a static measuring cup
- b) Couette’s principle: consist of a static bob and a rotating measuring cup

In a rotational test with controlled shear rate (CSR mode), the torque ( $T_q$ ) is measured by detecting the force tensor arising from internal viscous friction exerted by the sample on the rotating measuring bob surfaces. However, in a controlled stress (CSS mode) test, torque is applied to the sample and as a reaction the deflection or the rotational speed is measured which the measuring system gets towards the sample. The prerequisite for rheological measurements of

non-Newtonian fluids using the concentric cylinder geometry is a narrow annular gap of shearing, and the recommended ratio of inner to outer cylinder radii,  $\left(1 > \frac{R_b}{R_c} > 0.99\right)$  or  $1 < \delta < 1.01$  in order to ensure that adequate bulk flow is attained (Chhabra & Richardson, 1999: 43).

In order to derive basic equations for these measuring systems, the following assumptions are made (Van Wazer *et al.*, 1966: 52):

- a) The fluid is incompressible, and that the flow type is two-dimensional (i.e. neglecting the edge and end effects), steady-state (all time derivatives are zero), laminar flow. The criterion of laminar flow is the ratio of inertial force to viscous force, the Reynolds number,  $Re = \frac{\rho V D}{\eta}$ . In rotational instruments, the transition from laminar to turbulence is influenced by centrifugal forces. In the Couette measuring system, the inertial forces have a high stabilising effect, and consequently, the transition from laminar to turbulence is at much higher Reynolds number ( $Re$ ). However, for the Searle's measuring system, the centrifugal force tends to introduce instabilities (Van Wazer *et al.*, 1966: 85).
- b) The streamlines of flow are circles on the horizontal plane perpendicular to the axis of rotation (i.e. the velocity is a function of the radius only, and axial flow are assumed to be equal to zero, i.e. effect of centrifugal forces are negligible which is valid for small values of  $\omega$ ).
- c) There is no wall slip.
- d) The system is isothermal.

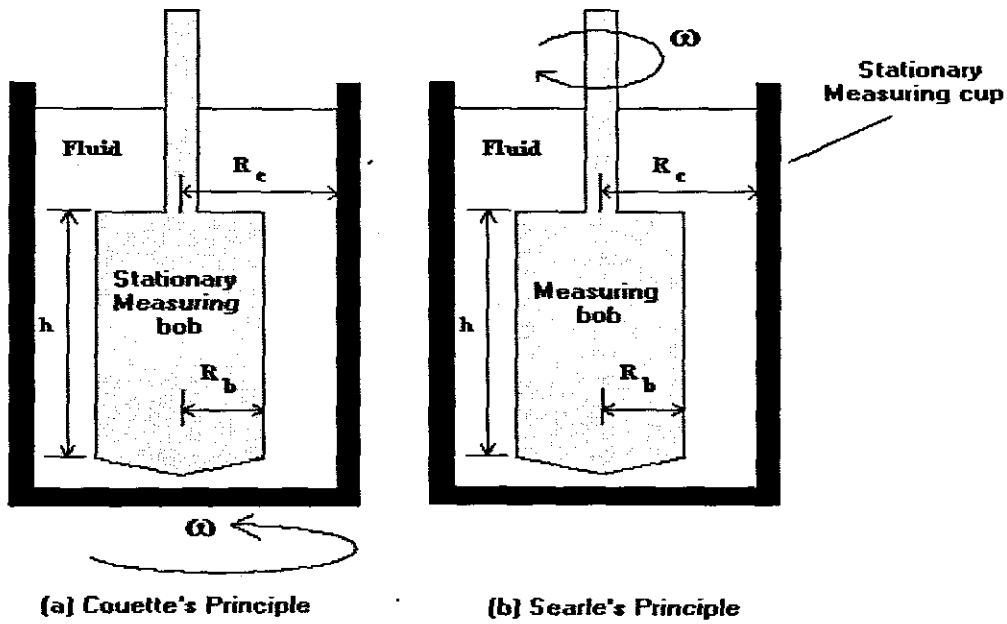


FIGURE 2. 8 Measuring Principle for concentric cylinder geometry.

For concentric cylinder geometry the following fundamental equation applies (Chhabra & Richardson, 1999; Paar Physica, 1995; Steffe, 1996: 158-171, 174-183; Van Wazer *et al.*, 1966: 47-61, 68-71).

$$\dot{\gamma}_{\text{rep}} = \omega \cdot \frac{1 + \delta^2}{\delta^2 - 1} = \frac{\pi n}{30} \left( \frac{1 + \delta^2}{\delta^2 - 1} \right); \quad \omega = n \cdot \frac{2\pi}{60} \text{ and } \delta = \frac{R_c}{R_b} \quad (2.37)$$

$$\tau_{\text{rep}} = \frac{1 + \delta^2}{2\delta^2} \cdot \frac{T_q}{2\pi h R_b^2 C_L} \quad (2.38)$$

$$\eta_{\text{rep}} = \frac{\tau_{\text{rep}}}{\dot{\gamma}_{\text{rep}}} \quad (2.39)$$

$\dot{\gamma}_{rep}$  is the representative or mean shear rate;  $\tau_{rep}$  is the representative or mean shear stress;  $\eta_{rep}$  is the representative or mean viscosity,  $\omega$  is the angular velocity;  $\delta$  is the radius ratio;  $n$  is rotational speed;  $T_q$  is the torque;  $h$  is gap length;  $R_b$  is radius of the bob;  $R_c$  is the radius of the cup and  $C_L$  is the end effect correction factor.

As is the case with tube viscometry, various factors incur serious errors in rheological measurements, and these factors include: end effects; wall slip; viscous heating; inertia and secondary flow; cavitation and eccentricities due to misalignment of the geometry. Vertical misalignment of the measuring system of the rheometer effect inaccuracies in measurements and this results in erroneous flow data. Such errors are not that significant as most coaxial cylinder rheometers are designed in such a way that the need for careful set-up is eliminated. However, it is important to calibrate the rheometer prior to testing. Some of these factors are corrected as follows:

### 2.6.2.1 End effects corrections

End effects that arise due to the shear flow at the bottom of the cylinder are determined by taking measurements of torque ( $T_q$ ) at a fixed rate of rotation with the annulus measuring gap filled to various heights ( $h$ ). The resulting data is plotted as torque versus the height of fluid in contact with the immersed length of the bob. The resulting curve should be linear with slope equal to the torque required to maintain the fixed rate of rotation per unit length of cylinder, and the  $h$ -intercept, which is found by extrapolating the straight line to zero torque is the effective height,

$h_0$ . The value of  $h_0$  is then substituted in the various equations, applying correction for the end effects in equation 2.38 results:

$$\tau_{\text{rep}} = \frac{1 + \delta^2}{2\delta^2} \cdot \frac{T_q}{2\pi(h + h_0)R_b^2 C_L} \quad (2.40)$$

Various bob designs have been developed to minimise end effects. The Mooney-Couette or Mooney-Ewart design has the lower end of the bob shaped as a truncated cone. Another bob design (which was developed by the German Institute of Standardization) that is commonly used has a reservoir on top and a recessed bottom. The shear rate at the bottom of the bob, for the Mooney-Ewart bob design, is equal to that in the annular measuring gap, if the conical angle ( $\theta$ ) is related to the cylinder radii by either of the following expression (Chabbra & Richardson, 1999: 44, Steffe, 1996: 174 - 175, Van Wazer *et al.*, 1966:69-70):

$$\theta = \tan^{-1} \left[ \frac{R_c^2 - R_b^2}{R_b^2 + R_c^2} \right] = \tan^{-1} \left[ \frac{\delta^2 - 1}{1 + \delta^2} \right] \quad (2.41)$$

$$\theta = \tan^{-1} \left( \frac{R_c - R_b}{R_c} \right) = \tan^{-1} \left[ \frac{\delta - 1}{\delta} \right] \quad (2.42)$$

Note that equation 2.41 is derived by equating equation 2.37 to the shear rate at the conical

section  $\left[ \dot{\gamma} = 2\Omega \left( \frac{\delta^2}{\delta^2 - 1} \right) \right]$ , by the method illustrated by Steffe (1996: 233, problem 3.8.15, see

Appendix B).

### 2.6.2.2 Wall Slip

The general basic expression, for purely viscous, shear-thinning, non-Newtonian fluids, which exhibit no yielding behaviour, that relates the angular velocity of the bob ( $\Omega$ ) to the shear stress in the gap is given by (assuming the slip velocity is zero):

$$\int_{\omega=0}^{\omega=\Omega} d\omega = \Omega = \frac{1}{2} \int_{R_b}^{R_c} f(\tau) \frac{d\tau}{\tau} \quad (2.43)$$

$\tau$  is the shear stress in the fluid,  $f(\tau) = \dot{\gamma}$  is the rate of shear,  $h$  is the length of measuring gap, and subscripts  $b$  and  $c$  refer to bob, and radii respectively.

The determination of the corresponding shear rates,  $f(\tau) = \dot{\gamma}$  from equations 2.43 and 2.46 is not so straightforward without knowledge of the fluid model. For example, with a Newtonian fluid,

$f(\tau) = \dot{\gamma} = \frac{\tau}{\eta}$ , integration of equation 2.43 yields an expression for the shear rate at the bob

(Nguyen and Boger, 1992: 56, Steffe, 1996: 164):

$$f(\tau_b) = \dot{\gamma}_b = \frac{2\Omega}{(1 - \delta^{-2})} \quad (2.44)$$

The solution of equation 2.43, for purely, viscous, non-Newtonian fluids with no yield stress, can be determined by the methods developed by Krieger and co-workers (Van Wazer *et al.*, 1966: 55 - 68). However, for purely viscous, yield-stress fluids, the shear stress decreases continuously

with  $r^2$  in the annulus. With Searle rheometers (i.e. rotating bob and stationary cup),  $\tau$  is maximum at the bob (at  $r = R_b$ ), and minimum at the cup (at  $r = R_c = \delta.R_b$ ). Thus the entire fluid is shear only if the yield stress,  $\tau_y$  is exceeded everywhere within the annulus i.e.  $R_b < r < R_c$ , implying:  $\tau_b > \tau_c \geq \tau_y$ ,  $\tau_b \geq \delta^2 \tau_y$  or  $T_o \geq 2\pi r^2 R_b^2 h \tau_y$ .

Under conditions where  $\tau_b > \tau_y > \tau_c$ , the fluid is partially sheared, as shown in Figure 2.8, only the fluid close to the bob is sheared, and where  $\tau_y$  is not yet exceeded, the fluid is stationary. The yield surface of radius,  $r = R_{crit}$  at which  $\tau = \tau_y$ , is given by:

$$R_{crit} = R_b \left( \frac{\tau_b}{\tau_y} \right)^{0.5} = \left( \frac{T_o}{2\pi h \tau_y} \right)^{0.5} \text{ for } \tau_b = \frac{T_o}{2\pi R_b^2 h} \quad (2.45)$$

$\tau_y$  is the yield stress of the fluid,  $h$  is the length of measuring gap,  $T_o$  is the torque of the measuring system, and subscripts b and crit refer to bob and critical radii respectively

The thickness of the sheared fluid layer ( $R_{crit} - R_b$ ) is the effective gap width, and it decreases with increasing rate of rotation,  $\Omega$ .

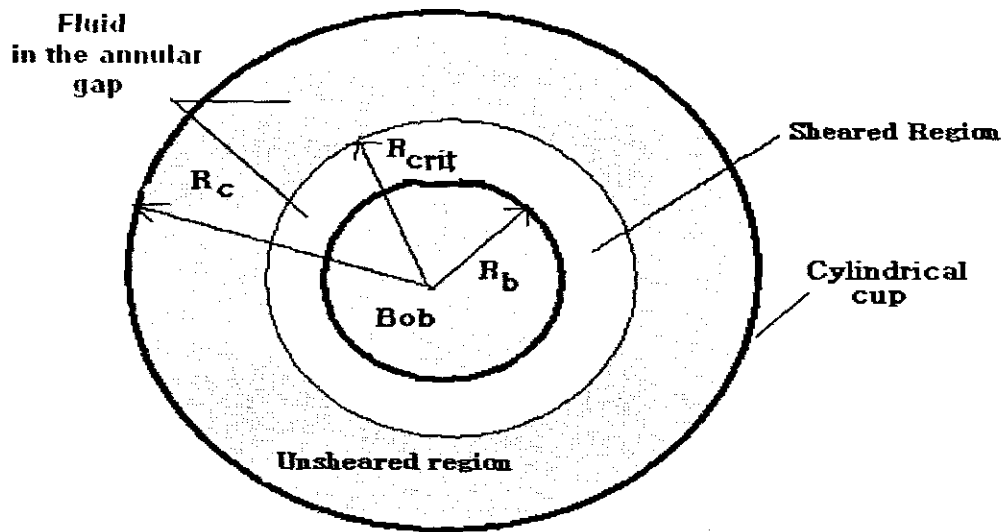


FIGURE 2. 9 Plug flow of yield stress fluids in concentric cylinder geometry.

Thus, for purely viscous, yield-stress fluids, in order to account for the yielding behaviour, equation is modified as follows:

$$\int_{\omega=0}^{\omega=\Omega} d\omega = \Omega = \frac{1}{2} \int_{R_b}^{R_{crit}} f(\tau) \frac{d\tau}{\tau} \quad (2.46)$$

Where  $\tau$  is the shear stress in the fluid,  $\tau_y$  is the yield stress of the fluid,  $f(\tau) = \dot{\gamma}$  is the rate of shear,  $h$  is the length of measuring gap,  $T_o$  is the torque of the measuring system, and subscripts  $b$ ,  $c$ , and  $crit$  refer to bob, cup and critical radii respectively

Wall slip effects due to separation in multiphase materials may cause serious errors in concentric cylinder systems. These errors may be corrected in the general expressions for angular velocity (equations 2.43 and 2.46) by adding a slip velocity term ( $V_s$ ). This slip term is a function of the wall shear stress at the bob and the cup:

$$\int_{\omega=0}^{\omega=\Omega} d\omega = \Omega = \frac{1}{2} \int_{R_b}^{R_c} f(\tau) \frac{d\tau}{\tau} + \frac{(V_s)_{\text{bob}}}{R_b} + \frac{(V_s)_{\text{cup}}}{R_c} \quad (2.47)$$

and

$$\int_{\omega=0}^{\omega=\Omega} d\omega = \Omega = \frac{1}{2} \int_{R_b}^{R_{\text{int}}} f(\tau) \frac{d\tau}{\tau} + \frac{(V_s)_{\text{bob}}}{R_b} + \frac{(V_s)_{\text{cup}}}{R_c} \quad (2.48)$$

In the absence of slip, all the slip terms are zero. Using the method of Mooney (1931) (which is discussed in detail in section 2.8.2), it is possible to correct slip by using numerous bobs, because measurements are required at different values of  $\frac{R_c}{R_b}$ .

However, some authors (Kiljanski, 1989, Yoshimura and Prud'homme, 1988) have developed methods for estimating the magnitude of the slip velocity,  $V_s$ , and the correction required for the shear rate as a function of gap spacing and applied shear stress. Wall slip effects can also be determined by the method of Cheng and Parker (1976), which makes use of a smooth bob and a rough bob for the same rheological tests. Slip effect can be reduced by the use of roughened cylindrical surfaces either by coating the surfaces with a layer of solid particles or by etching the

surfaces with deep grooves normal to the direction of shear (Chhabra & Richardson, 1999: 46, Nguyen and Boger, 1992: 54-60, Steffe, 1996: 181).

### 2.6.2.3 Viscous heating

The temperature rise in a fluid associated with viscous heating, as is the case with tube viscometry, causes erroneous rheological data during testing. These errors depend on the temperature of the measuring system boundaries; the geometry and speed of the measuring system; the fluid properties; as well as on the duration of the test. The rate of energy dissipated by

viscous flow  $\left(-\frac{dE}{dt}\right)$  is the product of the shear stress ( $\tau$ ) and the rate of shear ( $\dot{\gamma}$ ), i.e.

$-\frac{dE}{dt} = \tau \cdot \dot{\gamma}$ . When the system is in steady state, the rate of energy dissipation by viscous flow is

equal to the rate of heat conduction to the surroundings, and assuming that the system boundaries are maintained at a constant temperature, the resulting energy balance is given by:

$$-\frac{dE}{dt} = \tau \cdot \dot{\gamma} = -j\kappa \frac{d^2T}{dz^2} \quad (2.49)$$

Where  $j$  is the mechanical equivalent of heat,  $\kappa$  is the thermal conductivity of the fluid, and  $z$  is the distance from the bob surface.

Rheological properties are strongly influenced by temperature. Therefore modern rotational rheometers (and rotational viscometers) are equipped with effective temperature control units that

minimize or eliminate viscous heating problems by removing excess heat generated during testing (Steffe, 1996: 177-180, Van Wazer *et. al.*, 1966: 82-85).

#### 2.6.2.4 Cavitation

In a high shear environments, radial pressure drops become sufficient to effect partial evaporation a sample. This results in the formation and collapse of vapour cavities, and the phenomenon is known as Cavitation. Cavitation will occur when:

$$V_b > \sqrt{2(P_{atm} - P_{vap})} \quad (2.50)$$

For  $V_b$  is the linear velocity of the bob,  $P_{atm}$  is the atmospheric pressure,  $P_{vap}$  is the vapour pressure, note that  $V_b$  is related to the pressure drop across the gap,  $\Delta P$  by:

$$V_b = \left( \frac{\Delta P}{\rho} \right)^{0.5} \quad (2.51)$$

If present, cavitation may cause erroneous torque response in concentric cylinder rheological measurements (Steffe, 1996:182).

#### 2.6.2.5 Inertia and secondary flow

Equations developed for the analysis of rheological data assume that the streamlines are circular i.e. the flow is laminar. As mentioned earlier in the Searle's measuring system, the fluid near the inner surface tries to move outward due to centrifugal forces. This movement may create non-

streamline flow due to the presence of Taylor vortices. The dissipation of energy by these vortices leads to overestimation of the torque,  $T_q$ . The critical Reynolds number,  $Re$ , above which secondary motions (i.e. Taylor vortices) may occur for Newtonian fluids is given by:

$$Re_{crit} = \frac{\Omega R_c (R_c - R_b) \rho}{\eta} > 41.3 \sqrt{\frac{R_c}{R_c - R_b}} = 41.3 \sqrt{\frac{\delta}{\delta - 1}} \quad (2.52)$$

This stability criterion for Newtonian fluids (equation 2.52) may be written in terms of the Taylor number, which is denoted by  $T_a$ :

$$Ta_c = \frac{\rho^2 \Omega^2 R_b (R_c - R_b)^3}{\eta^2} < 3400 \quad 2.53 (a)$$

$\rho$  is the density of the material, but for non-Newtonian flow, the Taylor number is high (Chhabra & Richardson, 1999: 44, Steffe, 1996:174-182, Van Wazer *et al.*, 1966: 85). Numerous authors (Mizushima *et al.*, 1971, Capriz *et al.*, 1966, Walowit *et al.*, 1964, etc.) have shown the critical Taylor number  $Ta_c$  to a function of the radius ratio,  $\delta$  and the following expression relate  $Ta_c$  to the inverse radius ratio,  $\beta$  for  $\beta = \delta^{-1}$  for a particular concentric cylinder measuring system (Heywood, 2003, Heywood & Alderman, 2004):

$$Ta_{crit} = 2350 + \frac{1050}{\beta^{1.8}} \quad 2.53 (b)$$

And for negligible secondary effects, the criterion must be satisfied for Newtonian fluids:

$$\tau > \rho(\Delta R)^2 \frac{4\beta \Omega_c^2}{(1-\beta^2)^{0.5} Ta_c^{0.5}} \quad 2.53 (c)$$

A double logarithmic plot of the shear stress (in Pascals),  $\tau$  calculated from the inequality 2.53 (c) against the angular velocity of the bob  $\Omega$  (in radians/second) gives the laminar line limit with a slope of unity, and experimental data to the left of this (which has a slope of 2) correspond to laminar flow (Heywood, 2003, Heywood & Alderman 2004).

## 2.7 PREDICTION OF FLOW RATE AND PRESSURE DROP FROM RHEOMETRY

The frictional pressure drop - flow rate relationship is widely applied in the mechanical energy balance used to calculate the total head loss in a pipe network. This in turn allows for the estimation of the required power to be delivered by a pump (Govier and Aziz, 1972). Rabinowitch (1929) and Mooney (1931) developed an equation that relates the true shear rate at the wall (as measured by a rheometer) to the pseudo-shear rate (as measured in pipeline tests). Flow rate-pressure drop ( $Q - \Delta P$  or  $Q_v - \Delta P$ ) calculations for laminar flow in pipes may be made in various ways depending on the type of flow information available, and from rheometer measurements, the data is in the form of shear stress- shear rate values (in tabular and graphical). The flow rate, ( $Q$  or  $Q_v$ ) and pressure drop,  $\Delta P$  relation can be calculated directly by numerically evaluating the integral using equation 2.54, and calculating the corresponding pressure drop from equation 2.55. Equation 2.54 relates the shear stress at the wall,  $\tau_w$  to the volume of the fluid flowing per second through any cross-section,  $Q_c$ , and equation 2.55 relates the shear stress at the

wall to the magnitude of the pressure drop per unit length of pipe. These equations are shown below:

$$\frac{32Q_c}{\pi D^3} = \frac{32(Q_v - Q_s)}{\pi D^3} = \frac{8V_c}{D} = \frac{8(V - V_s)}{D} = \frac{4}{\tau_w^3} \int_0^{\tau_w} \tau^2 \dot{\gamma}(\tau) d\tau \quad (2.54)$$

$$\tau_w = \frac{D\Delta P}{4L} \quad (2.55)$$

$Q_c$  is the corrected volumetric flow rate ( $\text{m}^3/\text{s}$ );  $Q_v$  is the bulk volumetric flow rate ( $\text{m}^3/\text{s}$ );  $Q_s$  is the volumetric flow rate due to slip ( $\text{m}^3/\text{s}$ );  $D$  is the pipe diameter (m);  $V_c$  is the corrected velocity in the pipe (m/s);  $V$  is the bulk velocity in the pipe (m/s);  $V_s$  is the velocity in the pipe due to slip (m/s);  $\tau_w$  is the shear stress at the wall (Pa);  $\frac{-\Delta P}{L}$  is the pressure gradient (Pa/m),  $\dot{\gamma}(\tau)$  is the relationship between shear rate and shear stress depicted by the experimental data.

The expression  $\frac{32Q_c}{\pi D^3} = \frac{8V}{D}$  in equation 2.54 is called the apparent or pseudo shear rate. The plot of the wall shear stress ( $\tau_w$ ) against the pseudo-shear rate ( $\frac{8V}{D}$ ) is called the pseudo-shear rate diagram, and is characteristic of the flow behaviour of a material at a particular set of flow conditions (i.e. temperature, pressure, flow region, etc.)

In the absence of wall slip, all the slip terms (i.e.  $Q_s$  and  $V_s$ ) in equation 2.54 are zero, and hence equation 2.54 reduces to the following equation:

$$\frac{32Q_v}{\pi D^3} = \frac{8V}{D} = \frac{4}{\tau_w^3} \int_0^{\tau_w} \tau^2 \dot{\gamma}(\tau) d\tau \quad (2.56)$$

If the  $\tau-\dot{\gamma}$  can be accurately described by a simple rheological model (such as Power law; Yield-Pseudoplastic or Cross models, etc.) over the required range of practical interest, this flow or rheological model can be substituted for  $\dot{\gamma}(\tau)$ , thus allowing the integral in equation 2.56 to be evaluated analytically. The following flow rate,  $Q$  and pressure drop relations are obtained, if  $\dot{\gamma}(\tau)$  in equation 2.54 is substituted by the following rheological models, followed by subsequent integration:

a) The Herschel-Bulkley Flow Model, i.e. equation 2.4:

$$\frac{32Q_c}{\pi D^3} = \frac{32(Q_v - Q_s)}{\pi D^3} = \frac{8V_c}{D} = \frac{8(V - V_s)}{D} = \frac{4n}{K^n \tau_w^3} (\tau_w - \tau_y)^{1+n} \left[ \frac{(\tau_w - \tau_y)^2}{1+3n} + \frac{2\tau_y(\tau_w - \tau_y)}{1+2n} + \frac{\tau_y^2}{1+n} \right] \quad (2.57)$$

b) The Power Law Model, equation 2.5:

$$\frac{32Q_c}{\pi D^3} = \frac{32(Q_v - Q_s)}{\pi D^3} = \frac{8V_c}{D} = \frac{8(V - V_s)}{D} = \frac{4n}{(3n+1)K^n} \tau_w^{\frac{1}{n}} \quad (2.58)$$

c) The Simplified Cross Viscosity Model, i.e. equation 2.11

$$\frac{32Q_c}{\pi D^3} = \frac{32(Q_v - Q_s)}{\pi D^3} = \frac{8V_c}{D} = \frac{8(V - V_s)}{D} = \frac{4\tau_w^3}{\tau_w^3} \int_0^{\dot{\gamma}_w} \frac{\dot{\gamma}^3 \left[ 1 + \left( 1 - \frac{n}{\lambda} \right) (\lambda \dot{\gamma})^n \right]}{\left[ 1 + (\lambda \dot{\gamma})^n \right]^4} d\dot{\gamma} \quad (2.59)$$

Derivation of equation 2.59 is described in section 2.8.1.

## 2.8 FLOW IN PIPES OF CIRCULAR CROSS-SECTION

In various industries (namely mining, chemical; process; plastics; etc.) it is often necessary to pump fluids and complex mixtures over long distances from storage to various processing units and/or from one plant site to another. There may be substantial pressure drop in the pipe network, it is thus often necessary to consider problems of calculating the power requirements for pumping through a given pipe network. In order to understand the mechanism of the transport process, the flow pattern, and particularly the velocity distribution near the surface must be studied (Govier and Aziz, 1972, 3: 48).

When a fluid is flowing through a tube or over a surface, the flow pattern will vary with the velocity, the physical properties of the fluid and the geometry of the surface (Coulson and Richardson, 1990, 3: 48). This section is only confined to the steady-state laminar flow of time independent non-Newtonian materials, for which the viscosity model describing the flow curve is known. In steady-state flow, the time average velocity in the mainstream direction is constant (Coulson and Richardson, 1990, 3: 49).

Like Newtonian fluids, non-Newtonian materials may flow in laminar, transitional, or turbulence. Laminar flow is characterised by the absence of bulk movement at right angles to the main stream direction, though small amount of radial dispersion may occur as a result of diffusion, whereas turbulent flow is characterised by the rapid movement as eddies in random directions across the tube. As in the case of Newtonian flow, a finite distance of travel from the entrance of a pipe is required for development of stabilised flow (Govier and Aziz, 1972, 5: 182). For the purpose of this study, the Simplified Cross or Modified Bird-Carreau Structural Viscosity model

has been scrutinised more carefully, for the prediction of laminar flow of highly concentrated w/o emulsion explosives, although other models (namely Power Law and Yield-Pseudoplastic Flow Models) were also investigated.

### 2.8.1 Laminar Pipe Flow

In order to develop the equations that relate the rheograms to pipe flow, the following assumptions were made: the fluid is homogeneous (in the case of w/o emulsions, this assumption implies that the water solution droplets of the emulsion are evenly distributed throughout the pipe cross sectional area), there is steady state flow, the no slip assumption holds (i.e. velocity is zero at the pipe wall) and the assertion that the velocity gradient is zero at the pipe centre line holds. The prediction is made possible by applying the Rabinowitch (1929)-Mooney (1931) relation (i.e. equations 2.54 and 2.55 as mentioned in section 2.7). These equations are for steady state, stabilised, laminar pipe flow, and their general derivation is given below. The resulting equations although usually referred to as the Rabinowitch-Mooney relations, according to Savins, Wallick, and Foster (1962) were first developed by Herzog and Weissenberg (1928). Derivation of the Rabinowitch-Mooney relation from first principles is as follows (Govier and Aziz, 1972):

We start with the complete general constitutive equation for circular tube flow:

$$-\frac{du}{dr} = \dot{\gamma}(\tau) \quad (2.60)$$

A force balance over a cylindrical element of radius,  $r$  and length,  $dL$  yields:

$$\pi r^2 dP = 2\pi r \tau dL \quad (2.61)$$

$$\therefore \frac{dP}{dL} = \frac{2\tau}{r} \quad \text{and} \quad \frac{dP}{dL} = \frac{2\tau_w}{R} \quad (2.62)$$

$$\therefore r = \frac{R\tau}{\tau_w}, \quad r^2 = \frac{R^2\tau^2}{\tau_w^2}, \quad dr = \frac{R}{\tau_w}d\tau \quad \text{and} \quad \tau_w = \frac{D\Delta P}{4L} \quad (2.63)$$

The flow rate can be obtained by integrating the velocity profile:

$$Q_v = 2\pi \int_0^R ur dr \quad (2.64)$$

Integrating by parts and applying the no slip assumption ( $u_w = 0$ ), yields:

$$\frac{Q_v}{\pi R^3} = \frac{1}{\tau_w^3} \int_0^{\tau_w} \tau^2 \dot{\gamma}(\tau) d\tau \quad (2.65)$$

Applying the continuity equation  $Q_v = \pi R^2 V$  gives:

$$\frac{32Q_v}{\pi D^3} = \frac{8V}{D} = \frac{4}{\tau_w^3} \int_0^{\tau_w} \tau^2 \dot{\gamma}(\tau) d\tau \quad (2.66)$$

Equation 2.66 may be re-arranged and differentiated with respect to  $\tau_w$ , to yield a general relationship for the rate of shear at the wall:

$$\dot{\gamma}_w = \dot{\gamma}(\tau_w) = -\left(\frac{du}{dr}\right)_w = 3\left(\frac{8Q_v}{\pi D^3}\right) + \tau_w \frac{d\left(\frac{8Q_v}{\pi D^3}\right)}{d\tau_w} \quad (2.67)$$

Equation 2.67 in simple form:

$$\dot{\gamma}_w = \frac{8V}{D} \left( \frac{1+3n'}{4n'} \right) \quad (2.68)$$

Where,

$$n' = \frac{d \ln \tau_w}{d \ln \left( \frac{8V}{D} \right)} \quad (2.69)$$

Equation 2.68 relates the true shear rates obtained from rheometry to the pseudo-shear rates measured in pipe viscometry.

### 2.8.1.1 Simplified Cross or Modified Bird-Carreau Model

The rheological expression that needed to be integrated in the Rabinowitch-Weissenberg relation (i.e. equation 2.54) is given by the Simplified Cross model (i.e. equation 2.11) as follows: -

$$\eta(\dot{\gamma}) = \left( \frac{\eta_0}{1 + (\lambda \dot{\gamma})^n} \right) \quad (2.11)$$

Multiplying both sides of equation 2.11 by  $\dot{\gamma}$ , the resulting equation is:

$$\eta(\dot{\gamma})\dot{\gamma} = \tau(\dot{\gamma}) = \frac{\eta_0 \cdot \dot{\gamma}}{1 + (\lambda\dot{\gamma})^n} \quad (2.70)$$

Squaring and differentiating equation 2.70 results in the following two equations: -

$$[\tau(\dot{\gamma})]^2 = \frac{(\eta_0 \cdot \dot{\gamma})^2}{[1 + (\lambda\dot{\gamma})^n]^2} \quad (2.71)$$

$$d\tau(\dot{\gamma}) = \frac{\eta_0 \left[ 1 + \left( 1 - \frac{n}{\lambda} \right) (\lambda\dot{\gamma})^n \right] \cdot d\dot{\gamma}}{[1 + (\lambda\dot{\gamma})^n]^2} \quad (2.72)$$

Substituting equations 2.71 and 2.72 in equation 2.54 result in the expression given by equation 2.59 for the Rabinowtch-Weissenberg relation: -

$$\frac{32Q_c}{\pi D^3} = \frac{32(Q_v - Q_s)}{\pi D^3} = \frac{8V_c}{D} = \frac{8(V - V_s)}{D} = \frac{4\eta_0^3}{\tau_w^3} \int_0^{\dot{\gamma}_w} \frac{\dot{\gamma}^3 \left[ 1 + \left( 1 - \frac{n}{\lambda} \right) (\lambda\dot{\gamma})^n \right]}{[1 + (\lambda\dot{\gamma})^n]^4} \cdot d\dot{\gamma} \quad (2.59)$$

Note that  $\dot{\gamma}_w$  is the maximum shear rate at the pipe wall.

The corresponding values of flow rates and pressure drops can then be calculated from equation 2.59 using numerical methods and equation 2.55.

### 2.8.2 Investigation and Correction of pipe wall slip

In steady state, stabilized, laminar flow and in the absence of slip: the wall shear stress ( $\tau_w$ ) – apparent wall shear rate (or simply pseudo-shear rate,  $\frac{8V}{D}$ ) data for different tubes coincide, implying that the pseudo-shear rate is a unique function of the wall shear stress,  $\tau_w$  (Chhabra & Richardson, 1999: 104), as shown below in Figure 2.10.

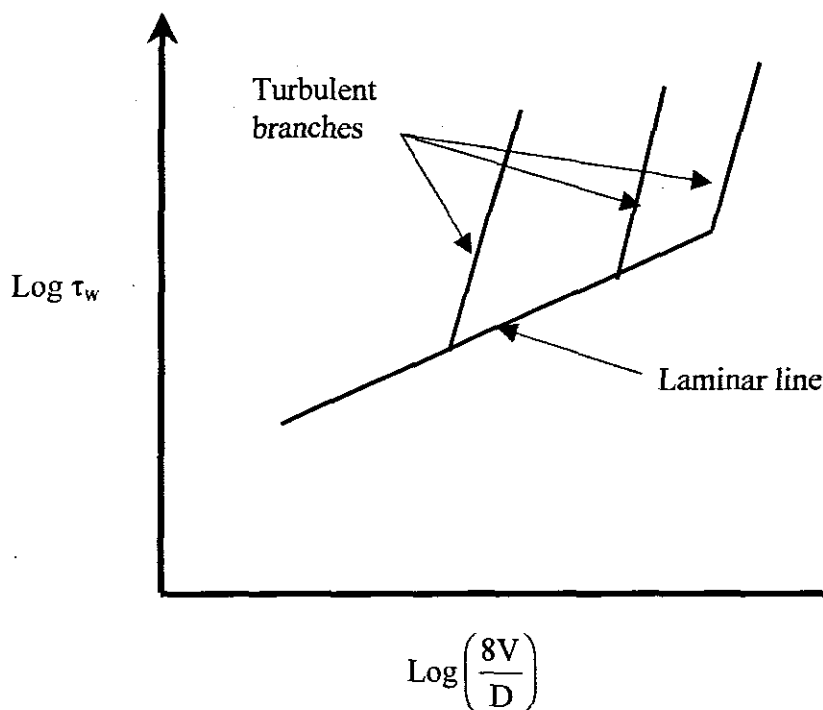


FIGURE 2. 10 Typical flow behaviour of materials  $\left(\tau_w - \frac{8V}{D}\right)$  in different pipe diameters.

However, for many dispersions, especially highly concentrated dispersion systems, i.e. emulsions and suspensions, in which the viscosities of the two phases are significantly different, the bulk material appears to slip on a pipe wall lubricating layer formed by the low viscosity material.

When trying to determine the flow behaviour of a material suspected of exhibiting slip, the procedure is to establish whether wall slip does occur, and how significant it is. This is accomplished by making measurements with tubes (or pipes) of various diameters. In the absence of slip, all data for different tubes coincide (i.e. all lie in the laminar line of that particular material, see Figure 2.10), implying that all the slip terms in equations 2.57, 2.58 and 2.59 are zero.

If slip is evident,  $\frac{8V}{D}$  will be the function of both the pipe diameter  $D$  and the wall shear stress  $\tau_w$ . All the slip terms will be different for different values of  $D$  at the same value of  $\tau_w$  as shown in Figure 2.11. It is clear from equation 2.54 that the effect of slip is greater in pipes of smaller diameters, and in general, the slip velocity (which is denoted by  $V_s$ ) increases with  $\tau_w$  and decreases with  $D$ , although in some cases  $V_s$  is independent of  $D$  (Holland and Bragg, 1995: 125-130).

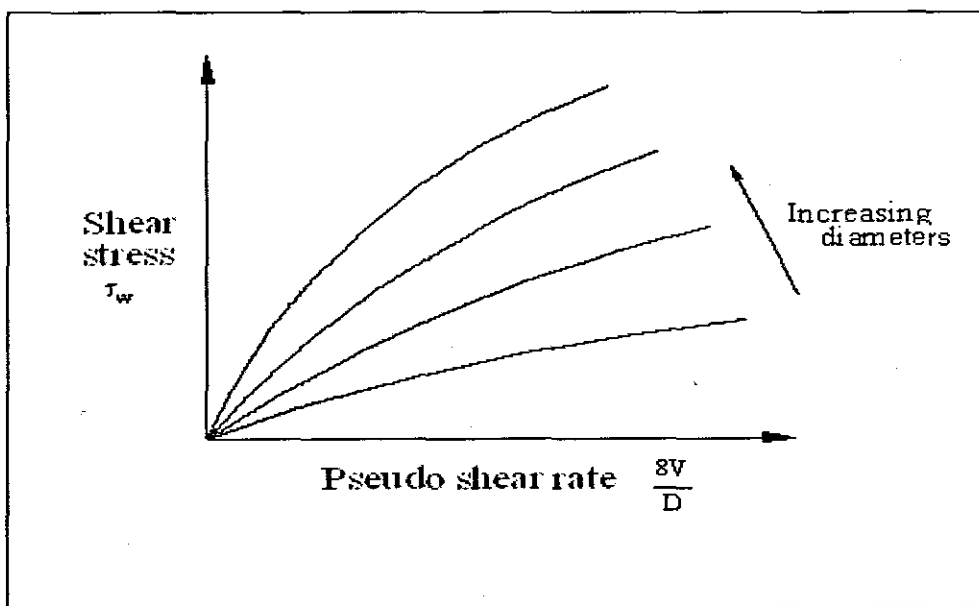


FIGURE 2. 11 Effect of slip in pipe of different diameters (Holland and Bragg, 1995: 127).

Based on the assumption by Schofield and Scott Blair in 1930 that the slip velocity,  $V_s$  was linearly related to  $\tau_w$  but independent of the pipe diameter,  $D$ , Mooney (1931) assumed that the following expression for  $V_s$ :

$$V_s = C_s \tau_w \quad (2.73)$$

Where  $C_s$  is the slip coefficient, thus the slip term in equation 2.54 can be written as follows:

$$\frac{8V_s}{D\tau_w} = \frac{8C}{D} \quad (2.74)$$

This expression was generalised by several workers (Cheng, 1984), writing the slip term as follows:

$$\frac{8V_s}{D\tau_w} = \frac{8C}{D^m} \quad (2.75)$$

The slip velocity,  $V_s$ , can then be determined from the plot of the apparent fluidity,  $\frac{8V}{D\tau_w}$  (reciprocal of the apparent viscosity obtained by dividing equation 2.54 by  $\tau_w$ ) against  $\frac{1}{D^m}$  using a suitable value of  $m$  so that the results are in a linear relationship (Holland and Bragg, 1995: 125 - 130). Figure 2.12 below shows plots of the apparent fluidity,  $\frac{8V}{D\tau_w}$  against  $\frac{1}{D^m}$ :

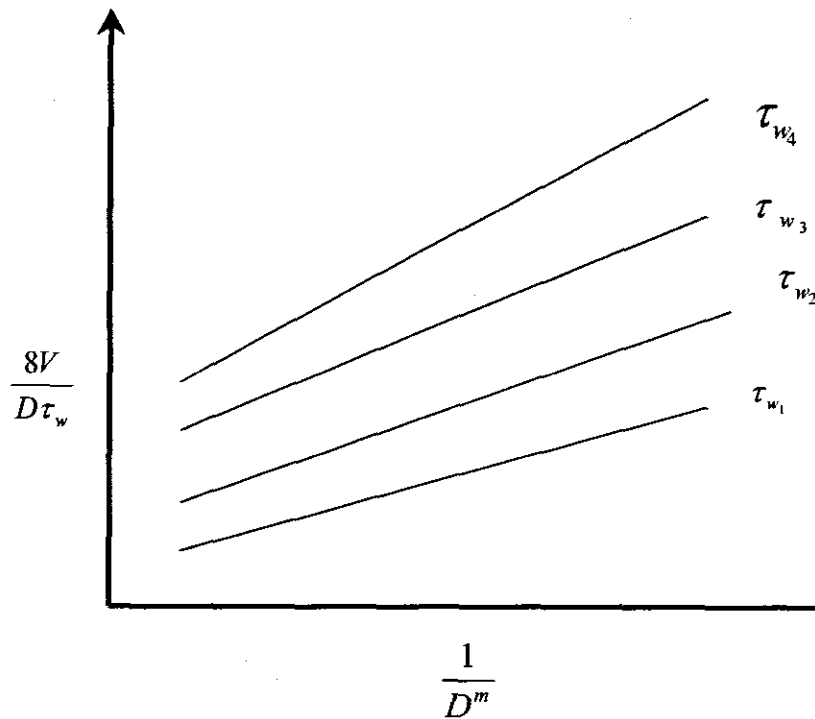


FIGURE 2.12 Apparent fluidity vs.  $\frac{1}{D^m}$  for  $m \geq 1$  (Holland and Bragg, 1995: 129).

Note that  $m$  is found by trial and error values greater of equal to 1. The gradient of the line is equal to  $8C$  for the corresponding value of  $\tau_w$  hence the value of  $V_s$  can be calculated for that value of  $\tau_w$ . The corrected flow rate is then calculated by subtracting slip flow ( $Q_s$  or  $V_s$ ) from the measured flow rate ( $Q_v$  or  $V$  respectively).

## 2.9 CONCLUSION

In this chapter, a comprehensive review of the theoretical rheological fundamentals and literature pertaining to the flow of emulsion, particularly high internal phase ratio emulsion explosives, has been presented.

# CHAPTER 3

## CHAPTER 3

### EXPERIMENTATION

#### 3.1 INTRODUCTION

This chapter provides a comprehensive description of the experimental methodology adopted for this study, the procedures used in the statistical analyses of experimental random errors, and the precautionary measures that were taken in order to eradicate experimental systematic errors. Description of the apparatus and instrumentation used for both pipe viscometry and rotational rheometry is also addressed, including the method used in the determination and analysis of the effect of wall slip.

*The experimental work was done with the following questions in mind:*

- a) Is it possible to use rheometry in the prediction of pumping characteristics for the transportation of explosive emulsions?
- b) Is the choice of a rheological or a flow model crucial in predicting the pumping characteristics of explosive emulsions, and thus crucial for the design of pipelines?

This chapter is subdivided into two sections:

Part I deals with pipe viscometry (i.e. layout of experimental facility, instrumentation and experimental methodology).

Part II deals with rotational rheometry (i.e. layout of experimental facility, instrumentation and experimental methodology).

### 3.2 Objectives of the Experimental Investigations:

The objectives were:

- To measure the pressure drops ( $\Delta P$ ) by means of pressure transducers, which were strategically located along the length of the test pipes, and flow rates ( $Q$ ) using the traditional Bucket-and-Stopwatch Method.
- To calculate the average pressure drop ( $\Delta P$ ) along the length of the pipe for each test pipe.
- To calculate the pressure gradient across the length of the pipe (i.e. pressure drop per unit length of pipe,  $\frac{\Delta P}{L}$ ) as a function of flow rate,  $Q$ , by means of pressure.
- To construct pseudo-shear rate diagrams  $\left( \tau - \frac{8V}{D} \text{ curves} \right)$  for each test pipe for use in the investigation of the wall slip effect. In the case of rheometry data the resulting pseudo shear rate diagrams are used to predict laminar pipeline transport data in the form of  $\Delta P$  vs.  $Q$  curves for this emulsion system.
- To compare the average  $\Delta P$  vs.  $Q$  curves obtained from each test pipe diameter with rheometry predictions.

### 3.3 SAMPLES

The emulsion system used in the study for both pipeline and rheological tests came from the same batch. The study material was a high internal phase ratio w/o emulsion system of a concentrated solution of nitrate salts of ammonia and calcium, which was emulsified in melt form as supersaturated, supercooled droplets into a hydrocarbon oil base. The Fudge Point or crystallisation point of the dispersed aqueous phase was approximately 52 °C, and the density of the emulsion system was approximately 1437 kg/m<sup>3</sup>. The concentration of the dispersed phase was approximately 94% (by mass), and contained less than 20% (by mass) of water. As a result, the dispersed phase was supersaturated. The distribution of the droplet size was very heterogeneous (i.e. this emulsion system was polydispersed), with a droplet size range of 1 µm to 6 µm. Less than 0.5% of pH-buffering additives and acids were added in the formulation to control the pH of the emulsion system.

The emulsion was stabilized by an emulsifying agent, which was added into a hydrocarbon oil phase comprised of straight chain paraffins and cyclic naphthenes with a chain length higher than 16, prior to its inclusion into the emulsion formulation. This resulting hydrocarbon oil base had a density of 900 kg/m<sup>3</sup>. The emulsifier comprised approximately of 10 to 20% (by mass) of the oil continuous phase, and was based on organic derivatives of *PIBSA* (*PIBSA* is an industry acronym for polyisobutylene succinic anhydride, especially alkanolamine derivatives), with a molecular mass in the range of 900 to 1300 grams per mole. The hydrophile-lipophile balance (or simply HLB) was low, i.e. between 2 to 4. The emulsion system was meta-stable at least for a duration of one month, although some changes in the formulation could produce instability. Instability mechanisms of this emulsion system were not due to droplets flocculation, droplets aggregation

or creaming, but arised only from some droplets coalescence, and crystallisation of the dispersed aqueous phase.

### 3.4 EXPERIMENTAL APPARATUS

The test work was conducted at two different experimental test facilities:

- a) Pipeline tests (or Pipe viscometry) were done at African Explosive Limited (AEL) experimental test facility.
- b) Rheometry was conducted at the Rheology Laboratory of the Cape Peninsula University of Technology Flow Process Research Centre, and the emulsion was approximately 14 days old when the tests commenced.

### 3.5 EXPERIMENTAL ERRORS

Engineers and scientists rely on their sound theoretical understanding of the principles governing physical, chemical and biological processes, and constantly utilise experimental data to test theoretical predictions and make critical decisions about process performance and design of process equipments based on careful analysis and interpretation of the experimental data. However, any experimental measurement is subject to some degree of uncertainty or measurement error, excluding the tally of discreet objects. A primary goal is to identify the reliability of the measurements, and a secondary objective is to identify the limitation in the physical property measurements. Thus, steps must be taken to evaluate measurement errors, and there are three steps in error analyses of most experiments. The first is the propagation of errors, which can be performed before the experiment is performed, the second is the determination of

the errors which is done during the experiment, and lastly the comparison with true accepted values is performed after the experiment is completed (Poshusta 2004). Experimental errors are grouped into three categories: gross, systematic and random errors.

*Gross errors* are errors due to blunders, equipment failure and power failures, and these are immediate cause for rejection of measurements.

*Systematic errors* are errors that affect the accuracy of the measuring instrument, and are often identified by independent calibration measurements or a systematic effect on the measurements. The *accuracy* of the measuring instrument is the measure of the deviation of the experimental result from the true accepted value. The most obvious sources of systematic errors in the case of both pipe viscometry and rotational rheometry are due to known conditions, and these conditions might be:

- Natural (temperature variation due to viscous heating, faulty calibration, hole pressure effect, entrance and end effects, wall slip effect, cavitation, and secondary flow effect).
- Instrumental (faulty calibration and incorrect alignment of the experimental setup)
- Personal (poor techniques and mistakes).

In this study, precautionary measures were taken to alleviate systematic errors, and their corrections are discussed in detail under relevant subsections below.

*Random errors* are errors, which arise from unpredictable and often, unspecified variations in experimental situation due to natural limitations of making physical measurements (e.g. mechanical vibration of experimental setup, magnetic and electrical interference). They affect the precision of a measurement. *Precision* is sometimes called “*repeatability*” or “*reproducibility*”, and is a measure of the variation between repeated measurements. In most cases, precision is improved by increasing the sample size (i.e. number of repeated measurements). Thus, averaging repeated measurements would often improve the precision of the measurements, provided

$\left| \frac{x_i}{\bar{x}} \right| < 2$ , for  $\bar{x}$  is the arithmetic mean, and  $x_i$  is the measurement. The precision of the measurement is indicated by the significant reported, and the least significant figure reported is the value associated with the error of the measurement, e.g.  $4.235 \pm 0.009$  kg. The distribution of the values will depend on the physical system, but will generally assume a *normal or Gaussian distribution* (see Appendix C).

### 3.5.1 Statistical analysis of experimental data

Statistics provide the necessary tools for quantifying random errors as well as assessing their effect on the conclusions drawn from the experimental data. The quality of the final research outputs from any statistical experiment depends on the quality of the raw experimental data. The most important summary statistics about the precision and accuracy of experimental measurements are grouped into two categories: those that measure the precision of the

measurements (i.e. the measure of repeatability or reproducibility of repeated measurements), and those that measure the accuracy of the results.

### 3.5.1.1 Precision of the measurements

The most important summary statistics that have been developed to measure the precision of repeated measurements are:

- The measure of central tendency which is usually characterised by the arithmetic mean (denoted by  $\bar{x}$ ), and is defined as follows:

$$\bar{x} = \frac{1}{N} \sum x_i \quad (3.1)$$

$N$  is the number of measurements and  $x_i$  is the experimental measurement. For a large number of measurements ( $N \geq 20$ ), the mean value  $\bar{x}$  is the most probable value.

- Secondly, the measure of dispersion, which is usually characterised by the standard deviation and by its variance (denoted  $s$  or  $s^2$  respectively). The standard deviation (also referred to as the mean square deviation) is the measure of the width of the spread about the mean value. The less precise is the measurement, the broader is the frequency distribution and the larger is the standard deviation and variance. For a finitely large sample ( $N \geq 20$ ), the standard deviation and variance are accurately presented by equations 3.2 and 3.3 respectively.

$$s = \sqrt{\frac{\sum_{i=1}^N (x_i - \bar{x})^2}{N-1}} \quad (3.2)$$

The variance is the standard deviation squared,

$$s^2 = \frac{\sum_{i=1}^N (x_i - \bar{x})^2}{N-1} \quad (3.3)$$

The precision or uncertainty of the mean value is presented by the standard deviation of the mean value (which is also referred to as the standard error,  $s_{\bar{x}}$ ), and is given by the following expression:

$$s_{\bar{x}} = \frac{s}{\sqrt{N}} \quad (3.4)$$

The value of the overall standard deviation ( $s$ ) is calculated from equation 3.2. For non-normal distribution, the results are usually reported as  $\bar{x} \pm \alpha$ , for  $\alpha$  is the confidence limit. This confidence limit  $\alpha$  defines the range on both sides of the mean within which the true average value can be expected to be found with a given level of confidence (i.e. the value within which the magnitude of the mean is certain to lie with a given level of confidence). The confidence level and number of measurements ( $N$ ) are often reported in brackets, e.g.  $25.325 \pm 10.427$  (95 %,  $N = 30$ ). Calculation of  $\alpha$  is given by equation 3.5.

$$\alpha = \pm \frac{ts}{\sqrt{N}} = \pm ts_{\bar{x}} \quad (3.5)$$

The value of  $t$  depends on both the type of frequency distribution and level of confidence assumed for the calculation. For a large sample ( $N \geq 20$ ) following the normal or Gaussian frequency distribution,  $t = 1, 2,$  and  $3$  for the confidence levels of 68.3 %, 95.5 % and 99.7% respectively. For non-normal frequency distributions, the table in Appendix D can be used to determine the values of  $t$  at a specified level of confidence  $\alpha$  and number of measurements  $N$ .

It could be seen from equation 3.5 that the standard error ( $s_{\bar{x}}$ ) is given by:

$$s_{\bar{x}} = \pm \frac{\alpha}{t} \quad (3.6)$$

Finally, the measure of shape which is usually characterised by its skewness,  $SK$  (i.e. the frequency distribution's degree of distortion from symmetry) and by its kurtosis,  $\alpha_4$  (i.e. the degree of concentration of data around the mode, the value with highest frequency, and kurtosis is also referred to as peakedness). The positional differences between the mean, median and mode (definitions given in the glossary) are used to create arithmetic measures of skewness. In the case of zero skewness ( $SK = 0$ ), there is a symmetrical or normal distribution where the mean is equal to both the mode and the median (see Appendix C). For positive skewness ( $SK > 0$ ), the frequency distribution tapers off more slowly toward the right of the mode, (Appendix F). For negative skewness ( $SK < 0$ ), the frequency distribution decreases more slowly towards the left of the mode, (Appendix E). A formula exists to measure kurtosis, however, the extent of kurtosis

can be easily determined by observing the frequency curve. The flatter the curve, the greater is the spread of the data and therefore the larger is the standard distribution (see Appendix F).

The descriptive summary statistics of the average rheological coefficients obtained in all the pipe diameters used is given in Appendix G.

### 3.5.1.1.1 Propagation of errors

When several experiments measure the same physical quantity and give a set of answers  $\bar{x}_i$  with different errors  $\alpha_i$ , then the best estimates of  $\bar{x}_{overall}$  and its accuracy  $\alpha_{overall}$  is found by statistically averaging the combined effect of the “N” number of statistical parameters obtained from analysis of different experimental sets of measurements. This is done as follows:

- The most probable value or the mean ( $\bar{X}_{overall}$ ) of the combined observation of N arithmetic averages ( $\bar{x}_i$  for  $i = 1, 2, 3, \dots, N$ ), and is given by:

$$\bar{X}_{overall} = \frac{\sum_{i=1}^N \frac{\bar{x}_i}{\alpha_i^2}}{\sum_{i=1}^N \frac{1}{\alpha_i^2}} \quad (3.7)$$

where the weighting function is the reciprocal of the square of the corresponding confidence limit,  $\alpha_i$ .

- The standard deviation ( $\alpha_{\text{overall}}$ ) of the mean for the combined observation of N confidence limits,  $\alpha_i$  ( $\alpha_i$  for  $i = 1, 2, 3, \dots, N$ ) is given by:

$$\frac{1}{\alpha_{\text{overall}}^2} = \sum_{i=1}^N \frac{1}{\alpha_i^2} \quad (3.8)$$

Note that  $\alpha_i$  and  $s_{\bar{x},i}$  in equation 3.7 and 3.8 can be interchanged depending on whether the frequency distribution is normal or not. Thus, each experiment is weighted by  $\frac{1}{\alpha_i^2}$ . In some sense,  $\frac{1}{\alpha_i^2}$  gives the measure of the information quality of that experiment. The combined measure of dispersion  $\alpha_{\text{overall}}$  or  $s_{\text{overall}}$  is also improved relative to any individual set, and is closest to the most precise original measurement (Benziger and Askay 2004, Carlson 2004, de Paula 2004).

### 3.5.1.2 Accuracy of measurements

The summary statistics used to evaluate the accuracy as well as the comparative performance of various (rheological) models make use of a larger number of performance indicators, in the form of error equations. To name a few of these error equations, there is log square error, standard error, absolute error, relative error, mean relative squared error, etc. For this study, only the mean relative squared error was used as a measure of accuracy, and for comparing the performance of the three rheological models.

$$E_{\text{rel}} = \frac{1}{N} \sqrt{\sum_{i=1}^N \left[ \frac{\left( \frac{8V}{D} \right)_{\text{exp},i} - \left( \frac{8V}{D} \right)_{\text{calc},i}}{\left( \frac{8V}{D} \right)_{\text{exp},i}} \right]^2} \quad (3.9)$$

$\left( \frac{8V}{D} \right)_{\text{exp},i}$  is the experimental value of the pseudo-shear rate obtained from pipeline tests, and

$\left( \frac{8V}{D} \right)_{\text{calc},i}$  is the pseudo-shear rate value predicted by the rheological model.

The degree of accuracy is indicated by the value of the error obtained, the smaller the value the more accurate is the model.

### 3.5.1.2.1 Propagation of errors

It is shown in statistical theory that the corresponding measure of dispersion of a derived quantity

$\left( \frac{8V}{D} \right)$  is given by:

$$s_{\frac{8V}{D}} = \sqrt{\sum \left[ \frac{\partial \left( \frac{8V}{D} \right)}{\partial m} \right]^2 s_m^2} \quad (3.10)$$

$m$  is any coefficient of a rheological model used to calculate  $\left( \frac{8V}{D} \right)$ , note that the measure of dispersion is the standard deviation ( $s$ ). Other measures, such as probable error, which are proportional to the standard deviation ( $s$ ), may be used. The standard deviation ( $s$ ) may be expressed fractionally, and thus, equation 3.10 leads to:

$$\frac{S_{8V}}{\left(\frac{8V}{D}\right)_{ave}} = \sqrt{\sum \left[ \frac{\partial \left(\frac{8V}{D}\right)}{\partial m} \right]^2 \left[ \frac{m}{\left(\frac{8V}{D}\right)_{ave}} \right]^2 \left[ \frac{S_m}{m} \right]^2} \quad (3.11)$$

Before the experiment was done, it was very important to predict the expected highest error (or maximum possible error), as this quantity is very useful in the design of experiments. It is the measure of the expected accuracy of the device used, or of a calculated quantity, given the accuracy of the measuring device needed for the calculation. The highest expected error quantifies the credibility of the devices and the measurement methods used in an experiment, and thus is another measure of the experiment's believability, (Brinkworth 1968, Baudouin 2003). It is analogous to equation 3.11, and is given by:

$$\left( \frac{\Delta \frac{8V}{D}}{\frac{8V}{D}} \right) = \sqrt{\sum \left[ \frac{\partial \left(\frac{8V}{D}\right)}{\partial m} \right]^2 \left[ \frac{m}{\frac{8V}{D}} \right]^2 \left[ \frac{\Delta m}{m} \right]^2} \quad (3.12)$$

Where  $\Delta \frac{8V}{D}$  is the computed absolute error of the pseudo-shear rate,  $\frac{8V}{D}$  is the averaged computed pseudo-shear rate,  $m$  is any averaged rheological coefficient of the models used, and  $\Delta m$  is the corresponding absolute error associated with that coefficient. The computed absolute error of the pseudo-shear rate  $\left( \Delta \frac{8V}{D} \right)$  is given by:

$$E_{\text{absolute}} = \Delta \frac{8V}{D} = \frac{1}{N} \sqrt{\left[ \sum_{i=1}^N \left( \frac{8V}{D} \right)_{\text{exp},i} - \left( \frac{8V}{D} \right)_{\text{calc},i} \right]^2} \quad (3.13)$$

Note that the expressions  $\frac{\Delta \frac{8V}{D}}{\frac{8V}{D}}$  and  $\frac{\Delta m}{m}$  in equation 3.12 are the mean squared relative errors

defined as:

$$E_{\text{rel}} = \frac{E_{\text{absolute}}}{\text{Averaged value}} \quad (3.14)$$

**PART 1**  
**PIPE VISCOMETRY:**  
**INSTRUMENTATION, EXPERIMENTAL**  
**METHOD, INTERPRETATION AND**  
**DISCUSSION OF RESULTS**

### 3.6 PIPE VISCOMETRY

The experimental test facility consisted of a pumping system to transport the emulsion through the pipe, and the fluid viscosity was then determined from the measured volumetric flow rate, applied pressure and the pipe dimensions (i.e. pipe diameter,  $D$ , and pipe length,  $L$ ). The complete pipe viscometer assembly consisted of the following: two fluid reservoirs, a mixing tank and a tanker as a discharge reservoir, five high density polyethylene (HDPE) pipes of internal diameters of 35.9 mm, 48.1 mm, 55.9 mm, 65.9 mm and 77.6 mm pipes of 45m in length, and a unit for controlling and measuring the applied pressure (i.e. four-stage Orbit progressive cavity pump which was fitted with a variable speed drive and differential pressure cells or pressure transducers, respectively).

#### 3.6.1 Layout of experimental test facility and Basic principles of operation

Figure 3.1 depicts the downstream assembly of the pipeline experimental facility, while Figure 3.2 is a schematic layout of the AEL pipeline test apparatus.



FIGURE 3. 1 Receiving tanker acting as a discharge reservoir.

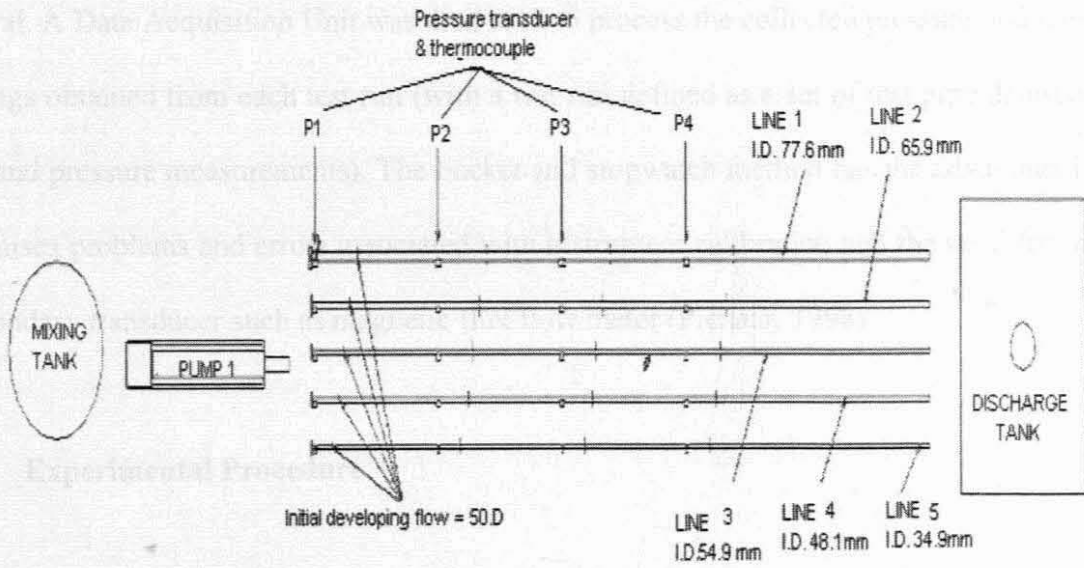


FIGURE 3. 2 Schematic layout of AEL experimental test facility.

As shown in Figure 3.2, the mixing tank was connected to a four-stage variable Orbit progressive cavity pump by means of a supply pipeline, and a 45m-test pipe of known diameter ( $D$ ) was used to connect the pump to the discharge tanker. In the complete pipe viscometer assembly, both reservoirs were 50m apart. The Orbit pump was used to transport the emulsion at a controlled rate from the mixing tank, through the 45m-test pipe of known diameter, to the discharge tanker. Each test pipe was fitted with a thermocouple and a pressure transducer at the pump outlet, as well as at distances of 10 m, 20 m, and 30 m along the length of the pipe.

The thermocouples were used to collect temperature readings, while pressure transducers were used to collect static pressure measurements. The bucket and stopwatch method was used to determine the mass flow rates, and in this procedure the flow rate is determined from first principle by literally weighing the fluid transported through a given pipe over a given time interval. A Data Acquisition Unit was then used to process the collected pressure and temperature readings obtained from each test run (with a test run defined as a set of test pipe diameter, force, time and pressure measurements). The bucket and stopwatch method has the advantage in that; it minimises problems and errors associated with instrument calibration and the need for the use of a secondary transducer such as magnetic flux flow meter (Pienaar, 1998).

### **3.6.2 Experimental Procedure**

All the study material, including pipeline experimental apparatus were sponsored by African Explosive Limited, a mining company based in South Africa. The experimental tests were done as follows:

- An entrance length of the order of fifty pipe diameters (50D) was adopted for the study to alleviate entrance effects.
- Consistency in pressure measurements was ensured by taking three static pressure measurements at intervals of 10m (P2, P3, P4). The resulting pressure drops between any two pressure points which were equidistant apart, should be the same for the same pump speed and same test pipe diameter (i.e.  $\Delta P$  between P2 and P3 =  $\Delta P$  between P3 and P4). The pressure drop between P2 and P4 pressure tapings is the sum of the pressure drops between P2 and P3, and between P3 and P4 (i.e.  $\Delta P$  between P2 and P4 =  $\Delta P$  between P2 and P3 +  $\Delta P$  between P3 and P4). The above argument also applies to the wall shear stresses, since  $\tau_w = \frac{D\Delta P}{4L}$ . Thus, the first evaluation was the pressure drop along the length of the pipe to ensure that a linear pressure profile was obtained, when calculated using different tapping distances, because the shear stress in the pipe is the same, provided that all flow conditions such as the flow rate and viscosity are constant. The pressure drop used for further analysis was from a tapping distance of 20m (P2 – P4, see fig 3.2).
- For each pipe diameter, the flow rate was varied by selecting a test pump speed (in revolutions per minute), and the resulting pressure drops and temperature were measured.
- This procedure was repeated for all the test pipes.

- The rheology of most materials is strongly influenced by changes in temperature, and thus all the test pipes were covered with shade nets as the tests were done outdoors, in an attempt to simulate the same temperature conditions for all the tests.
- It was also vital to monitor the temperature of the emulsion during testing, to detect any presence of viscous heating, and if present, determine its significance, and this was achieved by making use of thermocouples, which were distributed along the pipe length.
- The structure of high internal phase ratio emulsions (i.e. droplet size distribution) is extremely sensitive to shear (e.g. handling and pumping), thus sampling was done with great care at both the pump outlet and the pipe end, as shown in Figure 3.3. The sampling procedure was as follows:
  - a) After the test run was completed, the pump was switched off, and the pressurised emulsion was allowed to flow through the sampling valve, and this pressurised emulsion was then discarded.
  - b) This was followed by slowly rotating the pump manually, to allow the emulsion to slowly flow through the sampling valve.
- Samples were first taken for viscosity measurements on site using the Brookfield viscometer, before being sent for rheological studies at the Rheology Centre of the Cape Peninsula University of Technology Flow Process Research Centre.

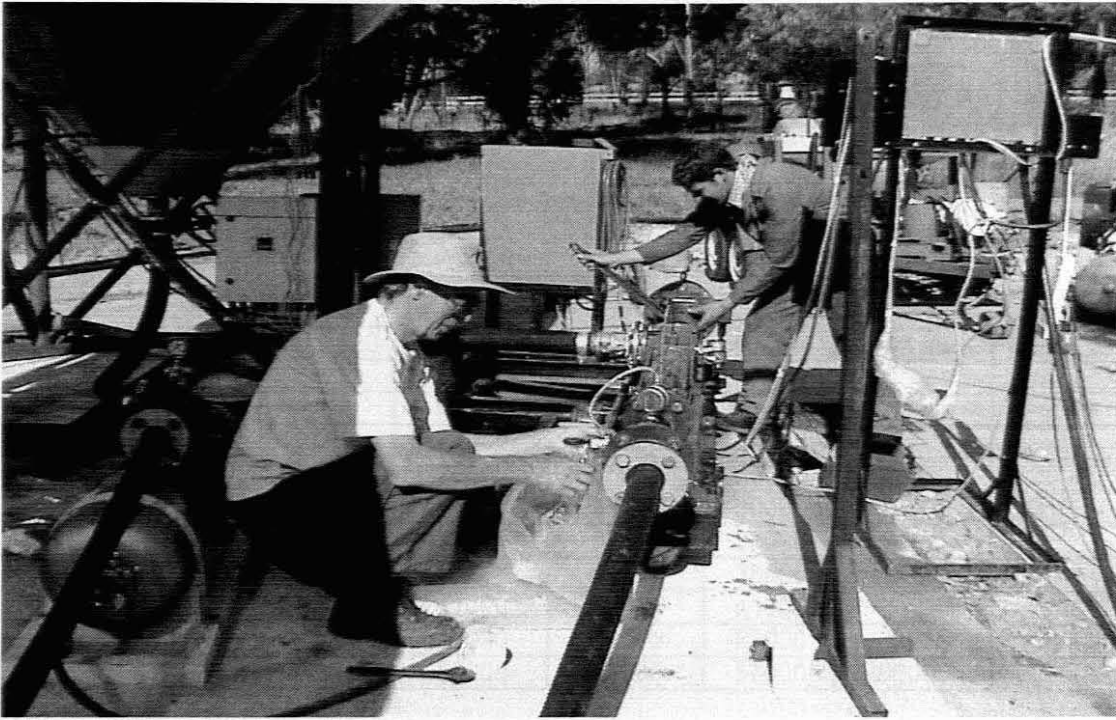


FIGURE 3.3 Sampling Procedure.

- The viscosities of the rheometry samples were then tested on site with a Brookfield viscometer, as this is standard quality control practice, before being packaged for rheometry testing. The Brookfield viscometer test rotational speed was set at 50 rpm and spindle size of 7 was selected. A factor of 800 (which is normally used for such test settings), was used to convert the data to centipoises or milli-Pascal.seconds (denoted as cP or mPa.s).

### 3.6.3 Pipeline experimental test results and data correction

The experimental pipeline test data obtained was in the form of pressure drop– flow rate - emulsion temperature-emulsion viscosity. This data was sub-divided into two sets, the first set was in the form of pressure drop or pressure gradient – flow rate relationship, to be used in the

prediction of pumping characteristics. The average pressure drop – flow rate data obtained from all the pipe diameters used are given below by tables 3.1 – 3.5, and graphically by Figure 3.4:

Table 3.1 Data for pipe diameter of 35.9 mm:

D(m)	Q (Kg/min)	P/m 10-20 (Pa)	P/m 20-30 (Pa)	P/m 10-30 (Pa)	Pav/m (Pa)	P/m min	P/m max
0.0359							
	3.6	27000	27000	27000	27000		
	4.8	28000	29000	28500	28500	28000	29000
	6.2	29000	31000	30000	30000	29000	31000
	8.9	33000	33000	33000	33000		
	12.2	35000	35000	35000	35000		
	20.2	41000	41000	41000	41000		
	42.4	52000	54000	53000	53000	52000	54000
	49.2	56000	58000	57000	57000	56000	58000

Table 3.2 Data for pipe diameter of 48.1 mm:

D(m)	Q (Kg/min)	P/m 10-20 (Pa)	P/m 20-30 (Pa)	P/m 10-30 (Pa)	Pav/m (Pa)	P/m min	P/m max
0.0481	11	21000	19000	20000	20000	19000	21000
	22	23000	24000	23500	23500	23000	24000
	32	28000	27000	27500	27500	27000	28000
	41	29000	30000	29500	29500	29000	30000
	50	31000	32000	31500	31500	31000	32000

Table 3.3 Data for pipe diameter of 55.9 mm:

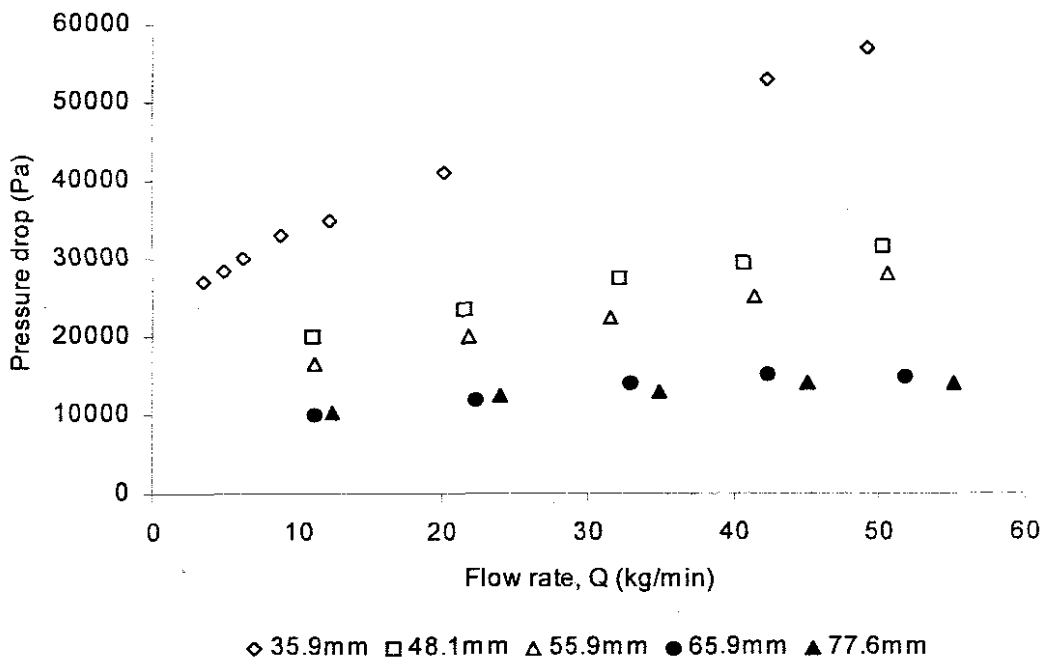
D(m)	Q (Kg/min)	P/m 10-20 (Pa)	P/m 20-30 (Pa)	P/m 10-30 (Pa)	Pav/m (Pa)	P/m min	P/m max
0.055	11	16000	17000	16500	16500	16000	17000
	21	20000	20000	20000	20000		
	31	22000	23000	22500	22500	22000	23000
	41	24000	26000	25000	25000	24000	26000
	51	26000	30000	28000	28000	26000	30000

Table 3.4 Data for pipe diameter of 65.9 mm:

D(m)	Q (Kg/min)	P/m 10-20 (Pa)	P/m 20-30 (Pa)	P/m 10-30 (Pa)	Pav/m (Pa)	P/m min	P/m max
0.065	11.6	6000	14000	10000	10000	6000	14000
	20.9	8000	16000	12000	12000	8000	16000
	32.5	9000	19000	14000	14000	9000	19000
	41.8	9000	21000	15000	15000	9000	21000
	48.8	9000	21000	15000	15000	9000	21000

Table 3.5 Data for pipe diameter of 77.6mm:

D(m)	Q (Kg/min)	P/m 10-20 (Pa)	P/m 20-30 (Pa)	P/m 10-30 (Pa)	Pav/m (Pa)	P/m min	P/m max
0.077	12.3	8000	13000	10000	10300	8000	13000
	23.8	8000	17000	12500	12500	8000	17000
	34.8	8000	18000	13000	13000	8000	18000
	45	9000	19000	14000	14000	9000	19000
	55.5	10000	18000	14000	14000	10000	18000

FIGURE 3. 4 System curve: Average pressure drop ( $\Delta P$ ) vs. Flow rate (Q).

The second set of results was in the form of flow rate - emulsion temperature-emulsion viscosity relationship, to be used as a quality control measure, as well as a measure of the effect and extent of viscous heating. Typical results are shown below in Table 3.6 for pipe diameters of 35.9 mm, 48.1 mm and 54.9 mm. The results shown are only for three diameters as similar results were obtained for the other two diameters (65.9mm and 77.6mm). The change in both viscosity and temperature of the emulsion is reported per unit length of pipe (Pa.s/m or °C/m.respectively) to enable these temperature effects to be quantified or estimated for any length of pipe subjected to similar pumping and ambient conditions.

Table 3.6 Results of quality control tests: Temperature and viscosity measurements.

	Q	$\eta_i$	$T_i$	$\eta_f$	$T_f$	$\Delta\eta$	$\Delta T$
	kg/m	mPa.s	°C	mPa.s	°C	mPa.s/m	°C/m
D = 35.9mm	3.551	30.8	34.4	31.6	30.7	0.018	-0.082
	4.827	30.0	34.6	32.0	32.5	0.044	-0.047
	6.222	29.6	37.1	31.2	34.5	0.036	-0.058
	8.908	28.0	35.5	31.2	34.9	0.049	-0.013
	12.186	28.0	36.2	30.0	37.0	0.044	0.018
	20.171	28.6	37.3	29.3	38.0	0.016	0.016
	42.384	30.8	37.7	31.2	37.2	0.009	-0.011
	49.155	31.0	36.2	30.4	38.2	-0.014	0.031
Average	29.7	36.2	30.9	35.4	0.025	-0.018	
D = 48.1mm	10.957	29.6	37.3	30.0	37.4	0.009	0.002
	21.448	30.0	38.0	29.2	36.9	-0.018	-0.024
	32.178	29.6	39.1	29.6	38.6	0.000	-0.011
	40.724	29.6	37.5	29.6	38.3	0.000	0.018
	50.244	32.0	37.5	32.0	38.2	0.001	0.016
	Average	30.2	37.9	30.1	37.9	-0.002	0.000
D = 55.9mm	11.111	33.5	32.5	33.4	31.1	-0.002	-0.031
	21.735	33.3	32.6	34.2	31.5	0.020	-0.024
	31.516	32.6	32.6	33.2	32.1	0.012	-0.011
	41.463	32.0	32.6	33.4	31.3	0.030	-0.029
	50.518	32.2	32.6	32.6	31.8	0.010	-0.018
	Average	32.7	32.6	33.4	31.6	0.014	-0.023

The following equations have been used for calculating the averages and percentage changes in quantity listed in Table 3.6:

$$\bar{T} = \frac{\sum_{k=1}^n T_k}{n} \quad \text{and} \quad \bar{\eta} = \frac{\sum_{k=1}^n \eta_k}{n} \quad (3.15)$$

$$\Delta T = \frac{(T_f - T_i)}{L} \quad \text{and} \quad \Delta \eta = \frac{(\eta_f - \eta_i)}{L} \quad (3.16)$$

$n$  is the number of observations per pipe diameter,  $T$  and  $\eta$  are the temperature and viscosity measurements per test run,  $L$  is the length of the test pipe which is 45 meters,  $\bar{T}$  and  $\bar{\eta}$  are the arithmetic averages for the temperature and viscosity measurements for each test diameter pipe.  $\Delta T$  is the change in temperature per unit length of pipe,  $\Delta \eta$  is the change in viscosity (as measured with the Brookfield viscometer) per unit length of pipe and subscripts  $f$  and  $i$  refer to the final and initial conditions while  $k$  is the summation subscript for a test run.

Table 3.6 shows the changes in both temperature and viscosity as a function of pumping rate, it is seen that the temperature of the material showed some small variations with an increase in the rate of pumping, showing an overall rise as the pumping rate was increased for the small diameter pipe (as expected in the case of viscous materials). However, irrespective of these temperature variations the viscosity of the material remained fairly stable, with only a slight change in viscosity in the range from 0.018 to 0.066 centipoises per unit length of test pipe. The percentage

change in shear viscosity was in the range of 0.06 % to 0.17 %, i.e.  $\% \Delta \eta = \left( \frac{\eta_f - \eta_i}{\eta_i} \right) \times \frac{100}{1}$ .

Serious errors in rheological data obtained from pipe viscometers arise from various factors, and these errors had to be corrected from the measured experimental data as discussed in Chapter 2. Thus, to justify for the absence of such corrections in the experimental data of this study, the following discussion has been included:

### 3.6.3.1 Entrance effects and their correction

In order to alleviate entrance effects as discussed in chapter 2, the following requirement should be met: An entrance length of the order of forty pipe diameters (i.e. 40D) for inelastic fluids was recommended for practical purposes. Trumpet-shaped or rounded pipe entrances must be employed. Pressure transducers or differential pressure cells should be strategically located, so that the effect of the entrance region did not influence experimental data.

Cylindrical pipes and an entrance length of the order of fifty pipe diameters (i.e.50D) were used for pipeline tests, and the lowest tapping distance (i.e. P2 in Figure 3.2) that was included in the calculations of pressure drops and shear stresses was located 10 meters from the entrance. The calculated entrance lengths,  $L_E$  for the different test pipes are given in Table 3.7 below, and the values of the resulting  $L_E$  are far lower than 10m, which is the distance of the initial lowest pressure tapping distance included in the calculations. Thus, the entrance region did not influence the experimental data.

Table 3.7 Entrance lengths  $L_E$  of the different test pipes.

Pipe diameter (m)	Fully developed flow, $L_E = 50D$ (m)
0.0359	1.795
0.0481	2.405
0.0559	2.795
0.0659	3.295
0.0776	3.880

### 3.6.3.2 Pipe end kinetic energy effects and correction

A detailed discussion on end effects has been presented previously, and it was mentioned that these end effects are eliminated, when long capillaries (or pipes) with  $\frac{L}{D} \geq 400$  are used. For the pipeline experiments, the length-to-diameter ratios  $\frac{L}{D}$  in the range of 664 to 1393 were used, which were sufficiently high enough for these effects to be negligible.

### 3.6.3.3 Hole pressure effect and correction

The hole pressure effect was alleviated by making use of identical pressure transducers at each sensing location. This was done to ensure that the hole pressure effect was cancelled out in the pressure drop ( $\Delta P$ ) calculations.

### 3.6.3.4 Viscous heating effect and correction

The effect of viscous heating and its correction has been presented in detail in chapter 2. It was mentioned that isothermal conditions are usually assumed in the derivation of the basic flow equations. However, temperature changes associated with frictional heat dissipation due to viscous heating and other uncontrolled ambient effects may cause serious experimental errors in the measurements obtained. It was thus essential to monitor temperature changes during experimental runs, and the average temperature and viscosity variations, i.e.  $\Delta T$  and  $\Delta \eta$  (calculated using equation 3.15 using data in Table 3.6) for the pipe diameters 35.9mm, 48.1mm and 55.9mm are shown below in Table 3.8. Table 3.8 is reproduced from Table 3.6.

Table 3.8 List of average temperature and viscosity variation per pipe test run.

Quantity	D = 35.9mm		D = 48.1		D = 55.9mm	
	Pipe inlet	Pipe outlet	Pipe inlet	Pipe outlet	Pipe inlet	Pipe outlet
$\Delta T$ ( $^{\circ}\text{C}$ )	36.2	35.4	37.9	37.9	32.6	31.6
$\Delta \eta$ (mPa.s)	29.7	30.9	30.2	30.1	32.7	33.4

In general, a change in the temperature of a material is usually accompanied by a change in viscosity, and the extent of such a change is indicative of the susceptibility of the material structure to temperature effects. It was seen that the temperature of the material at the pump exit was higher than that observed at the pipe exit (as evidenced from Tables 3.6 and 3.8), and thus, the observation signified an overall temperature drop as the material flowed through the test pipes. The variation in temperature might be attributed to cooling of the material as it flows from the pump through the pipe due to temperature difference between the pump environment and the

ambient surroundings which influence the temperature of the pipe walls. It could also be noticed in both Tables that the viscosity of the material increases as expected with a decrease temperature.

However, viscous heating is normally accompanied by a rise in the temperature of the material, and thus if viscous heating was evident in the tests, the temperatures of the material at the pipe exit would be higher than those observed at the pump outlet. Thus viscous heating was absent in pipeline tests, and no data correction was considered necessary for this effect.

### 3.6.3.5 Construction of pseudo-shear rate diagram and slip evaluation

The pressure drop or pressure gradient – flow rate experimental data was used to construct pseudo-shear rate diagrams, which is simply a graphical representation of the relationship between the wall shear stress,  $\left(\tau_w = \frac{D\Delta P}{4L}\right)$  and the pseudo-shear rate,  $\left(\frac{8V}{D}\right)$  for all the pipe diameter used, using the expressions given in brackets. The resulting pseudo-shear rate diagrams are given below by Figure 3.5, and these pseudo-shear rate diagrams were then used to evaluate the presence of slip in the pipe.

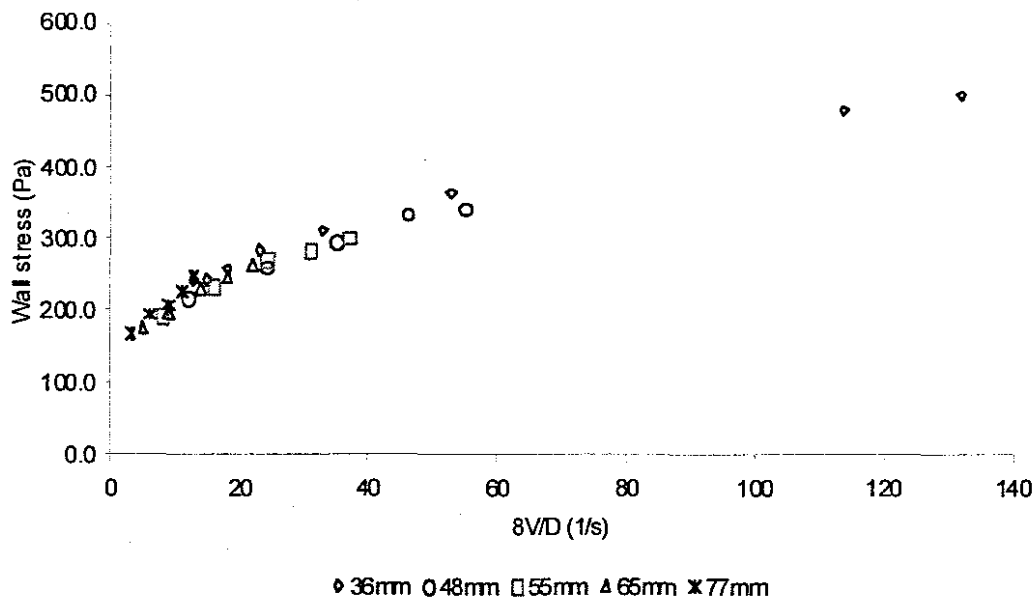


FIGURE 3.5  $\tau_w$  vs.  $\frac{8V}{D}$  of all pipe diameters.

Figure 3.5 shows that all the experimental data points are superimposed, and this serves as evidence for the absence of wall slip effect in the steady state, laminar flow of this emulsion system. An average pseudo-shear rate diagram, which is representative of the flow behaviour depicted by this emulsion system through the various test pipes, was calculated by averaging the pressure drops obtained for all the pipe diameters at the same pseudo-shear rate (i.e.  $\frac{8V}{D}$ ) value, and the resulting averaged pseudo-shear rate diagram is shown below in Figures 3.6 and 3.7. Figures 3.6 and 3.7 shows the fit of the average pseudo-shear rate diagram to experimental data obtained from all pipe diameters in both linear and double logarithmic scales. This averaged pseudo-shear diagram as shown as a straight line in Figure 3.7 is described by a Power Law expression depicted in the Figure. It could be seen that a good correlation was achieved as the

multiple regression coefficient  $r^2$  obtained was close to one (i.e. 0.965), and thus this equation could be used to extrapolate data outside the experimental window.

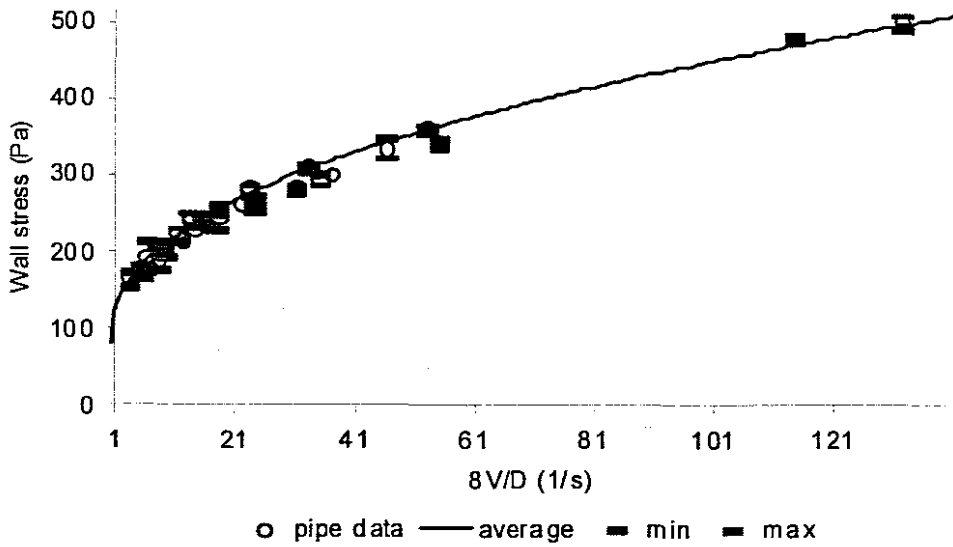


FIGURE 3.6 Averaged  $\tau_w$  vs.  $\frac{8V}{D}$ , diagram from all the pipe diameters, in linear scale.

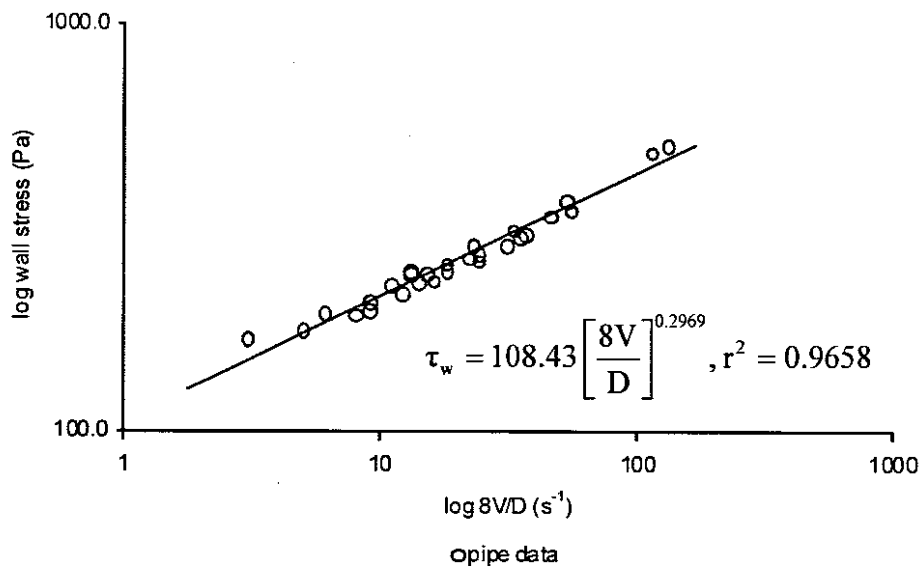


FIGURE 3.7 Averaged  $\tau_w$  vs.  $\frac{8V}{D}$  diagram from all diameters, logarithmic scale.

**PART II**  
**RHEOMETRY:**  
**INSTRUMENTATION, EXPERIMENTAL**  
**METHOD, INTERPRETATION AND**  
**DISCUSSION OF RESULTS**

### 3.7 RHEOMETRY

Rheometry was conducted using a rheometer MCR 300 from Paar Physica (a German Company) and a concentric cylinder measuring geometry CC 27 (described in section 3.7.1). Rheometer MCR 300 is a research grade rotational drag flow instrument designed according to Searle's measuring principle, and is equipped with a permanent magnet synchronous drive that allows both CR and CS rheological tests to be done in the same instrument. As mentioned earlier in Chapter 2 that temperature strongly influences the rheology and structure of most real materials, thus rheometer MCR 300 is equipped with an effective Temperature Control Unit, TEZ 300-C. This Temperature Control Unit was used to stabilise the temperature during testing, and thus, to alleviate viscous heating effects.

The complete rheometer MCR 300 assembly consists of an air compressor, an air regulator, the MCR 300 rheometer system, the temperature control unit, TEZ 300-C (equipped with in-built heating and cooling systems), and a computer data processing unit, US200 software, as shown below in Figure 3.8.

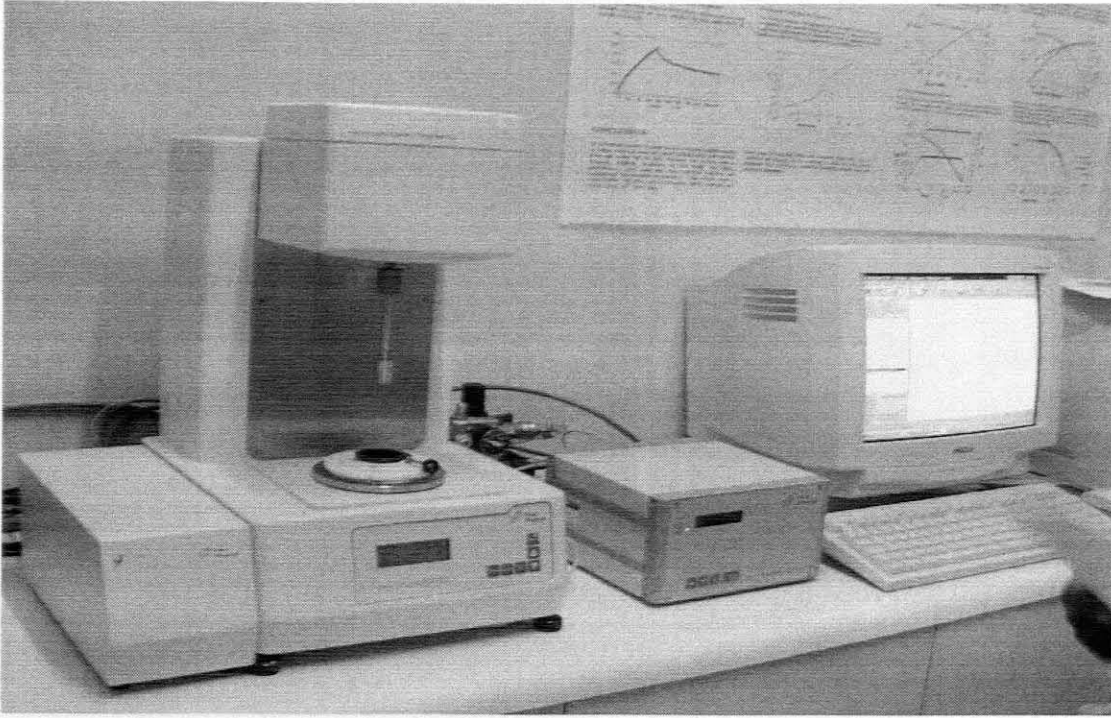


FIGURE 3. 8 Rheometer MCR 300 from PaarPhysica.

### 3.7.1 Concentric Cylinder Measuring system, CC 27

The measuring geometry was a concentric or coaxial cylinder geometry (denoted by CC 27). It consisted of a smooth cylindrical cup and a roughened cylindrical bob. The roughened bob surfaces were due to sandblasting, and this was done to alleviate the effect of wall slip. The bob was based on the Mooney-Couette or Mooney-Ewart design (i.e. has the lower end of the bob shaped as a truncated cone) to minimise end effects (see Fig. 3.9). The measuring bob diameter was 27mm and the gap measurement distance between the cup and the bob was 1mm.

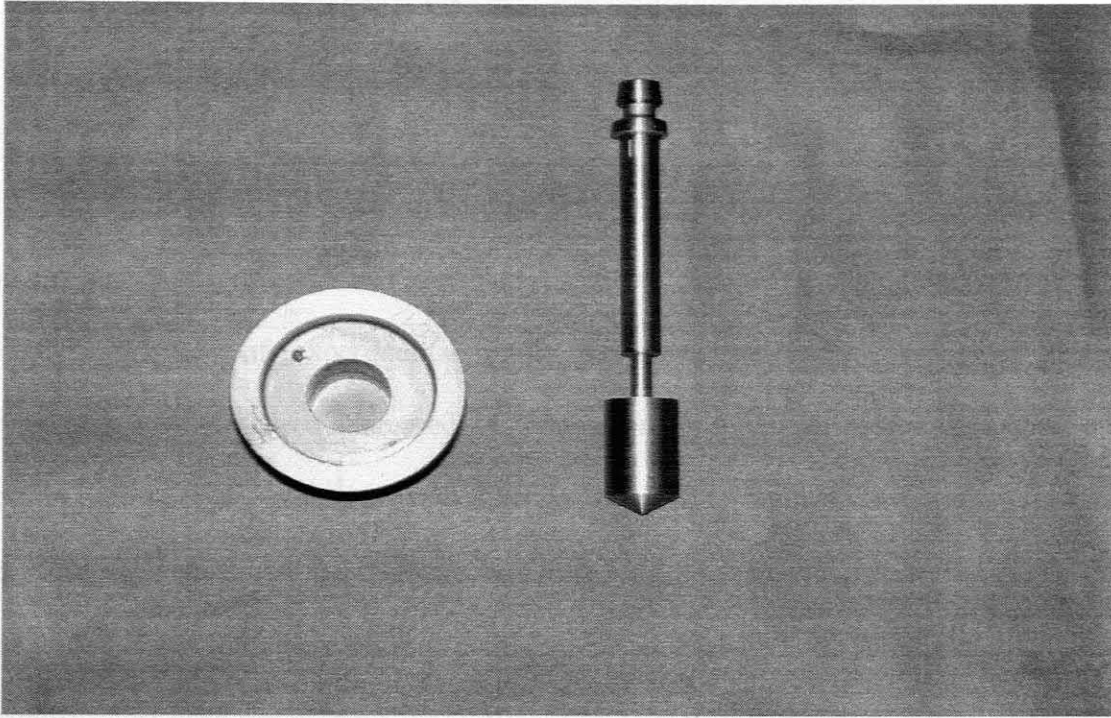


FIGURE 3. 9 Concentric cylinder geometry, CC27.

### 3.7.2 Experimental Procedure

As mentioned earlier, all the rheological studies were made on a rotational dynamic rheometer MCR 300 with CC27 measuring geometry. Samples for rheological measurements were taken from pipeline experiments, and were tested as received. Only a single region of deformation was used to determine the flow properties:

- Steady state flow measuring flow curves (shear stress versus shear rate) in the shear rate control mode was used.
- The shear rate was varied from  $0.0001$  to  $600 \text{ s}^{-1}$ .
- All the rheological measurements were conducted at a temperature of  $30 \text{ }^{\circ}\text{C}$ .

### 3.8 SUMMARY

A comprehensive description of both pipe viscometry and rheometry has been presented. It described in detail the instrumentation used for both types of rheological measurements (i.e. pipe viscometry and concentric cylinder rheometry) and the experimental methodology adopted for the study. Analyses of experimental errors associated with both types of rheological measurements have also been addressed. No corrections to the experimental data obtained were needed as precautionary measures were taken in advance to eradicate experimental systematic errors. Wall slip was found to be absent, and thus a single averaged pseudo-shear rate diagram represented the pipeline flow of this emulsion system through the different diameter pipes accurately.

# **CHAPTER 4**

## CHAPTER 4

### RESULTS AND DISCUSSIONS

#### 4.1 INTRODUCTION

This chapter provides a comprehensive description of the procedures used in the analyses of results, and the inherent discussions pertaining to the experimental findings are also presented. The primary purpose of this chapter is to analyse, compare and discuss the test results obtained from both rheometry and pipeline trial experiments.

Many formulae have been developed to relate the frictional pressure drop in pipe flow to the flow rate. The major application of these relationships is in the mechanical energy balance used to calculate the total head loss in a pipe network, which in turn allows for the estimation of the required power to be delivered by a pump (Govier and Aziz, 1972). Rabinowitch (1929) and Mooney (1931) developed an equation to relate the true shear rate at the wall (as measured by a rheometer) to the pseudo-shear rate (as measured in pipeline tests).

The Pressure drop – flow rate formulae mentioned above make use of rheological parameters obtained through rheological characterisation, hence the first step in the analysis was to embark on the rheological characterisation procedure of rheometer data, which was followed by calculation of pressure drops at different flow rates using averaged rheological constants obtained from characterisation.

Furthermore, highly concentrated w/o emulsion systems are thixotropic in nature, and this implies that these systems undergo structural decomposition when subjected to intense shearing

and tend to build-up a more viscous structure when shearing is stopped, as is the case of stopping flow in the pipeline. Thus, the effect of pre-shearing at different pump speeds is also presented.

This chapter is subdivided into two sections:

- First section deals with description of the flow curves, rheological models and characterisation, and the effect of flow rate on rheological properties.
- Second section deals with rheometry predictions of pumping characteristics, including detailed comparisons of such predictions to experimental data obtained from pipeline tests.

## 4.2 FLOW CURVES

Since all the experimental curves obtained from rheometry were similar, there was no need to show all these curves. Therefore, Figures 4.1 and 4.2 shown below are the typical logarithmic plots of viscosity curves and rheograms of explosive emulsions obtained from rheometry respectively.

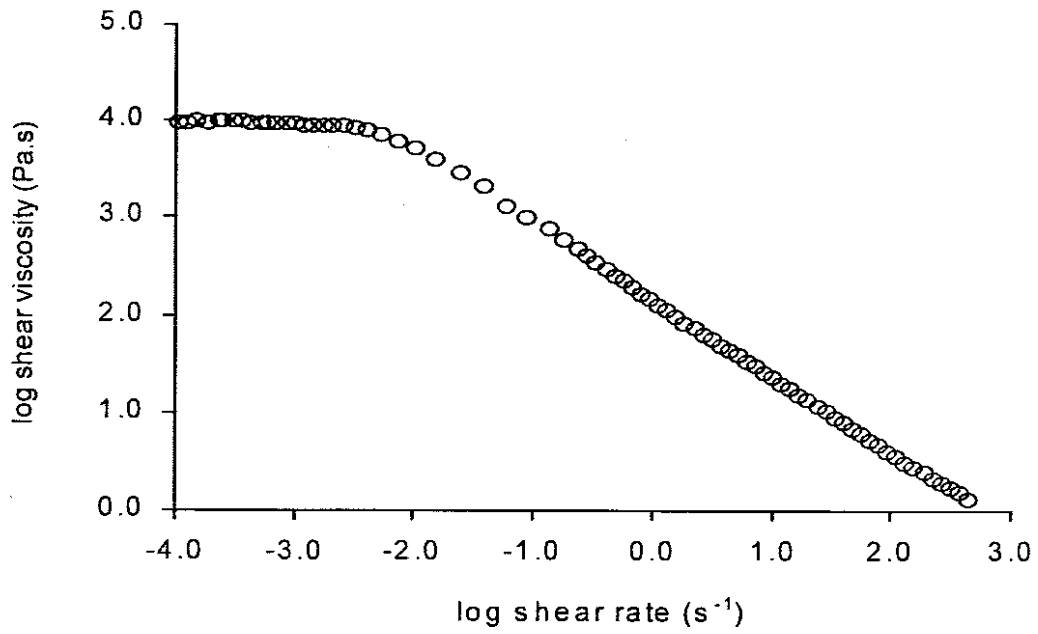


FIGURE 4.1 Typical viscosity curve in logarithmic scale.

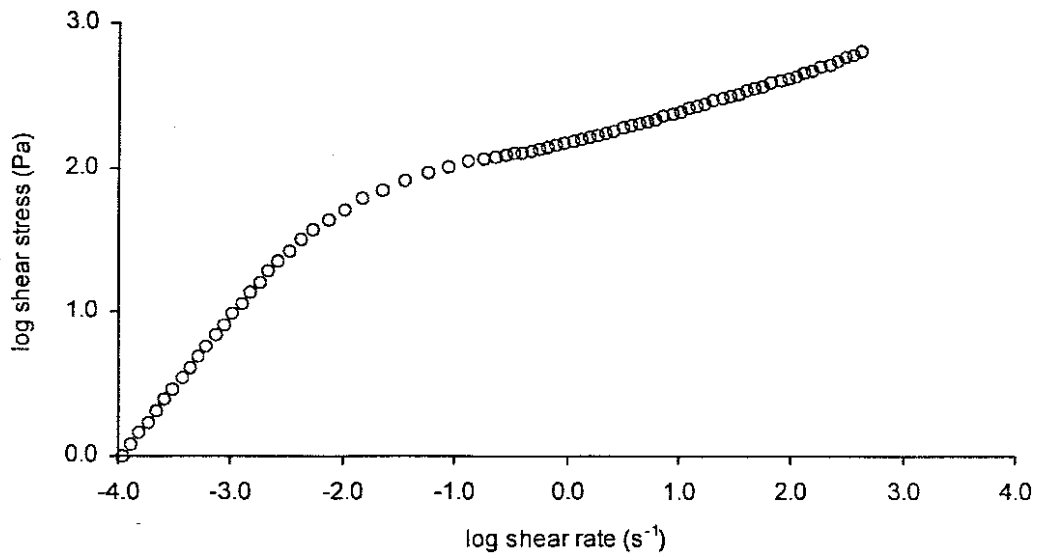


FIGURE 4.2 Typical flow curve in logarithmic scale.

The above Figures depict an emulsion system that exhibits a strong non-Newtonian behaviour. This is shown clearly by the existence of a lower Newtonian behaviour at very low rates of shear ( $\dot{\gamma} < 0.001 \text{ s}^{-1}$ ) and a strong shear-thinning region as the shear rate increases ( $\dot{\gamma} > 0.001 \text{ s}^{-1}$ ). Both Figures above depict a flow behaviour where the shear viscosity becomes sensitive to the applied shear stress or to the applied rate of shear. Mathematically speaking, this means that the shear viscosity becomes a function of the applied shear stresses or applied rates of shearing.

The study material exhibits two distinct regions of deformation behaviour. The first region of deformation occurs at very low rates of shear (i.e. in the shear rate region less than  $0.001 \text{ s}^{-1}$ ) where the material exhibits a constant response to the applied stresses. This zone of constant response is depicted by the horizontal plateau of the logarithmic plot of the viscosity curves, or by the lower linear region of the logarithmic plot of the rheograms having a constant slope of  $45^\circ$ . The low shear rate region is referred to as the lower limiting Newtonian region, and is usually characterised by the zero shear rate viscosity (denoted by  $\eta_0$ ) of the emulsion system. Numerous authors (Partal *et al.*, 1997, Princen, 1983, 1985, Princen and Kiss, 1986a, 1986b) have shown the dependence of the zero-shear viscosity to structural properties of emulsions, and such properties include droplet size and shape, polydispersity of the droplet size distribution and the rheological properties of the continuous phase.

The second region of deformation behaviour occurs in the shear rate region greater than  $0.001 \text{ s}^{-1}$ , as shown in Figures 4.1 and 4.2, where the flow behaviour deviates from Newtonian flow behaviour. This is evidenced by the exponential decrease in viscosity as the rate of shear

increases. This second region of deformation is referred to as the shear-thinning region of the rheogram.

From theoretical points of view (Cross 1965; Utracki 1980; Kozicki and Kuang 1993, etc.), one would expect three regions of deformation behaviour: a lower shear rate Newtonian region characterised by  $\eta_0$ , a shear thinning region at intermediate stresses or rate of shear, and lastly, a high shear rate Newtonian region characterised by  $\eta_\infty$  as shown below by Figure 4.3:

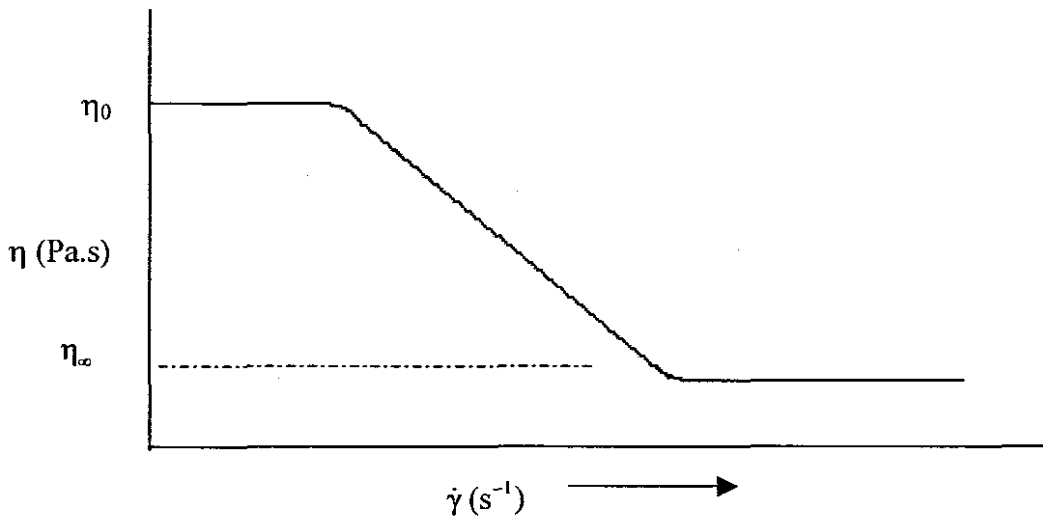


FIGURE 4.3 Typical theoretical flow behaviour expected from this emulsion system.

In all the rheological tests done on the study material, the high shear rate Newtonian limit was not evident as this can be clearly seen from Figures 4.1 and 4.2, despite the solid mathematical justification of its existence. This might be due to experimental limitation of the measuring instrument or other problems encountered at high rates of shear. The following section deals with flow models.

### 4.2.1 Rheological Models

#### *Introduction*

The measuring of viscous properties of flowing materials by means of sophisticated laboratory techniques occupy one of the central goals of rheology. These laboratory techniques are done in order to apply the results in predicting the behaviour of these materials in real technological equipments (pipelines, mixers, die swells, cyclones, etc.). Particularly for describing flow characteristics of these materials through pipelines. The central position in these problems is occupied by fitting experimental data by this or that approximating equation. These approximating equations are then integrated to predict the relationship between force and velocity, or in the case of flow through a pipe, the relationship between pressure gradient,  $\frac{\Delta P}{L}$ , and volume output,  $Q_v$ , or mass output,  $Q$ . As a general rule, a laboratory experimentator intends to measure the shear rate - shear stress dependence in a very wide range of shear rates exceeding in some cases eight decimal orders. Indeed, in many real cases the drop of apparent viscosity  $\eta = \left( \frac{\tau}{\dot{\gamma}} \right)$  as a function of shear rate is very impressive, reaching several decimal orders. The shear rate - shear stress dependence is referred to as the flow curve, and is denoted by  $\dot{\gamma}(\tau)$ .

In this study, only three flow models were used for rheological characterisation, and the best model was then used for predicting pumping characteristics of emulsion explosives. These models have been discussed in Chapter 2, but are repeated here for easy referencing, and are the Herschel-Bulkley, the Power Law and the Cross flow models, and they are expressed as follows:

- Yield-Pseudoplastic or Herschel-Buckley Flow Model  $\tau_w = \tau_y + K\dot{\gamma}^n$  (2.4)

- Pseudo-plastic or Power Law Flow Model  $\tau_w = K\dot{\gamma}^n$  (2.5)

- Cross Structural Viscosity Model  $\eta(\dot{\gamma}) = \frac{\eta_0}{1 + (\lambda \cdot \dot{\gamma})^n}$  (2.11)

The contribution of infinite (upper limiting) Newtonian shear viscosity  $\eta_\infty$  to the calculation of the apparent shear viscosities from Equation 2.7 was assumed negligible (i.e. mathematically,  $\eta_\infty = 0$ ), and thus Equation 2.7 was reduced to the simplified form of equation 2.11. The reasons for that assumption was that:

- (a) The magnitude of the infinite Newtonian shear viscosity  $\eta_\infty$  is extremely low compared to the zero shear limiting viscosity  $\eta_0$ , with their ratio of the order of  $10^5$ , i.e.  $\frac{\eta_0}{\eta_\infty} \approx 10^5$ .
- (b) The difficulty to measure its value at high rates of shearing due to both wall slip and secondary flow effects which become prevalent in high shear environments.

Normally, if the  $\dot{\gamma}(\tau)$  dependence has been measured, the  $Q(\Delta P)$  dependence can be calculated by numerical integration using the well-known Rabinowitsch-Weissenberg equation which is valid for any non-Newtonian fluid. This equation connects the so-named “average shear rate”

$\dot{\gamma}_{av} = \frac{8Q_c}{\pi D^3} = \frac{2V_c}{D}$  (or corrected volume output in other words) and shear stress at the wall of a pipe (or tube)  $\tau_w = \frac{D \Delta P}{4L}$  (i.e. the normalized pressure gradient). The Rabinowitsch-

Weissenberg equation is given by the following expressions:

$$\dot{\gamma}_{av} = \frac{1}{\tau_w^3} \int_0^{\tau_w} \tau^2 \dot{\gamma}(\tau) d\tau \quad (4.1)$$

For

$$\frac{8V_c}{D} = 4\dot{\gamma}_{av} \quad (4.2)$$

when equation 4.1 is substituted in equation 4.2 yields equation 2.56

$$\frac{32Q_v}{\pi D^3} = \frac{8V}{D} = \frac{4}{\tau_w^3} \int_0^{\tau_w} \tau^2 \dot{\gamma}(\tau) d\tau \quad (2.56)$$

In this equation, D is diameter of a pipe in (m),  $\dot{\gamma}(\tau)$  is the measured flow curve, and the subscript c stands for corrected value.

The  $Q(\Delta P)$  dependencies can also be calculated from Equation 2.56 by substituting the  $\dot{\gamma}(\tau)$  dependence depicted by these models or fitting equations, followed by evaluation of the resulting integrals analytically. The  $Q(\Delta P)$  dependencies basing on all these fitting equations are then compared with real experimental data obtained in industrial units used for pumping purposes. The resulting  $Q(\Delta P)$  dependences calculated analytically from the three commonly used fitting equations (namely, Herschel-Bulkey, Power Law and Cross flow models) using Equation 2.56 yield the following final analytical equations:

$$\frac{32Q_c}{\pi D^3} = \frac{32(Q_v - Q_s)}{\pi D^3} = \frac{8V_c}{D} = \frac{8(V - V_s)}{D} = \frac{4n}{K^n \tau_w^{\frac{1}{n}}} (\tau_w - \tau_y)^{\frac{1+n}{n}} \left[ \frac{(\tau_w - \tau_y)^2}{1+3n} + \frac{2\tau_y(\tau_w - \tau_y)}{1+2n} + \frac{\tau_y^2}{1+n} \right] \quad (2.57)$$

$$\frac{32Q_c}{\pi D^3} = \frac{32(Q_v - Q_s)}{\pi D^3} = \frac{8V_c}{D} = \frac{8(V - V_s)}{D} = \frac{4n}{(3n+1)K^n} \tau_w^{\frac{1}{n}} \quad (2.58)$$

$$\frac{32Q_c}{\pi D^3} = \frac{32(Q_v - Q_s)}{\pi D^3} = \frac{8V_c}{D} = \frac{8(V - V_s)}{D} = \frac{4\tau_0^3}{\tau_w^3} \int_0^{\dot{\gamma}_w} \frac{\dot{\gamma}^3 \left[ 1 + \left( 1 - \frac{n}{\lambda} \right) (\lambda \dot{\gamma})^n \right]}{\left[ 1 + (\lambda \dot{\gamma})^n \right]^2} d\dot{\gamma} \quad (2.59)$$

### *Analysis of Experimental Rheometry Data*

The procedure adopted for the analyses of rheometry data for comparison with pipeline data were done as follows:

The rheometry data was subjected to rheological characterisation using the three models (namely, the Herschel-Bulkley, the Power law and the Cross flow models) to describe all the flow curves obtained. Only data points in the laminar region were used for this purpose. The method adopted for rheological characterisation purposes utilised computer software for optimisation of the constants. The method is outlined below and was used for all characterisation purposes:

- A rheogram (or a viscosity curve in the case of the Cross model) was constructed using the true shear rate,  $\dot{\gamma}$  as the abscissa and wall shear stress,  $\tau$  (or apparent shear viscosity,  $\eta$  in the

case of the Cross model) as the ordinate. The following shear rate regions were selected for characterisation purposes: a shear rate range from 0.1 to 420 s<sup>-1</sup> was used for both the Herschel-Bulkley and the Power Law models, and for the Cross model, the complete experimental shear rate region of 0.0001 to 420 s<sup>-1</sup> was used.

- The corresponding values of shear stresses (or apparent shear viscosities in the case of the Cross model) were calculated using the appropriate constitutive rheological equation with arbitrarily selected coefficients.
- Using the method of least squares multiple regression analysis and correlation, a curve was fitted to the experimental data, and the resulting multiple correlation coefficient (denoted by  $r^2$ ) was calculated.
- Optimum values of rheological constants were obtained by maximising the value of the multiple regression correlation coefficient,  $r^2$  or by minimising the residual sum of squares.

The results of rheological characterisation using the three flow models for unpumped samples are shown below in tabular format by Tables 4.1 to 4.2. These tables show the list of all the rheological coefficients and the associated multiple regression correlation coefficients,  $r^2$ . Also included in these tables are the overall arithmetic averages of rheological constants. The associated confidence limits are calculated from equations 3.1 and 3.2 to 3.5 respectively. A 95.5 % level of confidence was assumed for all confidence limits calculations, and the number of observations, N (as grouped by number of unpumped samples) was four.

Table 4.1 Averaged coefficient of the Herschel-Bulkley model for unpumped samples.

Sample	$\tau_y$	K	n	$r^2$
1	27.335	101.722	0.318	0.998
2	23.459	96.566	0.277	0.999
3	23.419	103.483	0.262	0.996
4	20.000	118.056	0.242	0.993
Average	$23.553 \pm 4.770$	$104.957 \pm 14.660$	$0.275 \pm 0.051$	$0.997 \pm 0.003$

Table 4.1 shows the results of rheological characterisation using the Herschel-Bulkley flow model. The averaged coefficients are only valid in the shear rate region of 0.1 to 420 s<sup>-1</sup> for unpumped (or unsheared) emulsion samples, and were interpreted statistically as follows: With 95.5 % level of confidence, the yield stress was found to lie between 18.783 and 28.323 Pa (i.e. with a confidence limit of 4.770), the flow consistency coefficient K was between 90.297 and 119.617 Pa.s<sup>n</sup> (i.e. with a confidence limit of 14.660), the flow behaviour index n was between 0.224 and 0.326 (i.e. with a confidence limit of 0.051). These confidence intervals are calculated by adding and subtracting the corresponding mean confidence limits. The same interpretation applies to all the other coefficients of the other models. The multiple regression correlation coefficient  $r^2$  was between 0.989 and 1.000.

Table 4.2 Averaged coefficient of the Power Law model for unpumped samples.

Sample	K	n	$r^2$
1	132.643	0.236	0.994
2	136.122	0.230	0.997
3	127.131	0.233	0.995
4	136.550	0.223	0.994
Average	$133.112 \pm 6.928$	$0.230 \pm 0.009$	$0.995 \pm 0.002$

Table 4.2 shows the results of rheological characterisation using the Power Law flow model. These averaged means of the rheological coefficients as shown in Table 3.9 are valid in the shear

rate region of 0.1 to 420 s<sup>-1</sup> for unpumped (or unsheared) emulsion samples. A similar interpretation as above was applied, i.e. the 95.5 % level of confidence range for the flow consistency coefficient K was between 126.184 and 140.040 Pa.s<sup>n</sup> (i.e. with a confidence limit of 6.928), for the flow behaviour index n was between 0.221 and 0.239 (i.e. with a confidence limit of 0.009). The multiple regression correlation coefficient r<sup>2</sup> was between 0.992 and 0.999.

Table 4.3 Averaged coefficient of the Cross model for unpumped samples.

Sample	$\eta_0$	$\lambda$	n	r <sup>2</sup>
1	10000.405	127.774	0.830	0.999
2	11000.000	125.000	0.840	0.999
3	12000.000	120.000	0.820	0.983
4	10999.878	129.497	0.850	0.998
Average	11000.071 ± 1298.966	125.568 ± 6.601	0.835 ± 0.021	0.995 ± 0.012

Table 4.3 shows the results of rheological characterisation using the Cross model. The means of the coefficients as shown in Table 3.10 are valid in the shear rate region of 0.0001 to 420 s<sup>-1</sup> for unpumped (or unsheared) emulsion samples. The 95.5 % level of confidence range for the zero shear viscosity  $\eta_0$  was between 9701.744 and 12299.676 Pa.s (i.e. with a confidence limit of 1298.966), for the Cross coefficient  $\lambda$  was between 118.967 and 132.169 s (i.e. with a confidence limit of 6.601), for the Cross index n was between 0.814 and 0.856 (i.e. with a confidence limit of 0.021). The overall multiple regression correlation coefficient r<sup>2</sup> was between 0.971 and 1.000.

It could be seen from these Tables that different values of rheological coefficients were obtained from all the models used for unpumped samples taken from the same emulsion system. This could be attributed to inhomogeneity of the emulsion system, probably due to polydispersity of the droplet size distribution, as all the samples were unsheared prior to rheological testing.

The arithmetic averaged rheological coefficients tabulated above in Tables 4.1 to 4.3 are also presented below graphically in Figures 4.4 to 4.6 by points in a wide range of shear rates. The figures below depict the three possible approximations (solid lines) of the experimental data points.

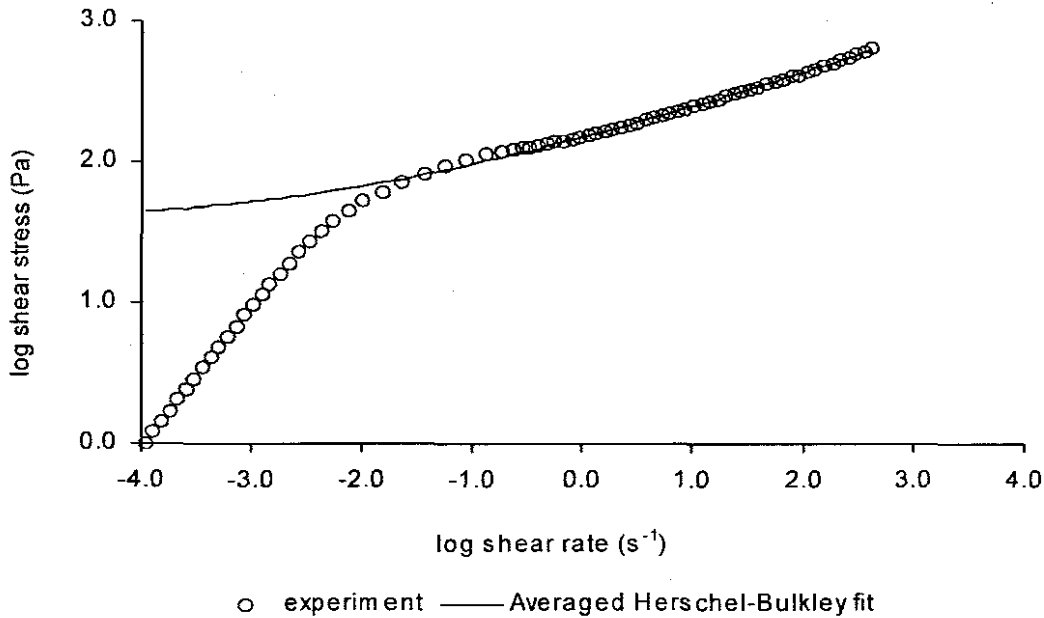


FIGURE 4.4 Herschel-Bulkley approximation of the experimental data

It could be seen from Figure 4.4 that this model depicts the absence of both the lower and the upper Newtonian asymptotes (namely the zero and the infinite shear viscosities, denoted by  $\eta_0$  and  $\eta_\infty$  respectively). This is contrary to experimental findings for this emulsion system, since the presence of the lower Newtonian region and the absence of a yielding behaviour were evident. In order to get a satisfactory fit of the rheological model over the medium and high shear rate region, data at the low shear rate region was excluded in the analysis ( shear rates below  $0.1 \text{ s}^{-1}$  as seen in Figure 4.4).

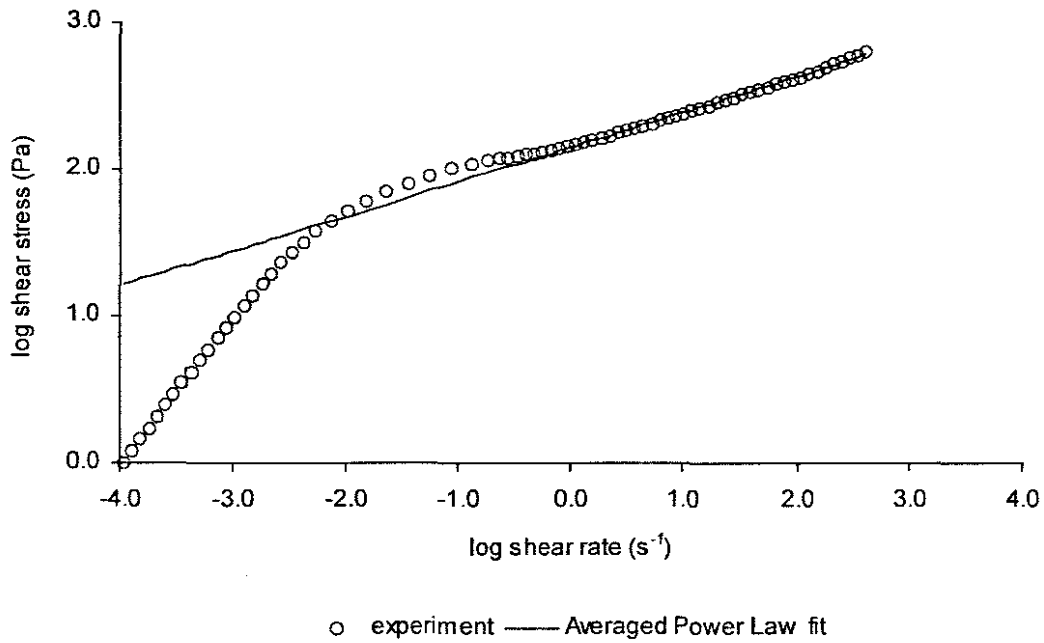


FIGURE 4.5 Power Law Approximation of the experimental data.

It could be seen from Figure 4.5 that this model described only the shear-thinning region of the overall rheogram of this emulsion system (shear rate region greater than  $1.0 \text{ s}^{-1}$ ). As was the case with the Herschel-Bulkley model, it did not describe the lower Newtonian shear rate region.

Thus, both models (i.e. the Herschel-Bulkley and Power law) are inadequate at the low shear rate range due to the existence of the lower limiting Newtonian branch on the flow curve.

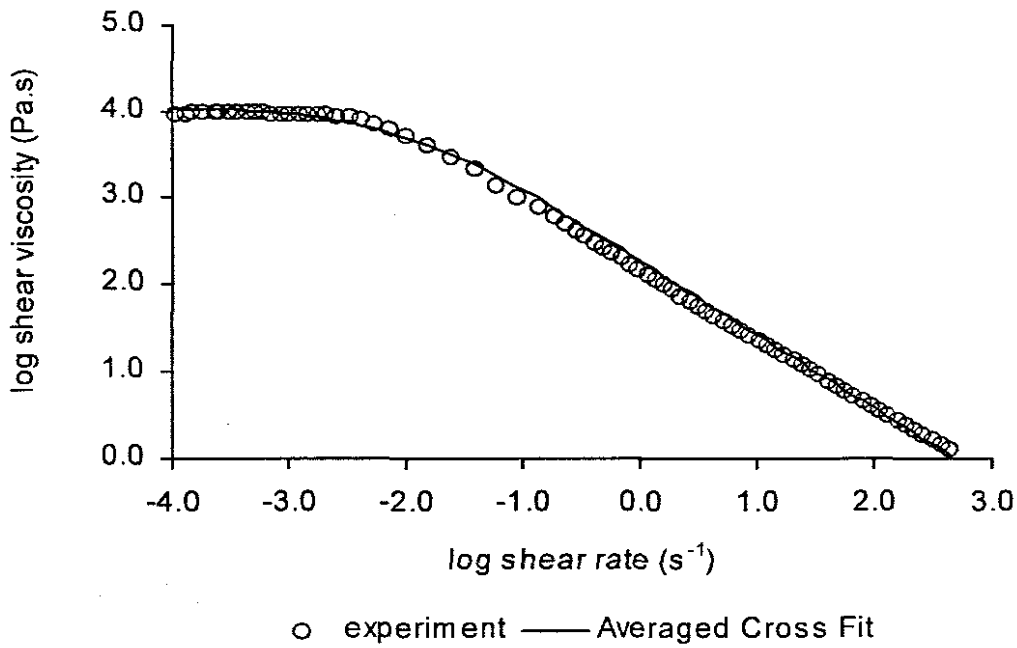


FIGURE 4.6 Approximation of the experimental data for the emulsion by the Cross model.

It could be seen from Figure 4.6 that the Cross model fully describes the flow behaviour (i.e. flow curve) depicted by the emulsion system over the entire shear rate range. Thus, it was chosen as the best and preferred model for subsequent investigations, which include the qualitative determination of the effect of pumping on the rheology of emulsion explosives and the approximation of pumping conditions of this emulsion system from rheometry. This selection was based on the following two reasons: (i) It describes the flow curve depicted by this emulsion system over the entire shear rate range, (ii) Its rheological parameter  $\eta_0$  has some physical significance in that its magnitude is correlated to the structure of the emulsion system. In fact,  $\eta_0$  could serve as a quality control measure as its magnitude is correlated to the structural properties of the emulsion system (which include the Sauter mean droplet size, effective volume fraction of dispersed phase, droplets deformability, elasticity of the structure, etc.), and thus, pumping-

induced structural changes of the emulsion system can be detected and quantified from variation in the value of  $\eta_0$ .

However, any of the other two models (Herschel-Bulkley and Power Law models) could also be used for predicting pumping characteristics as they describe the flow behaviour depicted by this emulsion system reasonably well in the shear rate region between 1 and 420  $\text{s}^{-1}$  (see Appendix I). It is worth-mentioning that the shear rate range of practical interest for pumping applications normally excludes the lower shear rate range and usually ranges from 10 to 1000  $\text{s}^{-1}$ . This is the shear rate range where most models find wide practical (industrial) applications.

An investigation on the effect of pumping (or pre-shearing) rate on the rheology of emulsion explosive was conducted to determine the extent of such an effect on their rheology qualitatively. Only the Cross model was used in this investigation as shear induced-structural changes (which include changes in the mean droplet size, droplet size distribution, etc.) could be determined both qualitatively (and quantitatively) from the variation in the value of its parameters.

#### **4.2.2 Effect of Pumping on the Rheological Properties of Emulsion Explosives**

The averaged coefficients of the Cross model obtained from rheological characterisation of unpumped samples were as follows:  $\eta_0 = 11000 \text{ Pa}\cdot\text{s}$ ,  $\lambda = 125.6 \text{ s}$ ,  $n = 0.84$  (see Table 4.3). In order to determine whether pre-shearing induced by different pump speeds had a significant effect on the flow behaviour depicted by this material, pipeline tests were done at different pump speeds for each test pipe. Subsequently, samples were taken for rheological testing and characterisation (using the Cross model) to determine qualitatively the effect of different degrees

of pre-shearing on the rheology of emulsion systems. The resulting coefficients of the Cross model were then compared with those obtained for unpumped samples, and were also compared against one another (as grouped by the degree of pre-shearing). It is also worth-mentioning that a portion of the resultant deformation is imparted to the emulsion system at the pump outlet (i.e. at the pipe entrance region where the material converges on entering the pipe).

If pre-shearing had an effect, the rheograms and thus the Cross model coefficients obtained would be different for the same sample collected from the same diameter pipe after being subjected to varying degrees of pre-shearing. The effect of pump speed on the flow properties of this material is shown below in Figures 4.7 to 4.12 and by Tables 4.4 to 4.6.

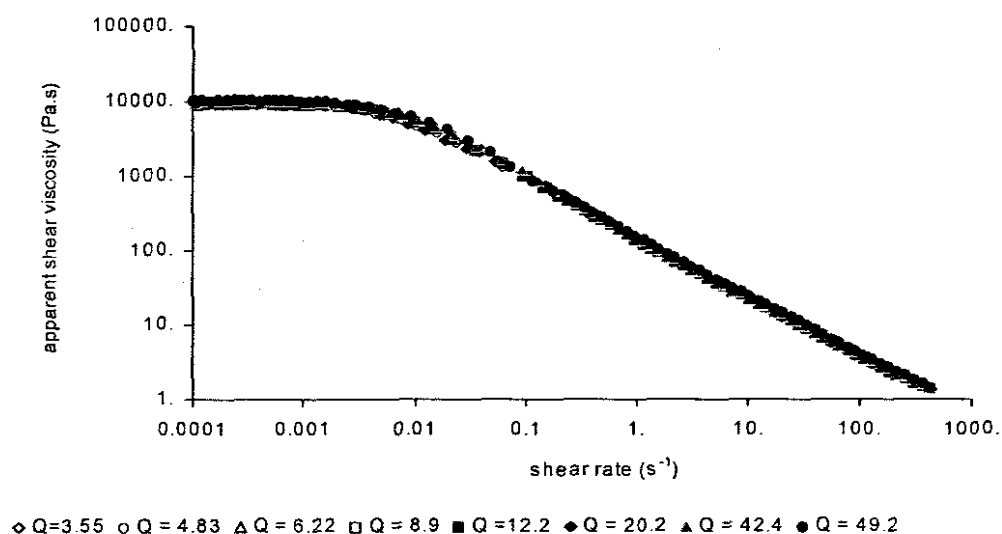


FIGURE 4.7 Viscosity curves obtained from pipe diameter 35.9mm as function of flow rate  $Q$  (kg / min), i.e. as a function of pump speed.

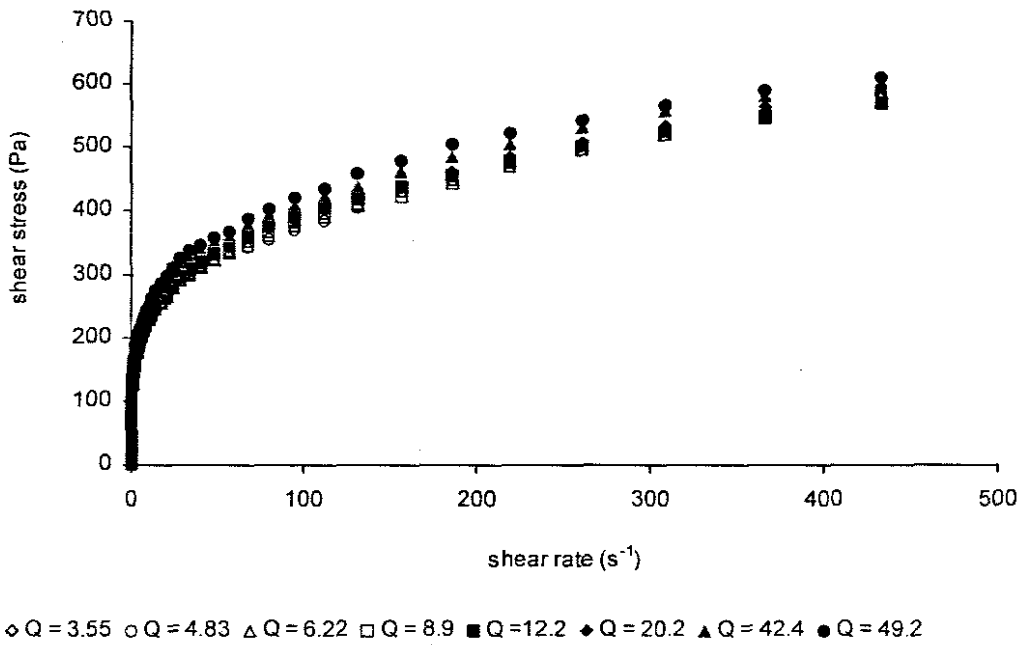


FIGURE 4.8 Rheograms obtained from pipe diameter 35.9mm as function of flow rate  $Q$ (kg / min), i.e. as a function of pump speed.

Table 4.4 Cross coefficients obtained at different pumping speeds for  $D = 35.9$  mm.

$Q$ (kg.min <sup>-1</sup> )	$\eta_0$ (Pa.s)	$\lambda$ (s)	$n$
3.55	11000	124	0.850
4.83	10800	125	0.850
6.22	10900	125	0.80
8.90	10800	124	0.85
12.20	10500	125	0.850
20.20	10900	124	0.850
42.40	11800	124	0.850
49.40	12600	125	0.850
Average	10957	124.50	0.850

Figures 4.6 to 4.7 and Table 4.4 depict the effect of different pump speeds for pipe diameter of 35.9 mm, which is indicative of small diameter steady state laminar flow of this emulsion system.

Figure 4.7 depict the linear plots of the viscosity curves obtained on double logarithmic scale, while Figure 4.8 depict the linear plots of the rheograms obtained.

It could be seen from these Figures that different pump speeds effect different rheological changes to the emulsion systems, and this is depicted by the existence of different rheograms for the same emulsion system when the emulsion system was subjected to different pumping speeds, as could be evidenced from Figure 4.8. Table 4.4 depicts the coefficients of the Cross model obtained from rheological characterisation of the data. . It could be seen from Table 4.4 that different values of zero-shear viscosities  $\eta_0$  and Cross relaxation times  $\lambda$  were obtained. Thus, pre-shearing affects both the lower Newtonian domain (shear rate region  $< 0.01 \text{ s}^{-1}$ ) and the shear-thinning region (shear rate region  $> 0.01 \text{ s}^{-1}$ ) of the flow curve. The effect of different degrees of pre-shearing was found to be insignificant in the shear-thinning region as evidenced by the values of the Cross index  $n$  and Cross relaxation time  $\lambda$  tabulated in Table 4.4 that describe this shear rate region. However, the zero shear viscosity  $\eta_0$  showed was a gradual decrease in  $\eta_0$  (from 11000 to 10500 Pa) and then by a gradual increase (from 10500 to 12600 Pa) when the emulsion was subjected to both lower and higher degrees of pre-shearing respectively (i.e. for  $3.55 \text{ kg}\cdot\text{min}^{-1} < Q < 12.2 \text{ kg}\cdot\text{min}^{-1}$  and  $Q > 12.2 \text{ kg}\cdot\text{min}^{-1}$  as evidenced from Table 4.4.

A decrease in  $\eta_0$  is usually accompanied by a rise in the value of the Sauter mean diameter (denoted by  $d_{\text{saut}}$ ) of the dispersed phase droplets (Princen 1983, Pal *et al.*, 1991, Pal 1996, Mason 1996, Jager-Le'zer, *et al.*, 1999, Malkin *et al.*, 2004) which is associated with increased rates of coalescence and flocculation (or formation of larger droplets and globules) encountered at low rates of shearing. An increase in  $\eta_0$  is usually accompanied by a decrease in the value of the the

Sauter mean diameter of the dispersed phase droplets which is associated with increased rates of droplets refinement and deflocculation (or formation of smaller droplets and rupture of large globules) encountered at high rates of shearing. This refinement of the dispersed phase droplets can be attributed mainly to the intense shearing action (i.e. high shear stresses) exerted to the emulsion system inside the pump at higher rates of pumping, but also to the deformation energy imparted on the material as it converges at the pipe entrance.

In general, coalescence and droplets flocculation predominates at flow rates lower than  $12.2 \text{ kg}\cdot\text{min}^{-1}$ , while droplets refinement and deflocculation predominates at flow rates higher than  $12.2 \text{ kg}\cdot\text{min}^{-1}$  for pipe diameter of 35.9mm. Thus, pre-shearing changes the physical properties of the emulsion system (i.e. mean droplets size and droplets size distribution) as manifested by changes in the rheological properties of the emulsion system.

The effect of pump speed on the rheology of this emulsion system for pipe diameters  $D$  of 48.1mm is shown in Figures 4.9 to 4.10 and by Table 4.5.

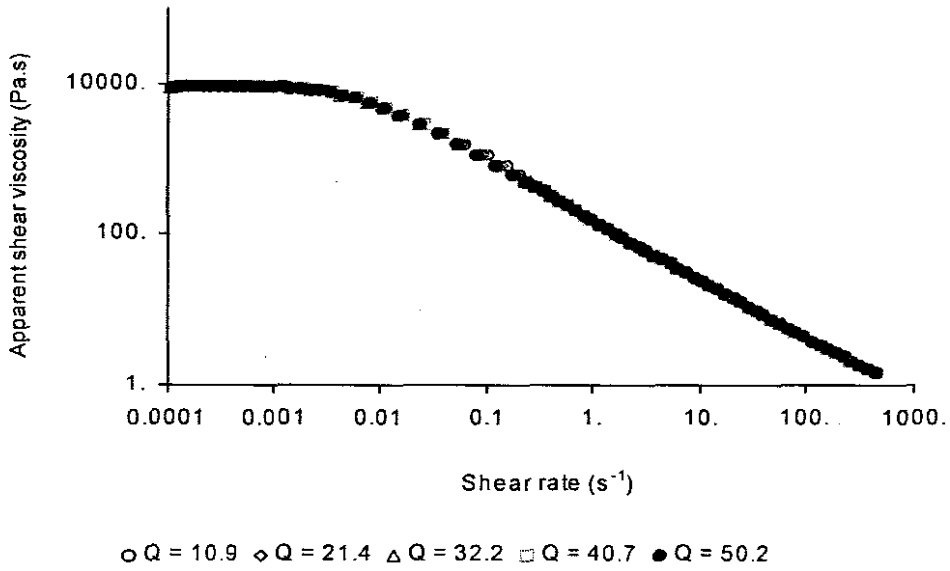


FIGURE 4.9 Viscosity curves obtained from diameter pipe 48.1mm as function of flow rate  $Q$  (kg / min), i.e. as a function of pump speed.

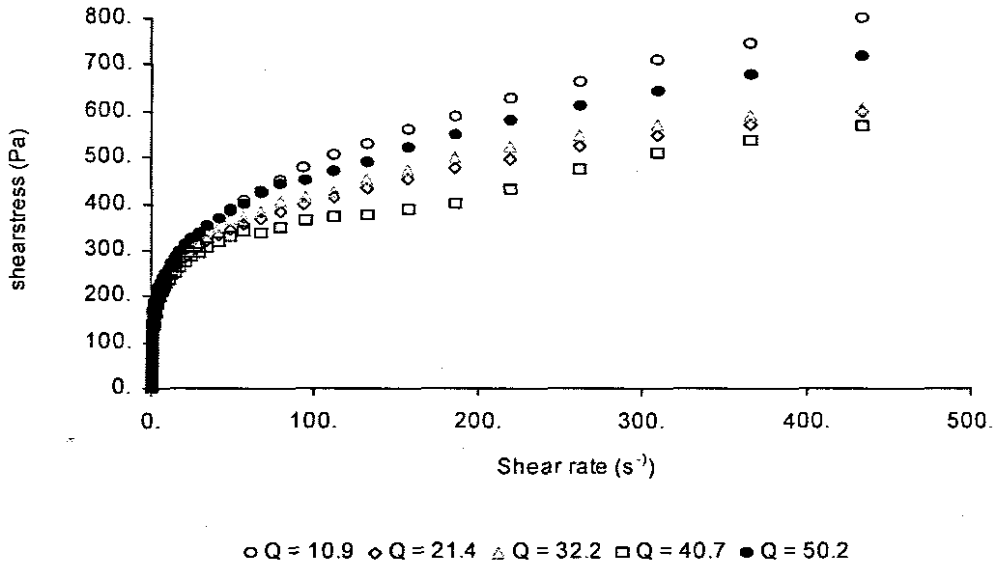


FIGURE 4.10 Rheograms obtained from diameter pipe 48.1mm as function of flow rate (kg / min), i.e. as a function of pump speed.

Table 4.5 Cross coefficients obtained at different pumping speeds for  $D = 48.1$  mm.

$Q$ ( $\text{kg}\cdot\text{min}^{-1}$ )	$\eta_0$ (Pa.s)	$\lambda$ (s)	$n$
10.9	10400	124	0.84
21.4	10400	126	0.84
32.2	10200	124	0.84
40.7	10500	126	0.84
50.2	10400	125	0.84
Average	10380	125.00	0.84

Figures 4.9 to 4.10 depict the effect of pump speed for the intermediate diameter steady state flow of this emulsion system. Figure 4.9 depict the linear plots of the viscosity curves obtained on double logarithmic scale, while Figure 4.10 depict the linear plots of the rheograms obtained. It could be seen that pre-shearing showed a similar effect on the rheological behaviour of emulsion systems as could be evidenced from Table 4.5.  $\eta_0$  showed a gradual decrease from 11000 Pa (for unpumped sample) to 10200 Pa and by gradual increase from 10200 Pa to 10400 Pa.

The effect of pre-shearing observed for samples taken from all other pipe diameters greater than 48.1 mm (pipe diameters of 54.9, 65.9 and 77.6 mm) is shown graphically by Figures 4.11 to 4.12 and in tabular format by Table 4.6. The flow in these pipes is indicative of large diameter laminar flow of this emulsion system. Figure 4.11 depict the linear plots of the viscosity curves obtained on double logarithmic scale for the diameters of 65.9 mm while Figure 4.12 depict the linear plots of the rheograms obtained from the same pipe diameter. These Figures are typical of the rheograms obtained from the 54.9 mm and 77.6 mm diameter pipes. It could be seen that these Figures and Table 4.6 depict a similar pre-shearing effect on the rheology of this emulsion

system as observed in all the other pipe diameters. The overall results of the effect of pump speed or pre-shearing on the rheological properties is presented graphically in Appendix K.

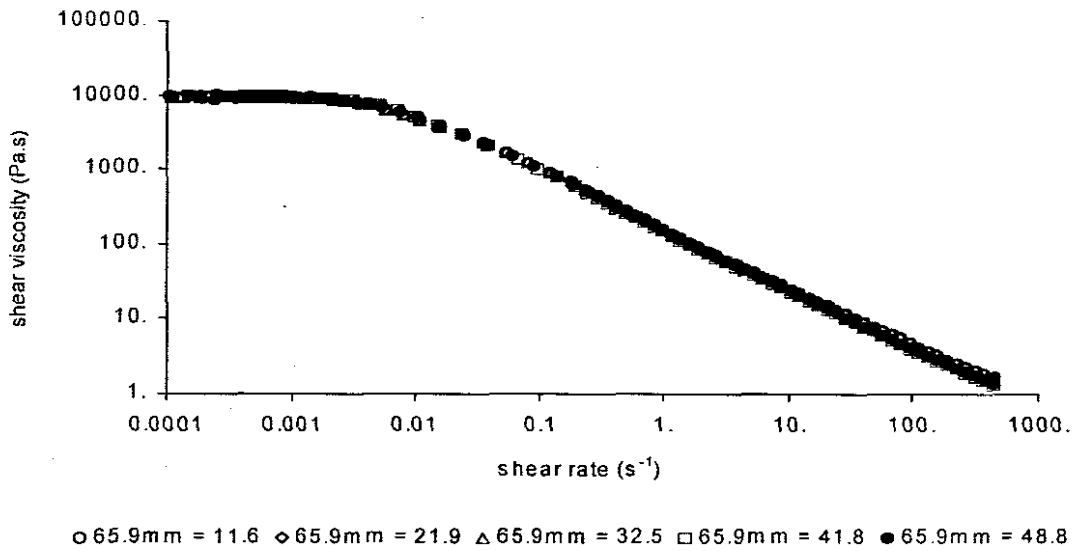


FIGURE 4.11 Viscosity curves obtained from diameter pipes of 65.9 mm as function of flow rate (kg / min), i.e. as a function of pump speed.

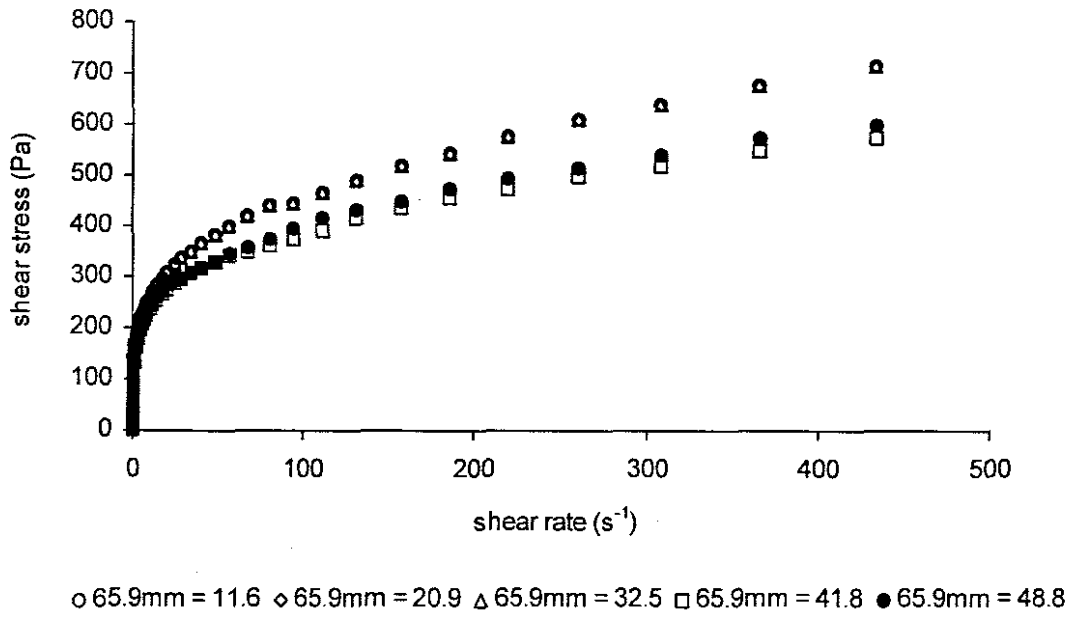


FIGURE 4.12 Rheograms obtained from diameter pipe 65.9mm as function of flow rate (kg / min), i.e. as a function of pump speed.

Table 4.6 Cross coefficients obtained at different pumping speeds for D = 54.9, 65.9 and 77.6 mm.

Diameter (mm)	Q (kg.min <sup>-1</sup> )	$\eta_0$ (Pa.s)	$\lambda$ (s)	n
55.9 mm	11.1	11150	124	0.85
	21.7	11200	125	0.84
	31.5	11000	124	0.84
	41.5	11100	126	0.84
	50	11500	125	0.84
	Average	11190	124.80	0.84
65.9 mm	11.6	11150	124	0.85
	21.9	11200	125	0.84
	32.5	11200	124	0.84
	41.8	11800	125	0.84
	48.8	11500	125	0.84
	Average	11370	124.60	0.84
77.6 mm	12.3	11150	124	0.83
	23.8	11200	124	0.83
	34.8	11300	125	0.83
	45.0	11200	125	0.85
	55.9	11500	125	0.84
	Average	11270	124.60	0.84

It is thus concluded from Figures 4.6 to 4.11 and Tables 4.4 to 4.6 that pre-shearing affects the flow or rheological properties of emulsion systems. Emulsion samples subjected to different degrees of pre-shearing exhibited different flow behaviours as evidenced by the different flow curves and rheological coefficients (i.e. variation in  $\eta_0$ ) obtained for each pipe diameter. The changes in the flow properties was attributed to different degrees of shear-induced structural changes occurring within them inside the pump due to different shear environments as well as at the pipe entrance when the emulsion system converged on entering the various test pipes.

However, a similar response of the zero-shear viscosity of the emulsion system  $\eta_0$  to variations in pump speed (as depicted by Q) was observed for all the pipes tested.

It is evident from Tables 4.4 to 4.6 that the  $\eta_0 - Q$  relation obtained for all the test pipes can be categorised into three regions (the third region is not evident but is supported by theory):

- Region of low or intermediate shear stresses which are encountered at low and moderate pump speeds where the rates of flocculation and coalescence of the dispersed phase droplets are predominant, resulting in decreased  $\eta_0$  and increased  $d_{saut}$ .
- Region of high shear stresses which are encountered at high pump speeds where the rates of deflocculation and refinement of the dispersed phase droplets are predominant resulting in increased  $\eta_0$  and decreased  $d_{saut}$ .
- Finally, a region of very high shear stresses encountered at very high speeds where additional increase in pump speeds produces no significant change in both  $\eta_0$  and  $d_{saut}$ , depicting a limiting value of  $d_{saut}$  (Sherman, 1968: 15 to 21).

The two opposing processes (i.e. coalescence - flocculation and refinement – deflocculation) of dispersed phase droplets are normally accompanied by a change in rheological properties, such as zero shear viscosity, elastic modulus, etc. The former processes (i.e. coalescence and flocculation) effect a decrease in rheological properties, while the latter processes (droplet refinement and deflocculation) normally effect an increase in rheological properties. This must be due to the fact

that the flow properties of high internal phase ratio emulsions are strongly influenced by the packing, the deformability and the intrinsic elasticity of the dispersed phase droplets, as well as by the strength, the tenacity and the rheology of the interfacial surfactant film separating the droplets.

However, both the elasticity and deformability of the droplets are controlled by their Laplace pressure (defined as the ratio of the interfacial tension to droplet radius,  $\frac{\Gamma}{r}$ ), and thus depend sensitively on droplet size, while the packing of the droplets is controlled by both their size distribution and by the internal phase ratio or internal volume fraction of the emulsion system (Mason *et al.*, 1996). The larger is the droplet size, the smaller is its elasticity (as measured by  $\eta_0$ ) and the higher is its deformability. The reverse applies for small droplets, and thus emulsion with smaller droplets are relatively more stable compared to those containing larger droplets due to increased rheological properties manifested by increased elastic properties and reduced deformability.

These shear-induced structural changes as manifested by variation in the rheological properties (different coefficients of the Cross model obtained for all test conditions of Q and D tabulated in Tables 4.4 to 4.6 were insignificant for industrial pipeline transport of these emulsion systems. Thus, these coefficients were averaged and weighted as shown in Tables 4.7 and 4.8. Averaging of the rheological coefficients was done statistically following the theory presented in subsection 3.5.1.1, which deals with error analysis. This was done as follows:

a) The 95.5% level of confidence was assumed for all the calculations and Appendix D was used to determine the values of  $t$  for use in equation 3.5. The results are shown below by Table 4.7.

Table 4.7 Averaged rheological coefficient of the Cross model for all D.

D (mm)	$\eta_0$	$\lambda$	$n$	$r^2$
0 (unpumped)	11000	125.586	0.835	0.995
35.9	10957	124.570	0.850	0.996
48.1	10380	125.000	0.842	0.992
55.9	11190	124.800	0.842	0.997
65.9	11370	124.600	0.842	0.998
77.6	11270	124.600	0.836	0.998
Average	11027.83	124.84	0.841	0.996

Thus, the overall averaged coefficients for the Cross model in the shear rate region of 0.0001 to 420  $s^{-1}$  for this emulsion system were interpreted as follows: With 95.5 % level of confidence, the zero shear viscosities  $\eta_0$  were between 10729 and 11327 Pa.s, the Cross relaxation times  $\lambda$  were between 124.5 and 125.18 s, the Cross indices  $n$  were between 0.836 and 0.846 and the multiple regression correlation coefficients  $r^2$  were between 0.994 and 0.998.

b) Secondly, These averaged rheological coefficients were analysed statistically and the summary statistics of the averaged rheological coefficients are given in Appendix G. These summary statistics were calculated using a Statistics software, and some were also verified manually using equations 3.1 to 3.5. The results were interpreted as follows:

It is seen from Appendix G that all the frequency distribution curves of the averaged rheological constants were non-normal since the value of skewness,  $SK \neq 0$  and the kurtosis  $\alpha_4 \neq 3$ . The

value of skewness for the frequency distribution of  $\eta_0$  was found to be negative ( $SK < 0$ ), and the kurtosis (or peakedness) of the frequency distribution curves was less than 3 ( $\alpha_4 < 3$ ), thus depicting a negatively skewed platikurtic frequency distribution curve (see Appendix E and F), which was associated with large dispersions (or broad distribution) of the mean values. The skewness of the frequency distribution curve for the averaged Cross coefficients  $\lambda$  and  $n$  were found to be positive ( $SK > 0$ ), and the corresponding kurtosis were found to be less than 3, respectively. This depicts positively skewed platikurtic frequency distribution curves for  $\lambda$  and  $n$  respectively, associated with broad distribution of the mean values.

From the statistical analyses of the averaged rheological constants, it was seen that the frequency distributions of the averaged rheological constants were non-normal. In almost all the cases, the kurtosis was found to be platikurtic (or flatter), except for the frequency distribution of the averaged  $\lambda$  which was found to be leptokurtic. The frequency distributions of the averaged rheological constants for the different sets of measurements (as grouped by the test pipe diameter used) were large, and was improved relative to any individual set of measurements by the use of weighted averaged coefficients.

c) Thirdly, the statistical overall weighted averages of the rheological coefficients and their corresponding combined confidence limits were then calculated from equations 3.7 and 3.8. These weighted averaged rheological constants were representative of the flow behaviour depicted by this emulsion system in an unsheared state and when flowing in the various test pipes. The weighted averaged rheological constants were subsequently used in the prediction of

pumping characteristics of this emulsion system from rheometry. The list of the weighted overall averages of rheological constants is shown in Table 4.8.

Table 4.8 Weighted averaged rheological constants of all the three flow models.

Flow Model	Weighted averaged rheological constants		
Cross	$\eta_0 = 11027.83 \pm 80.24$	$\lambda = 124.84 \pm 0.30$	$n = 0.841 \pm 0.004$

### 4.3 PREDICTION OF FLOW RATE AND PRESSURE DROP FROM RHEOMETRY.

The purpose of this sub-section is to compare the predictions of pumping characteristics calculated from rheometry to the actual pipeline flow data measured from corresponding test pipes. Initially, comparison of the predicted pseudo-shear rate diagram to the actual pseudo-shear rate diagram  $\left( \tau_w \text{ vs. } \frac{8V}{D} \right)$  obtained from pipeline tests is done. This is followed by comparison of the predicted system curves to the actual system curves (i.e.  $\Delta P$  vs.  $Q$ ). The results of such comparisons are illustrated below by Figures 4.13 to 4.18.

Construction of the averaged pseudo-shear rate diagram (i.e.  $\tau - \left( \frac{8V}{D} \right)$  relations) from rheometry is done using weighted averaged rheological constants of the Cross model tabulated in Table 4.9 and equation 2.58. Figure 4.13 depicts rheometry prediction of the averaged pseudo-shear rate diagram together with ten measurements from pipe tests.

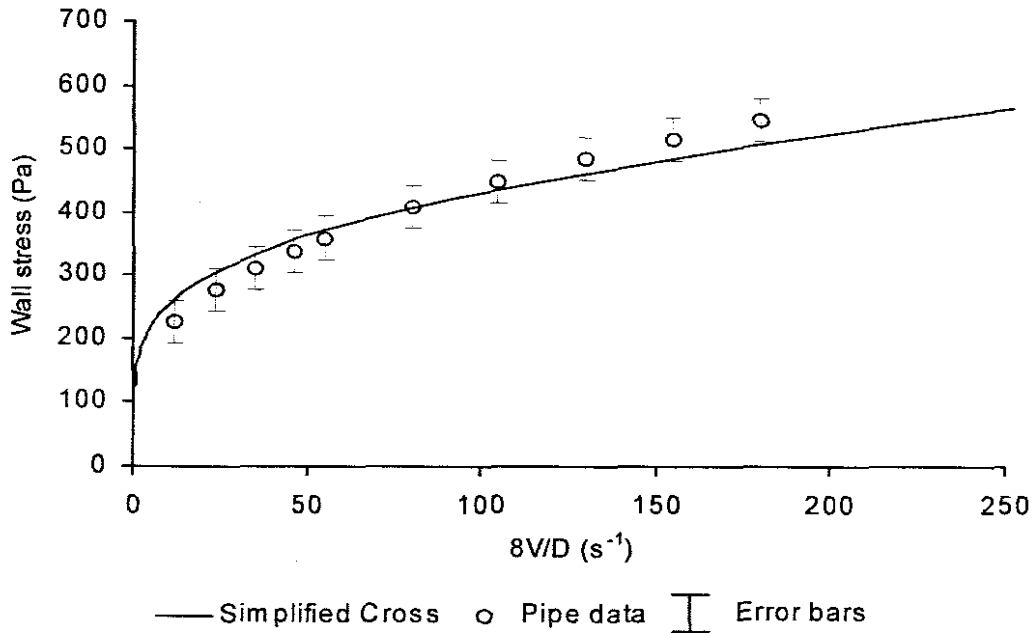


FIGURE 4.13 Pseudo-shear rate diagram constructed from the Cross model.

It is evident from Figure 4.13 that a good practical agreement was obtained between rheometry predictions and pipeline test data as the predictions lie within the standard error band of the experiment measurements. This conclusion is supported by the following estimation of possible errors tabulated in Table 4.9 as calculated from equations 3.9 and 3.12.

Table 4.9 List of possible errors for high internal phase ratio emulsion explosives.

Rheological Models	Mean Square Relative Error, $E_{rel}$	Maximum Possible Error
Simplified Cross	0.133	$1.90 \times 10^{-2}$

It is seen from Table 4.9 that both the mean squared relative error (of 0.133) and the maximum possible error (of  $1.90 \times 10^{-2}$ ) associated with the use of Cross model in rheometry prediction of pumping conditions is quite small. The percentage maximum error of 1.90% for the

approximations using the Cross model is far lower than the acceptable engineering limit of 5% normally used for approximation purposes.

The system curves ( $\Delta P$ -  $Q$  relations) were then constructed from the averaged pseudo-shear rate diagram using Equations 2.54 and 2.53 with  $\Delta P = \frac{4L\tau}{D}$  and  $Q = \left(\frac{8V}{D}\right)\left(\frac{\pi D^3}{32}\right)$  respectively. The comparison of pumping predictions from rheometry are presented by Figures 4.14 to 4.18 together with the results of direct measurements from corresponding pipe test.

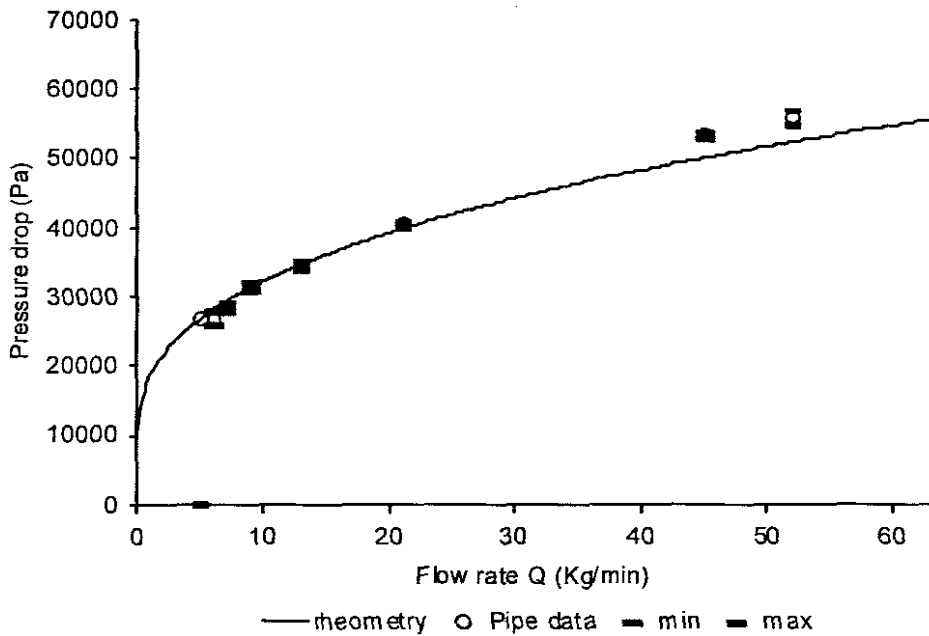


FIGURE 4.14  $\Delta P$  vs.  $Q$  for  $D = 35.9\text{mm}$ .

Figure 4.14 above depict comparison made for pipe diameter,  $D = 35.9\text{mm}$ , which depict the case of small diameter, steady-state, laminar pipeline flow of this emulsion system. It could be seen from this figure that a good agreement between rheometry and actual pipe flow is evident.

Figures 4.15 and 4.16 shown below depict a similar comparison for pipe diameters  $D$  of 48.1mm and 55.9mm respectively, which depict a case for intermediate diameter; steady state; laminar pipeline flow of this emulsion system. It could also be seen that a good correlation was achieved for these diameters.

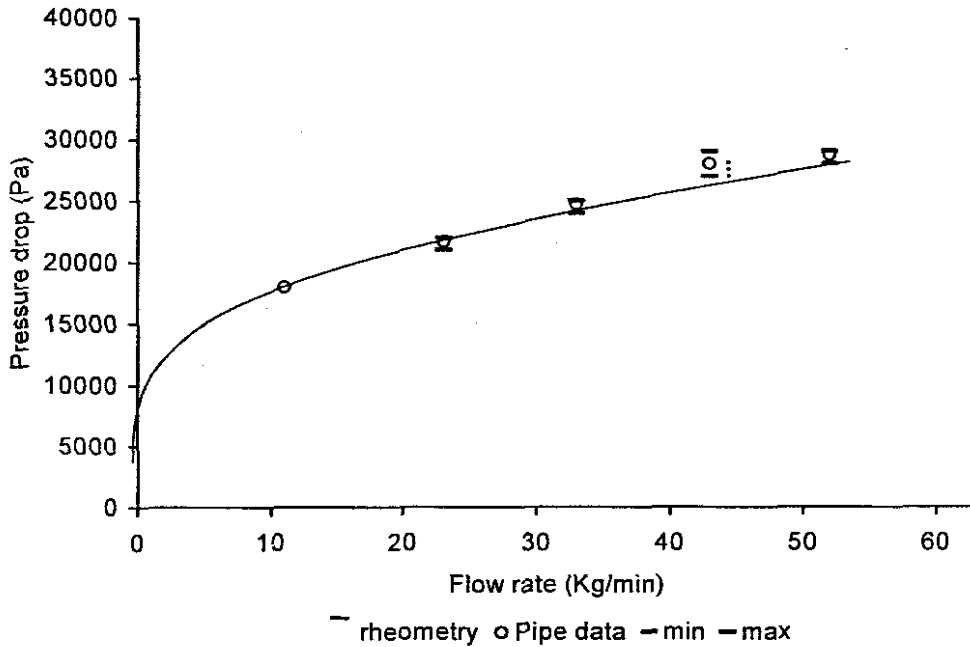


FIGURE 4.15  $\Delta P$  vs.  $Q$  for  $D = 48.1\text{mm}$ .

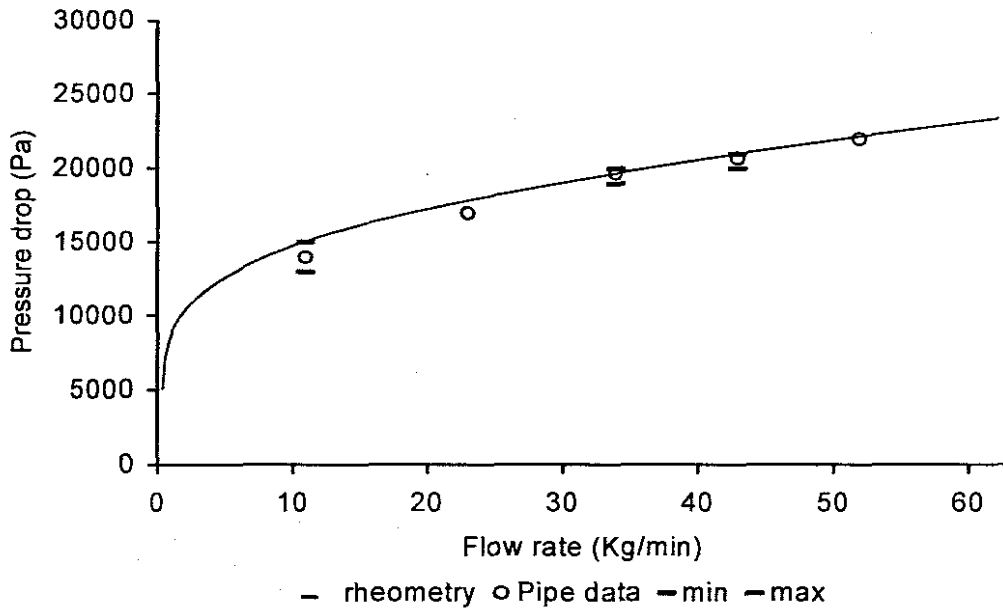
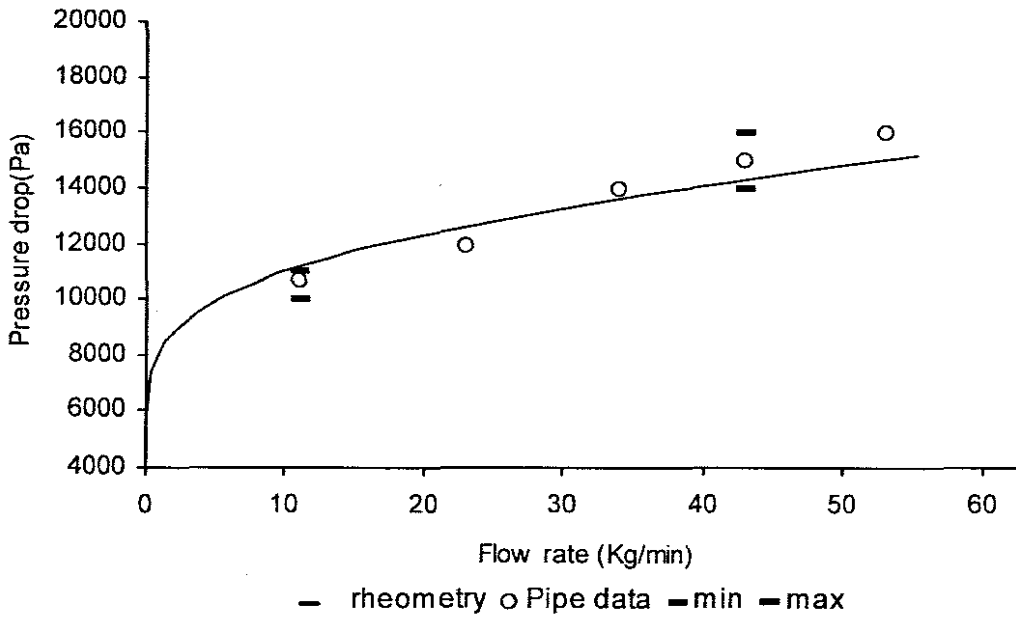
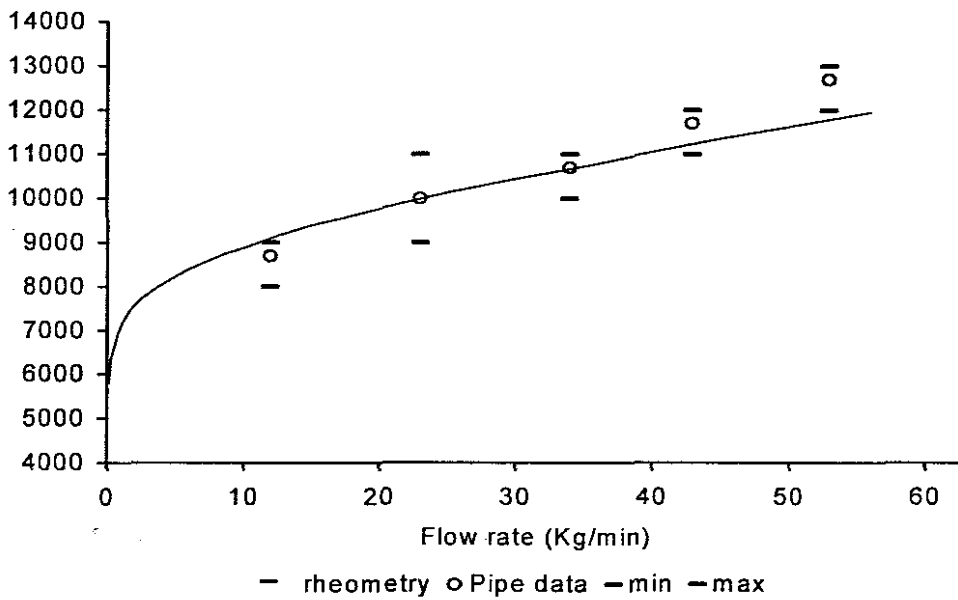


FIGURE 4.16  $\Delta P$  vs.  $Q$  for  $D = 55.9\text{mm}$ .

The case of large diameter; steady-state; laminar pipeline flow of this emulsion is illustrated by Figures 4.17 and 4.18 for pipe diameters,  $D = 65.9\text{mm}$  and  $77.6\text{mm}$ ,

FIGURE 4.17  $\Delta P$  vs.  $Q$  for  $D = 65.9\text{mm}$ .FIGURE 4.18  $\Delta P$  vs.  $Q$  for  $D = 77.6\text{mm}$ .

It is also evident from Figures 4.17 and 4.18 that a good correlation was achieved for both test pipes, since the predicted pressure drops were within the allowable pressure drops range. It is thus concluded that all rheometry predictions covering all steady state laminar flow conditions of practical interest (ranging from small, intermediate to large diameter laminar flow of this emulsion system) gave good agreements with actual pipeline flow.

*In general, rheometry is sufficient and valid for estimating the pumping characteristics of explosive emulsions for all the pipe diameters of practical interest.*

#### 4.4 SUMMARY

A comprehensive description of the techniques used in the analyses of the experimental results has been presented. Inherent discussions pertaining to the experimental findings have also been addressed. The following investigations have been presented:

- a) Whether pump speed significantly affects changes on the rheological properties of emulsion explosives associated with structural changes of emulsion system under shear.
- b) Whether rheometry can be applied successfully and accurately in prediction of pumping characteristics of emulsion explosives.

Good correlations were achieved between rheometry predictions and pipeline data irrespective of the choice of the model used (evidenced from Appendix I). Different pump speeds were found to

effect different shear-induced structural changes on the emulsion system which were manifested by the observed changes in rheological properties, particularly by the variation in the values of  $\eta_0$  obtained. However, such structural changes were found to be insignificant for industrial pipeline transportation of these emulsion system. Rheometry was found to predict the pumping characteristics of emulsion system reasonably well in all the test pipes used in the study, and can thus be used successfully in predicting pumping characteristics.

# **CHAPTER 5**

## CHAPTER 5

### SUMMARY AND CONCLUSION

#### 5.1 INTRODUCTION

This Master's dissertation was devoted at developing rheological methods of testing, characterisation

and correlation for highly concentrated w/o emulsion explosive systems, in order to develop a basis for predicting pumping characteristics from rheometry.

However, numerous studies on the rheology of emulsion explosives ignored their long distance pipeline transportation, as well as correlation of their steady state flow properties obtained from rheometry in prediction of the pumping requirement for long distance pipeline application, despite the fundamental economic benefit that could be derived from such studies.

This work seeks to make a direct contribution to the understanding of steady state laminar flow of high internal phase ratio (i.e. highly concentrated) emulsion explosive systems, more specifically to make use of rheometry in prediction of pumping characteristics for application in long-distance transport of these systems.

#### 5.2 SUMMARY

Long-distance pipeline transport of bulk emulsion explosives has become a viable economic option over traditional explosives (i.e. nitroglycerine dynamites, dry blasting agents, slurry explosives) due to a variety of factors which include cost, safety, performance, etc. Prediction of

pumping characteristics for long distance pipeline transport of emulsion explosives from rheometry has important economic advantages associated with it, in that, it minimises the effort (i.e. time and labour) and cost (test material and test equipments) associated with pipeline trial experiments.

Presently, rheological characterisation of emulsion explosives is well documented (Bampffield & Cooper, 1988, Utracki, 1980). However, very little or none has been done for this emulsion system, pertaining to the use of rheometry for application in their long-distance pipeline transportation. This Master's dissertation seeks to correct this omission from published literature, and use rheometry to predict pumping characteristics for long-distance transport of these high internal phase ratio (or highly concentrated) emulsion explosives.

Three flow models have been used for rheological characterisation, and these are the Herschel-Bulkley Model, the Power Law Model and the Simplified Cross models. The performance of these models were then evaluated and compared to the actual rheograms depicted by this emulsion system. The rheological coefficients of the best model obtained through rheological characterisation were then used to predict the laminar pipeline flow of this emulsion system. Its performance (best model) was then evaluated by comparing the pipeline flow predictions obtain from rheometry to the actual pipeline data obtained from pipeline test experiments.

The experimental work was conducted at two experimental test facilities, pipeline tests were done at the AEL experimental test facility, while rheometry was performed at the Rheology Laboratory of the Cape Peninsula University of Technology Flow Process Research Centre. The

experimental methodology (i.e. instrumentation, experimental procedure and treatment of results) adopted for the study, as well as the discussion of the experimental findings have been fully described in Chapter 3. The study material was a high internal phase ratio w/o emulsion explosive system having an internal phase ratio of approximately 94%, the composition and properties of this emulsion explosive system has also been presented in detail in the previous chapter.

From analysis of the results, it was found that the viscous characteristics of highly concentrated w/o emulsion explosive systems are strongly non-Newtonian, and that their flow behaviour is characterised by the existence of two regions of deformations: a lower Newtonian region of deformation (i.e. lower Newtonian asymptote which is characterised by the zero-shear viscosity, denoted by  $\eta_0$ ) in the shear rate region lower than  $0.001 \text{ s}^{-1}$ ; and a strong shear thinning region in the shear rate region above  $0.001 \text{ s}^{-1}$ . Absence of the upper Newtonian region of deformation (i.e. upper Newtonian asymptote which is characterised by the infinite-shear viscosity, denoted by  $\eta_\infty$ ) contrary to proposals by numerous authors (Cross 1965; Utracki 1980; Kozicki and Kuang 1993 etc.) was evident in all the rheological measurements, and this could be attributed to experimental limitations.

It was also found that both the Power Law model and Herschel-bulkley could be applied partially to describe the rheology of this emulsion system with reasonable accuracy. The former model is applicable down to a shear rate limit of  $1 \text{ s}^{-1}$ , while the latter model is applicable from a shear rate limit of  $0.01 \text{ s}^{-1}$  upwards. The Simplified Cross model described the rheology of this emulsion system with reasonable accuracy over the entire steady state laminar shear rate range of 0.0001 to

420 s<sup>-1</sup>. However, all the flow models used in the study predicted the pipeline flow reasonably well as evidenced from comparison with actual pipeline test data (see Appendix I for Herschel-Bulkley and Power Law models), and thus the choice of the rheological model was found to be insignificant for pipeline design purposes. The only difference between these models is the lower shear rate domain, which is not applicable to pipeline flow. The Cross model was preferred over the other two model mainly because its coefficient  $\eta_0$  is correlated to the structure of the emulsion system, thus pumping-induced structural changes can be detected and quantified from variation in its value. Pre-shearing at different pumping speeds was found to induce two opposing processes in the emulsion system, namely coalescence – flocculation and refinement – deflocculation of the dispersed phase droplets. Refinement – deflocculation of dispersed droplets was found to be predominant at high shear rates (high pump speeds). This process was manifested by an increase in  $\eta_0$  which is associated with decreased  $d_{saut}$ , normally accompanied by increased elastic and viscous effects. Coalescence – flocculation of droplets was found to be predominant at low and intermediate shear stresses (moderate pump speeds), and this process was manifested by a decrease in  $\eta_0$  which is associated with increased  $d_{saut}$ , normally accompanied by decreased elastic and viscous properties.

### 5.3 CONCLUSION

In view of all the findings and inherent discussions presented in this Master's dissertation, the following conclusions can be drawn:

- The laminar flow of highly concentrated w/o emulsions explosive (as could be evidenced from Appendix j) used in this study can be successfully modelled using any of the three

models, namely the Simplified Cross model, the Herschel-Bulkley and the Power Law models.

- The constitutive rheological equation that best describes the flow behaviour of a given material, depends not only on the behaviour of that material, but also on the quality and selected range of shear viscosity data available for that material, as well as on the shear rate range of practical application. Thus, the choice of the rheological model is not crucial in the prediction of pipeline flow.
- All three flow models used in this study can be used to predict the pipeline flow reasonably well, and thus rheometry can be used to predict the pumping characteristics of emulsion explosives accurately.
- The Simplified Cross model fully describes the rheology of emulsion explosive, and is preferred over the other two models since structural changes induced by shearing (either inside the pump or when flowing inside a pipe) can be detected from the zero shear viscosity of this model, and thus  $\eta_0$  can be used as a quality control measure.
- Pre-shearing at different pumping speeds effects different degrees of shear-induced structure changes, and thus has an effect on the rheological properties of emulsion explosive systems. Intermediate shear stresses associated with moderate pump speeds induce coalescence and flocculation of dispersed phase droplets, while high stresses associated with high pump speeds effect deflocculation and refinement of droplet aggregates and droplets respectively.

- For shear sensitive materials (i.e. emulsion in general), the use of structural viscosity models (to mention but the least Cross, Carreau) is recommended, as their constants (especially  $\eta_0$ ) are correlated to structural parameters of the material (such as droplet size; shape of droplets; polydispersity of the droplet size distribution; deformability of the droplets; effective volume fraction of the dispersed phase), and can thus be used as a quality control measure.
- It was also found essential to use statistical analysis of random errors whenever repeated measurements of the same quantity are done for averaging purposes of the individual observations. This could eliminate ambiguity in the interpretation of the experimental observation as well as to establish some range within which the mean value is likely to be found with a certain level of confidence. The highest and lowest values in the frequency ranges establish both the higher and lower limit of the pumping prediction calculated from rheometry.

#### 5.4 FUTURE RESEARCH RECOMMENDATIONS

As a consequence of this study, a number of areas have been identified as possible future research initiatives:

- Effect of pre-shearing at various pumping speeds on the rheology of high internal phase ratio (or simply HIPR) w/o emulsion explosives with the objective of correlating the pump speed to the shear-induced structural changes, in terms of suitable rheological structural parameters (such zero shear viscosity, elastic modulus, Sauter mean diameter of the droplets, size distribution of droplets, etc.). This could aid with emulsion formulations.

- Effect of variation in temperature of the HIPR emulsion explosive systems on their rheology with the objective of quantifying temperature-effects in terms of suitable rheological structural parameters (such zero shear viscosity, elastic modulus, Sauter mean diameter of the droplets, size distribution of droplets, etc.). This could also aid with emulsion formulations.
- Determination of time effects on the rheological behaviour of HIPR emulsion explosive systems in terms of suitable time dependent rheological models (theoretical or empirical) for application in pump start-up operations after pumping have been stopped for some time.

## 5.5 FINAL CONCLUSION

An experimental and analytical rheological investigation has been embarked upon, to develop rheological methods of testing, characterisation and analysis in order to predict pipeline flow of high internal phase ratio emulsion (or simply HIPRE) explosives from rheometry. The following final conclusion can be made:

- The literature relevant to the flow of emulsion explosives has been reviewed.
- Rheological methods of testing and characterisation have been established.
- Analysis of results were done, and evidence have shown that rheometry could accurately predict the pumping characteristics of HIPRE explosives irrespective of the choice of a rheological model used in prediction of pipeline pumping characteristics.

- The effect of pump speed was insignificant for industrial transportation of emulsion explosive systems.
- Recommendations for future research work have been made.

# REFERENCES

## REFERENCES

- Adamson, A W.. 1990. *Physical chemistry of surfaces, 5<sup>th</sup> Ed.* New York: Wiley, 525-544.
- Anon. Presentation and Interpretation of Engineering Data [online]. Available: [http://www.eng.uwaterloo.ca/~che100/Chapter2\\_content.htm](http://www.eng.uwaterloo.ca/~che100/Chapter2_content.htm) [21 August 2004].
- Anon. Combining Experimental Errors [online]. Available: [http://www.home.clara.net/rod.beavon/err\\_comb.htm](http://www.home.clara.net/rod.beavon/err_comb.htm) [21 August 2004].
- Anon. Errors vs. Mistakes [online]. Available: [http://webphysics.iupui.edu/NH/Projects/TEAMS\[2\]/err2.htm](http://webphysics.iupui.edu/NH/Projects/TEAMS[2]/err2.htm) [21 August 2004].
- Bampffield, H. A. & Cooper, J. 1988. Emulsion Explosives, Part 7 in “ *Encyclopedia of emulsion technology, Volume 3*, Marcel Dekker, Ink. N. Y. & Bassel.
- Bancoft, W. D. 1915. The Theory of Emulsification, VI, *J. Phys. Chem.* 19 (4): 275 - 309.
- Bagley, E. B. 1957. End Corrections in the Capillary Flow of Polyethylene, *J. Appl. Phys.* 28: 624 - 627.
- Barnea, E. & Mizrahi, J. 1973. A generalized approach to the fluid dynamics of particulate systems, Part 1: General correlation for fluidization and sedimentation in solids multiparticle system. *Chem. Eng. J.* 5: 171-189.
- Barnes, H. A. & Walters, K. 1985. The yield stress myth? *Rheologica. Acta*, 24: 323-326.
- Barnes, H. A 1995. A review of the slip (wall depletion) of polymer solutions, emulsions and particle suspensions in viscometers: Its cause, character and cure, *J.Non-Newtonian Fluid Mech.*, 56: 221-251.

- Barnes, H. A. 1999. The yield stress – a review or “*παντα ρει*”-everything flows? *J. Non-Newtonian Fluid Mech.*, 81: 133–178.
- Baudouin, M. M. 2003. Contraction and Expansion Losses for non-Newtonian fluids. MTech. Master's dissertation, Cape Technikon, Cape Town, South Africa.
- Benziger, J. B. & Askay, I. A. 1999. Notes on Data Analysis [online]. Available: <http://www.princeton.edu/~che346/Notes/Analysis.pdf> [21 August 2004].
- Boger, D.V. 1982. Circular entry of inelastic and viscoelastic fluids. In: Mujumdar, A. S. & Mashelka, R. A. (editors). *Advances in Transport Processes, Volume II*. New York: Hosted Press, John Wiley & Sons, 43-104.
- Bogue, D. C. 1959. Entrance Effects and Prediction of Turbulence in Non-Newtonian Flow, *Ind. Eng. Chem.* 51: 874 - 878.
- Bower, C., Gallegos, C., Mackley, M. R. & Madiedo, J. M. 1999. The rheological and microstructural characterization of the non-linear flow behavior of concentrated oil-in-water emulsions. *Rheol Acta.* 38: 145 – 159.
- Brinkworth, B. J. 1968. *An Introduction to Experimentation*. London: English University Press.
- Capriz, G., Ghelardoni, G. & Lombardi, G. 1966. Numerical Study of the Stability Problem for Couette Flow, *Phys. Flui.* 9 (10): 1935 - 1936.
- Carlson, G. A. 2000 – 2004. Experimental Errors and Uncertainty [online]. Available: [http://www.stchas.edu/faculty/gcarlson/physics/docs/Error\\_and\\_Uncertainty.pdf](http://www.stchas.edu/faculty/gcarlson/physics/docs/Error_and_Uncertainty.pdf) [21 August 2004].
- Chabbra R. P. & Richardson, J. F. 1999. *Non-Newtonian flow in the process industries*. Oxford: Butterworth Heiniman.

- Cheng, D. C-H. & Parker, B. R. 1976. The determination of wall slip velocity in the coaxial cylinder viscometer: *Proc. 7<sup>th</sup> Int. Congr. on Rheol.*, Gotenberg, Sweden, 518-519.
- Cheng, D. C-H. 1984. Further observations on the rheological behaviour of dense suspensions. *Power Technology*. 37: 255–273.
- Collins, M. & Schowalter, W. R. 1963. Behaviour of non-Newtonian fluids in the entry region of a pipe. *AIChE. J.* 9: 804 – 809.
- Coulson, J. M. & Richardson, J. F. 1990. *Chemical Engineering. Volume 1.* 4<sup>th</sup> ed. Oxford: Pergamon Press.
- Cross, M. M. 1965. Rheology of non-Newtonian fluids: A new flow equation for Pseudoplastic systems, *J. Colloid Sci.*, 20: 417-423.
- de Paula, J. C. Data Analysis [online]. Available: <http://www.haverford.edu/chem/302/data.pdf> [21 August 2004].
- Dervisoglu, M. & Kokini, J. L. 1982. Steady shear Rheology and fluid mechanics of four semi-solids foods. *J. Food Sci.* 51: 541–545, 625.
- Edwards, A. L. 1979. *Multiple Regression And Analysis of Variance and Covariance*, San Francisco: W. H. Freeman.
- Einstein, A. 1906. Eine neue Bestimmung der Molekul dimension, *Annln Phys.* 19: 289.
- Einstein, A. 1911. Berichtigung zu meiner Arbeit: Eine neue Bestimmung der Molekul dimension *Annln Phys.* 34: 591.
- Freundlich, h., 1928. Ueber Thixotropie, *Kolloid-Z.* 46: 289.

- Gee, R. E. & Lyon, J. B. 1957. Nonisothermal Flow of Viscous Non-Newtonian Fluids, *Ind. Eng. Chem.* 49: 956 – 960
- Govier, G. W. & Aziz, K. 1972. *The Flow of Complex Mixtures in Pipes*, van Nostrad Reinhold Co.
- Griffin, W. C. 1949. Classification of Surface-Active Agents by HBL, *J. Soc. Cosmet. Chem.* 1: 311.
- Griffin, W. C. 1954. Calculation of HBL Values of non-Ionic Surfactant *J. Soc. Cosmet. Chem.* 5: 249.
- Herzog, R. L. & Weissenberg, K. 1928. Ueber die thermische, mechanische und röntgenoptische Analyse der, *Kolloid Z.* 46: 277 - 289.
- Heywood, N. 2003, Lecture notes: Rheology and flow of non-Newtonian materials, Cape Town: Cape Technikon, 31 March – 04 April.
- Heywood, N. & Alderman, N 2004. Important Considerations when Making Rheological Measurements on Pastes. In: *International Seminar on Paste and Tailings*. Cape Town, 31 March – 02 April: [Paper 4].
- Holland, F. A. & Bragg, R. 1995. *Fluid Flow for Chemical Engineers*. 2<sup>nd</sup> Ed. London: Edward Arnold, 108-130.
- Huang, C. R. 1988. Characterisation of thixotropic fluids. In Cheremisinoff N. P. (ed). *Encyclopedia of fluid Mechanics*, Vol. 7 – Rheology and Non Newtonian flows. Huston: Gulf Publishing Co.: 3-17
- Jager-Lezèr, N., Tranchant, J., Alard, V., Vu C., Tchoreloff, P. C. & Grossiord, J. 1998. Rheological Analysis of highly concentrated w/o emulsions, *Rheol. Acta.*, 37: 128–138.

- Jansen, K.M.B., Agterof, W. G. .M. & Mellema, J. 2001. Viscosity of surfactant stabilized emulsions, *J. Rheol.* 45: 1359-1371.
- Kiljanski, T. 1989. A method for the correction of wall-slip in a Couette rheometer. *Rheol. Acta.* 21: 325 – 332.
- Kozicki, W. & Kuang, P. Q. 1993. Prediction of Lower / Upper Limiting Viscosities, *Canadian J of Chem .Eng.*, 71: 329–331.
- Lacroix, C., Aressy, M. & Carreau, P.J. 1997. Linear viscoelastic behavior of molten polymer blends: a comparative study of the Palierne and Lee and Parks models, *Rheol. Acta.*, 36: 416-428.
- Langefield, A., Schmitt, V., & Stebbe M. J. 1999. Rheological behaviour of fluorinated highly concentrated reverse emulsions with temperature. *J. Colloid and Interface Sci.*, 218: 522 – 528.
- Larson, R. G. 1999. The structure and Rheology of complex fluids, New York: Oxford University, 270.
- Leviton, A. & Leighton, A. 1936. Viscosity Relationships in Emulsions Containing Milk Fat, *J. Phy. Chem.* 40 (1): 71 - 80.
- Macosko, C. W. 1994. *Rheology: principles, measurements and applications*. New York: VCHPublishers.
- Malkin, A. Ya. 1994. *Rheology Fundamentals*. Canada: ChemTec, 1: 1-3, 4: 62–66.
- Malkin, A. Ya., Masalova, I., Slatter., P & Wilson., K. 2004. Effect of droplet size on the rheological properties of highly concentrated w/o emulsions, *Rheoigical Acta.*, 43: 584–591.
- Manca, S., Lapsin, R., Partal, P. & Gallegos, C. 2001. Influence of surfactant addition on the rheological properties of aqueous Welan matrices, *J. Rheol.*, 40: 128-134.

- Masalova, I., Malkin, A. Ya., Slatter., P & Wilson., K. 2003. The rheological characterization and pipeline flow of highly concentrated water-in oil emulsions, *J. Non-Newton. Fluid Mech.*, 112: 101–114.
- Mason, T. G., Bibette, J. & Weitz, D. A. 1996. Yielding and Flow of Monodisperse Emulsions, *J. Colloid and Interface Sci.*, 179: 439-448.
- Mezger, T. G. 2002. *The Rheology handbook: for users of rotational and oscillatory rheometers*, Hannover, Germany: Viententz Verlag, 29.
- Michiyosi, L., Mizumo, R. & Hoshia, Y. 1966. Studies on the flow of slurries through pipes, Part 1: Entrance region of laminar flow. *Int. Chem. Engn.* 6: 373 – 381.
- Mizushina, T., et al. 1971. *Kagaku Kogaku.* 35: 1116.
- Mooney, M. 1931. Explicit formulas for slip and fluidity. *J. Rheol.* 30: 337–357.
- Myers, D. 1992. *Surfactant Science and Technology*, 2<sup>nd</sup> Ed, New York: VCH, 232–241.
- Nawab, M. A. & Mason, S. G. 1958. The viscosity of dilute emulsions, *Trans. Faraday Soc.* 54: 1712.
- Nguyen, Q. D. & Boger D. V. 1992. Measuring the flow properties of yield stress liquids, *Ann. Rev. Fluid Mech.*, 24: 47-8.
- Otsubo, Y. & Prud'homme, R.K. 1994. Rheology of oil-in-water emulsions, *Rheol. Acta*, 33: 29-37.
- Otsubo, Y. & Prud'homme, R. K. 1994. Effect of drop size on the flow behavior of oil-in-water emulsions, *Rheol. Acta*, 33: 303-306.
- Paar Physica, 1995. *Rotational Rheometry*. Germany: Physica Messtechnik GmbH.

- Paar Physica: *Operating Instruction. 2000. Modular Compact Rheometer MCR 300*. Germany: Physica Messtechnik GmbH.
- Paar Physica: TEZ 300. 2000 – 2001. *Temperature Unit TEZ 300 : Operating Instructions*. Germany: Physica Messtechnik GmbH, 3-10.
- Pal, R. 1990. On the Flow Characteristics of Highly Concentrated Oil-in-Water Emulsions, *Chem. Eng. J.* 43: 53-57.
- Pal, R., Yuhua Y. & Masliyah, J. 1991. Rheology of Oil-in-Water Emulsions with Added Solids, *Chem. Eng. Sci.*, 46: 985-994.
- Pal, R. 1996. Effect of droplet size on the rheology of emulsions, *AIChE J.*, 42:3181-3190.
- Pal, R. 1997. Scaling of relative viscosity of emulsions, *J. Rheol.*, 41: 141-150.
- Pal, R. (2001). Novel viscosity equations for emulsions of two immiscible liquids, *J. Rheol.*, 45: 509-520.
- Partal, A., Guerrere, A., Berjano, M. & Gallegos, C. 1997. Influence of concentration and temperature on the flow behavior of oil-in water emulsions stabilized by sucrose palmitate. *JAOCS.*, 74: 10.
- Pienaar, V. 1998. Non-Newtonian Fitting Losses. NHD Dissertation, Cape Technikon, Cape Town, South Africa.
- Pons, R., Solans C., Stebe M. J., Erra P. & Ravey J. C. 1992. Stability and rheological properties of gel emulsions, *Progr. Colloid Polymer Sci.*, 89: 110-113.
- Poshusta, R. D.. Error Analysis [online]. Available:  
[http://www.poshusta.chem.wsu.edu/Sci\\_comp/datanal/errors.htm](http://www.poshusta.chem.wsu.edu/Sci_comp/datanal/errors.htm) [21 August 2004].

- Princen, H. M. 1983. Rheology of foams and highly concentrated suspensions. I: Elastic properties and yield stress of a cylindrical model system, *J. Colloid & Interface Sci.*, 91: 160-17.
- Princen, H. M. 1985. Rheology of foams and highly concentrated suspensions. II: Experimental study of the yield stress and wall effects for concentrated oil-in-water emulsions, *J. Colloid & Interface Sci.*, 105: 150-171.
- Princen, H. M. & Kiss, A. D 1986a. Rheology of foams and highly concentrated suspensions. III: Static shear modules, *J. Colloid & Interface Sci.*, 112: 427-437.
- Princen, H. M. & Kiss, A. D. 1986b. Rheology of foams and highly concentrated suspensions. IV An experimental study of the shear viscosity and yield stress of concentrated emulsions, *J. Colloid & Interface Sci.*, 128: 176-187.
- Rabinowitsch, B. Z. 1929. Ueber Ueber die viskosität und elastizität von solen. *Z. Physik. Chem.*, 145A: 1.
- Rajagopal, E. S., 1960. *Z. Phys. Chem.*, 23: 342.
- Randal, G. G., Sun, R. & Shook, C. A. 2000. Laboratory Investigation of Inversion of Heavy Oil Emulsions, *Canadian J. of Chem. Eng.*, 78: 757-763.
- Richardson, E. G. 1950. The formation and flow of emulsion, *J. Colloid Sci.* 5 (4): 315 - 419.
- Richardson, E. G. 1953. The flow of the emulsions, *J. Colloid Sci.* 8: 387 - 373.
- Schofield, R. K. & Scott Blair, G. W. 1959. Transition from laminar to turbulence flow. *AIChE. J.* 5: 433 - 435.
- Savins, J. G., Wallick, G. C. & Foster, W. R. 1962. *Soc. Petrol. Engrs. J.* 2: 211.

- Sherman, P. 1968. *Rheology of Emulsions. In Emulsion Science*. New York: Academic Press, 217 – 342.
- Slatter, P. T. 1999. The Role of Rheology in the Pipelining of Mineral Slurries, *Min. Pro. Ext. Met. Rev.*, 20: 281 – 300.
- Slatter, P. T. & Chhabra, R. P. 2002. Lecture notes: The Flow of Non-Newtonian Slurries and Sludges, Cape Town: Cape Technikon, 16 July – 19 July.
- Steffe, J. F. 1996. *Rheological Methods in Food Engineering*, East Lansing: Freeman.
- Taylor, G. I. 1932. The viscosity of fluid containing small droplets of another, *Proc. R. Soc. (London) Ser. A*. 138: 41 - 48.
- Thomas, D. G. 1965. Transport characteristics of suspension: VIII. A note on the viscosity of Newtonian suspensions of uniform spherical particles, *J. Colloid Sci.* 20 (3): 267-288.
- Toor, H. L. 1956. The Energy Equation for Viscous Flow – Effect of Expansion on Temperature Profile, *Ind. Eng. Chem.* 48: 922 – 926.
- Toor, H. L. 1957. Heat Generation and Conduction in the Flow of a Viscous Compressible Liquid, *Trans. Soc. Rheol.* 1: 177 - 190.
- Utracki, L. A. 1980, The Rheology of Basic Emulsion Explosives, *ERL Report no. EL. 0812, Category B*.
- Usher, S. P., De Kretser, R. G. & Scales, P. J. 1998. Origins of Thixotropy, *8<sup>th</sup> Inter. Conference on Rheology*, Adelaide, 211-213.
- Van Wazer, J. R., Lyons, J. W., Kim, K. Y. & Colwell, R. E. 1966. *Viscosity and Flow Measurement: A Laboratory Handbook of Rheology*, New York: Interscience.

- Walowit, J., Tsao, S. & Diprimas, R. C. 1964. Stability of flow between...., *J. Appl. Mech.* 31: 585.
- Whorlow, R. W. 1992. *Rheological Techniques, 2<sup>nd</sup> Ed.* New York: Ellis Horwood.
- Willemse, I. 1991. *Statistical Methods and Financial Calculations*, Cape Town: Juta.
- Yoshimura, A. S. & Prud'homme, R. K. 1988. Wall slip corrections for couette and parallel disk viscometers. *J. Rheol.* 32: 53–67.

# APPENDICES

## APPENDIX A

Appendix A1: Hydrophile-Lipophile Balance ranges and their application (Myers, 1992)

Range	Application
3 - 6	w/o emulsions
7 - 9	Wetting
8 - 18	o/w emulsions
3 - 15	Detergency
15 - 18	Solubilization

$$HLB_{\text{mix}} = (f_A \times HLB_A) + (1 - f_A)HLB_B,$$

$f_A$  is the weight fraction of A in the surfactant mixture

Appendix A2: HLB scales

Surfactant solubility behaviour in water			
No dispersibility in water	{	0 2 4	w/o emulsion
Poor dispersibility	{	6	
Milky dispersion; unstable	{	8	
Milky dispersion, stable	{	10	Detergency
Poor dispersibility	{	12	
Translucent to clear solution	{	14	Solubilizer
Clear solution	{	16	
		18	
			o/w emulsion

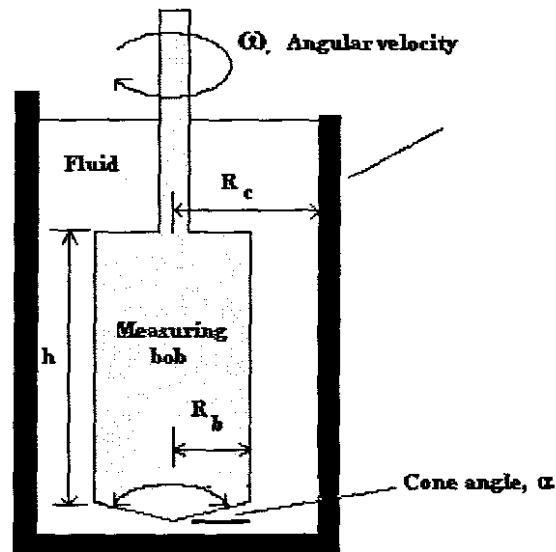
## APPENDIX B

Derivation of an equation for calculation the cone angle,  $\alpha$  for coaxial cylinder geometry:

Cylinder radius:  $R_c$

Bob radius:  $R_b$

Cylinder height:  $h$



Concentric cylinder rheometry

### Equations for the mean or representative shear rate:

(a) Annular measuring gap:

$$\dot{\gamma}_{rep} = \omega \cdot \frac{1 + \delta^2}{\delta^2 - 1} = \frac{\pi n}{30} \left( \frac{1 + \delta^2}{\delta^2 - 1} \right); \quad \omega = n \cdot \frac{2\pi}{60} \text{ and } \delta = \frac{R_c}{R_b}$$

A

(b) Conical section:

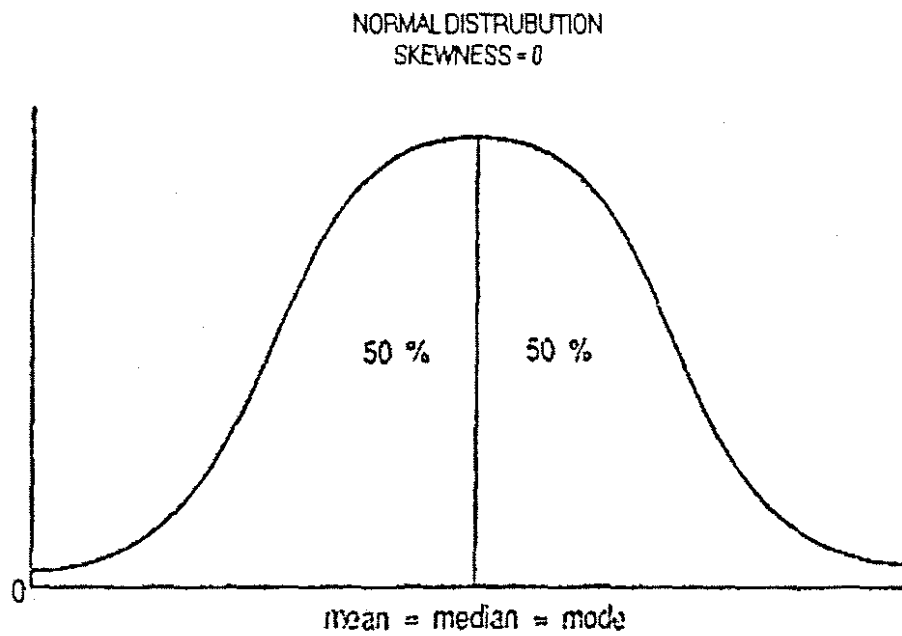
$$\dot{\gamma}_{\text{rep}} = \frac{\omega}{\tan \alpha} \quad \text{B}$$

Equating equations A and B yields:

$$\tan \alpha = \frac{\delta^2 - 1}{1 + \delta^2} = \frac{R_c^2 - R_b^2}{R_c^2 + R_c^2} \Rightarrow \alpha = \tan^{-1} \left( \frac{R_c^2 - R_b^2}{R_c^2 + R_c^2} \right) = \tan^{-1} \left( \frac{\delta^2 - 1}{1 + \delta^2} \right)$$

## APPENDIX C

Normal or Gaussian Frequency Distribution (Willemse, 1991: 61).



**APPENDIX D**

Values of  $t$  at a function of confidence level  $\alpha$  and number of measurements  $N$ .

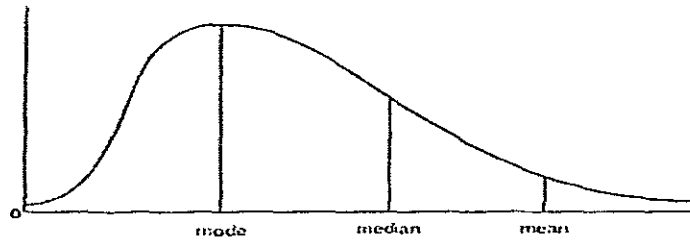
(Willemse, 1991: 253)

N	t ( 90 % )	t ( 95 % )	t ( 99 % )
2.00	6.314	12.706	63.657
3.00	2.920	4.303	9.925
4.00	2.353	3.182	5.481
5.00	2.132	2.776	4.604
6.00	2.015	2.571	4.032
7.00	1.943	2.447	3.707
8.00	1.895	2.365	3.449
9.00	1.860	2.306	3.355
10.00	1.833	2.262	3.250
11.00	1.812	2.228	3.169
12.00	1.796	2.201	3.106
13.00	1.782	2.179	3.055
14.00	1.771	2.160	3.012
15.00	1.761	2.145	2.997
16.00	1.753	2.131	2.947
17.00	1.746	2.120	2.921
18.00	1.740	2.110	2.898
19.00	1.734	2.101	2.878
20.00	1.729	2.093	2.861
21.00	1.725	2.086	2.845
22.00	1.721	2.080	2.831
23.00	1.717	2.074	2.819
24.00	1.714	2.069	2.807
25.00	1.711	2.064	2.797
26.00	1.708	2.060	2.787
27.00	1.706	2.056	2.779
28.00	1.703	2.052	2.771
29.00	1.701	2.048	2.763
30.00	1.699	2.045	2.756
31.00	1.697	2.042	2.750
32.00	1.696	2.040	2.744
33.00	1.694	2.037	2.738
34.00	1.692	2.025	2.733
$\infty$	1.645	1.960	2.576

## APPENDIX E

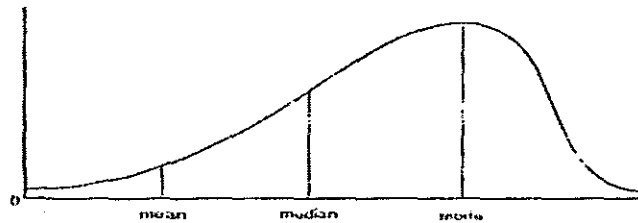
Skewness of a Frequency Distribution Curve (Willemse, 1991: 62).

STATISTICAL METHODS AND FINANCIAL CALCULATIONS  
 POSITIVELY SKEWED DISTRIBUTION  
 SKEWNESS  $> 0$



(3) The converse is true for negatively skewed distributions.

NEGATIVELY SKEWED DISTRIBUTION  
 SKEWNESS  $< 0$



The positional differences among mean, median and mode can be used to create arithmetic measures of skewness.

Pearson's first coefficient of skewness  $SK = \frac{\text{mean} - \text{mode}}{\text{standard deviation}}$

Pearson's second coefficient of skewness  $SK = \frac{3(\text{mean} - \text{median})}{\text{standard deviation}}$

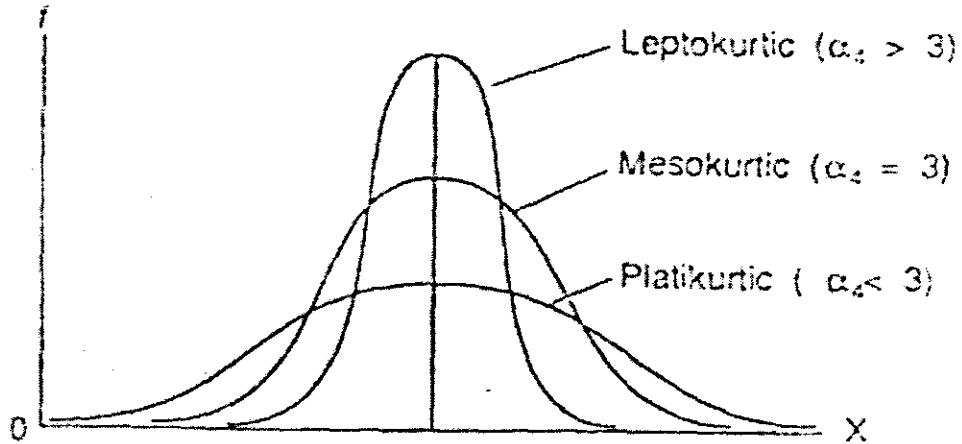
If  $\text{mean} = \text{median} = \text{mode}$ ,  $SK = 0$

If  $\text{mean} > \text{median} > \text{mode}$ ,  $SK > 0$  but smaller than 3.

If  $\text{mean} < \text{median} < \text{mode}$ ,  $SK < 0$  but greater than -3.

## APPENDIX F

Kurtosis or Peakedness of a Frequency Distribution Curve (Willemse, 1991: 63).



The mesokurtic curve indicates a normal distribution.  
The platykurtic curve indicates a large dispersion.  
The leptokurtic curve indicates a small dispersion.

## APPENDIX G

### Summary Statistics of Cross Rheological Model.

The following table lists the summary statistics of all the Cross coefficients obtained from rheological characterisation. They are calculated using Microsoft Excel statistic software, and provide the following numerical measures about the frequency distributions of the coefficients obtained: Measures of central tendency (mean, median and mode), measures of dispersion (standard deviation, variance, minimum and maximum) and measures of shape (skewness and kurtosis). These measures are described in Chapter 3 section 3.5.1.

Summary statsics	$\eta_0$	$\lambda$	n	$r^2$
Mean	11027.83	124.84	0.841	0.996
Standard Error	122.23	0.14	0.002	0.001
Median	11027.83	124.80	0.842	0.997
Mode	#N/A	#N/A	0.842	#N/A
Standard Deviation	323.39	0.37	0.005	0.002
Sample Variance	104583.47	0.13	0.000	0.000
Kurtosis	2.88	2.51	1.206	0.765
Skewness	-1.47	1.51	0.627	-1.071
Range	990.00	1.07	0.015	0.006
Minimum	10380.00	124.50	0.835	0.992
Maximum	11370.00	125.57	0.850	0.998
Sum	77194.83	873.88	5.888	5.976
Count	7.00	7.00	7.000	6.000
Confidence Level(95.0%)	299.09	0.34	0.005	0.002

**APPENDIX H**

Averaged rheometry data obtained from all the pipe diameters used in the study:

## Appendix H1

Pipe diameter, D = 35.9 mm		
Average shear rate, $s^{-1}$	Average shear stress, Pa	Average shear viscosity (Pa.s)
0.0001	1.02	9408.15
0.0001	1.22	9523.89
0.0002	1.46	9465.51
0.0002	1.74	9576.85
0.0002	2.07	9618.69
0.0003	2.47	9517.60
0.0003	2.94	9594.06
0.0004	3.49	9550.82
0.0004	4.14	9475.76
0.0005	4.92	9506.15
0.0006	5.84	9495.19
0.0007	6.94	9429.93
0.0009	8.23	9322.91
0.0011	9.76	9245.16
0.0013	11.56	9187.42
0.0015	13.72	9071.92
0.0018	16.25	8907.10
0.0022	19.26	8687.81
0.0027	22.79	8486.82
0.0033	26.99	8127.73
0.0042	31.93	7670.30
0.0054	37.75	6996.14
0.0072	44.59	6226.30
0.0099	52.54	5308.14
0.0143	61.78	4312.37
0.0219	72.11	3300.00
0.0351	83.25	2371.04
0.0589	94.57	1606.63
0.0953	104.07	1091.81
0.1461	110.77	758.05
0.1973	114.29	579.22
0.2422	116.42	480.72
0.2888	118.39	410.02
0.3424	120.82	352.82
0.4033	123.68	306.66
0.4841	126.44	261.18
0.5739	129.76	226.11
0.6803	133.32	195.99
0.8086	137.07	169.52
0.9578	141.26	147.49
1.1400	145.69	127.80
1.3494	150.50	111.53
1.6000	155.75	97.34
1.8931	161.44	85.28
2.2438	167.25	74.54
2.6600	173.56	65.25
3.1513	180.31	57.22
3.7394	187.31	50.09
4.4294	194.56	43.93
5.2500	202.19	38.51
6.2206	210.06	33.77
7.3713	218.50	29.64
8.7369	227.06	25.99
10.3750	236.31	22.78
12.3000	245.50	19.96
14.5250	255.63	17.60
17.2063	266.37	15.48
20.4000	277.31	13.59
24.2000	288.63	11.93
28.6875	300.56	10.48
34.0000	311.81	9.17
40.2875	323.62	8.03
47.7313	335.37	7.03
56.5813	347.50	6.14
67.0313	362.44	5.41
79.4375	376.31	4.74
94.1313	390.68	4.15
111.8750	405.38	3.62
132.0000	423.06	3.21
157.0000	443.06	2.82
186.0000	464.00	2.49
220.0000	486.69	2.21

## Appendix H2

Pipe diameter, D = 48.1 mm		
Average shear rate, s <sup>-1</sup>	Average shear stress, Pa	Average shear viscosity (Pa.s)
0.0001	1.01	8941.07
0.0001	1.21	9069.46
0.0002	1.44	9330.38
0.0002	1.72	9156.11
0.0002	2.05	9225.62
0.0003	2.44	9344.33
0.0003	2.91	9326.70
0.0004	3.46	9317.43
0.0004	4.12	9256.47
0.0005	4.89	9230.81
0.0006	5.81	9238.35
0.0007	6.89	9210.96
0.0009	8.19	9094.02
0.0011	9.71	9235.81
0.0013	11.52	9030.22
0.0015	13.66	8971.16
0.0019	16.38	8691.93
0.0023	19.17	8455.98
0.0028	22.68	8143.16
0.0035	26.84	7659.26
0.0044	31.73	7216.86
0.0058	37.49	6492.29
0.0078	44.17	5664.04
0.0108	51.94	4806.05
0.0158	60.77	3858.12
0.0238	70.63	2966.31
0.0369	81.31	2201.20
0.0583	92.36	1583.75
0.0912	102.93	1128.26
0.1370	111.23	811.88
0.1879	116.11	617.95
0.2370	119.12	502.63
0.2857	121.93	426.77
0.3414	124.61	365.00
0.4057	127.41	314.05
0.4822	130.41	270.44
0.5730	134.00	233.86
0.6804	137.21	201.66
0.8075	141.31	174.99
0.9582	145.70	152.06
1.1400	150.30	131.84
1.3470	155.31	115.30
1.6000	160.80	100.50
1.8930	166.30	87.85
2.2470	172.39	76.72
2.6600	178.60	67.14
3.1500	185.80	58.98
3.7380	193.10	51.66
4.4300	200.60	45.28
5.2510	208.50	39.71
6.2210	216.70	34.83
7.3710	225.70	30.62
8.7340	234.80	26.88
10.3600	244.87	23.64
12.3000	255.30	20.76
14.5100	266.30	18.35
17.2100	278.10	16.16
20.4000	290.30	14.23
24.2000	302.90	12.52
28.7100	315.40	10.99
34.0000	328.50	9.66
40.2800	341.80	8.49
47.7300	354.50	7.43
56.6000	367.51	6.49
67.0300	381.31	5.69
79.4300	399.29	5.03
94.1500	411.70	4.37
111.8000	429.27	3.84
132.0000	449.00	3.40
157.0000	471.10	3.00
186.0000	494.00	2.66
220.0000	520.80	2.37

## Appendix H3

Pipe diameter, D = 55.9 mm		
Average shear rate, s <sup>-1</sup>	Average shear stress, Pa	Average shear viscosity (Pa.s)
0.0001	1.01	9314.46
0.0001	1.22	9562.99
0.0001	1.43	9635.57
0.0002	1.70	9408.27
0.0002	2.12	9803.47
0.0003	2.43	9709.35
0.0003	2.92	9663.70
0.0004	3.47	9661.31
0.0004	4.12	9571.51
0.0005	4.92	9592.47
0.0006	5.83	9553.19
0.0007	6.90	9513.16
0.0009	8.18	9531.67
0.0010	9.73	9583.96
0.0012	11.59	9426.63
0.0014	13.59	9471.62
0.0018	16.25	9206.36
0.0021	19.12	8941.07
0.0026	22.42	8533.02
0.0034	26.69	7963.72
0.0042	31.50	7466.68
0.0055	36.51	6640.40
0.0076	43.06	5675.40
0.0106	49.66	4702.19
0.0156	57.87	3712.21
0.0236	67.19	2845.67
0.0365	77.49	2124.75
0.0577	88.50	1534.13
0.0866	98.48	1136.63
0.1280	107.53	840.05
0.1808	114.91	635.58
0.2341	119.24	509.34
0.2866	122.53	427.52
0.3414	124.97	366.04
0.4061	127.73	314.54
0.4823	130.64	270.86
0.5734	134.31	234.24
0.6800	137.87	202.75
0.8067	141.71	175.66
0.9576	145.93	152.39
1.1390	150.77	132.37
1.3460	155.80	115.75
1.6000	161.32	100.83
1.8910	166.96	88.29
2.2480	173.43	77.15
2.6600	179.49	67.48
3.1510	186.50	59.19
3.7400	193.72	51.80
4.4290	201.27	45.44
5.2500	209.09	39.83
6.2210	217.49	34.96
7.3720	226.57	30.73
8.7350	235.87	27.00
10.3900	245.65	23.64
12.3000	255.93	20.81
14.5000	266.71	18.39
17.2000	278.35	16.18
20.4000	289.96	14.21
24.2100	301.42	12.45
28.7100	313.04	10.90
34.0000	325.87	9.58
40.2900	338.63	8.40
47.7400	353.44	7.40
56.5300	368.50	6.52
67.0400	386.96	5.77
79.4700	405.21	5.10
94.1300	413.62	4.39
111.4000	432.51	3.88
132.0000	453.14	3.43
157.0000	479.13	3.05
186.0000	503.22	2.71
220.0000	530.24	2.41

## Appendix H4

Pipe diameter, $D \approx 65.9$ mm		
Average shear rate, $s^{-1}$	Average shear stress, Pa	Average shear viscosity (Pa.s)
0.0001	1.01	9314.46
0.0001	1.22	9562.99
0.0001	1.43	9635.57
0.0002	1.70	9408.27
0.0002	2.12	9803.47
0.0003	2.43	9709.35
0.0003	2.92	9663.70
0.0004	3.47	9661.31
0.0004	4.12	9571.51
0.0005	4.92	9592.47
0.0006	5.83	9553.19
0.0007	6.90	9513.16
0.0009	8.18	9531.67
0.0010	9.73	9583.96
0.0012	11.59	9426.63
0.0014	13.59	9471.62
0.0018	16.25	9206.38
0.0021	19.12	8941.07
0.0026	22.42	8533.02
0.0034	26.69	7963.72
0.0042	31.50	7466.68
0.0055	36.51	6640.40
0.0076	43.06	5675.40
0.0106	49.66	4702.19
0.0156	57.87	3712.21
0.0236	67.19	2845.67
0.0365	77.49	2124.75
0.0577	88.50	1534.13
0.0866	98.48	1136.63
0.1280	107.53	840.05
0.1808	114.91	635.58
0.2341	119.24	509.34
0.2866	122.53	427.52
0.3414	124.97	366.04
0.4061	127.73	314.54
0.4823	130.64	270.86
0.5734	134.31	234.24
0.6800	137.87	202.75
0.8067	141.71	175.66
0.9576	145.93	152.39
1.1390	150.77	132.37
1.3460	155.80	115.75
1.6000	161.32	100.83
1.8910	166.96	88.29
2.2480	173.43	77.15
2.6600	179.49	67.48
3.1510	186.50	59.19
3.7400	193.72	51.80
4.4290	201.27	45.44
5.2500	209.09	39.83
6.2210	217.49	34.96
7.3720	226.57	30.73
8.7350	235.87	27.00
10.3900	245.65	23.64
12.3000	255.93	20.81
14.5000	266.71	18.39
17.2000	278.35	16.18
20.4000	289.96	14.21
24.2100	301.42	12.45
28.7100	313.04	10.90
34.0000	325.87	9.58
40.2900	338.63	8.40
47.7400	353.44	7.40
56.5300	368.50	6.52
67.0400	386.96	5.77
79.4700	405.21	5.10
94.1300	413.62	4.39
111.4000	432.51	3.88
132.0000	453.14	3.43
157.0000	479.13	3.05
186.0000	503.22	2.71
220.0000	530.24	2.41

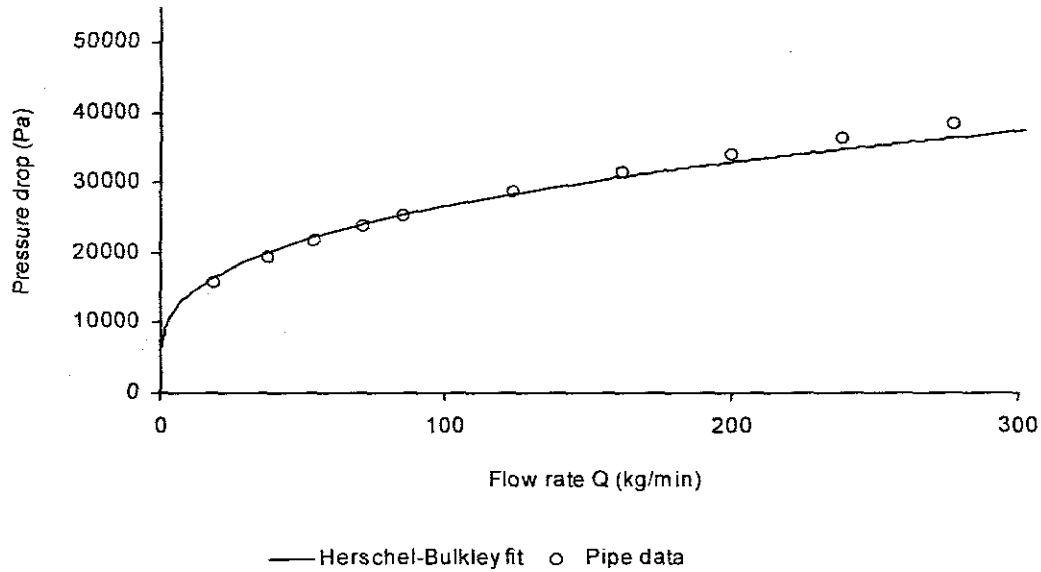
## Appendix H5

Pipe diameter, D = 77.6 mm		
Average shear rate, $s^{-1}$	Average shear stress, Pa	Average shear viscosity (Pa.s)
9314.4564	1.01	8941.07
0.0001	1.21	9069.46
0.0002	1.44	9330.38
0.0002	1.72	9156.11
0.0002	2.05	9225.62
0.0003	2.44	9344.33
0.0003	2.91	9326.70
0.0004	3.46	9317.43
0.0004	4.12	9256.47
0.0005	4.89	9230.81
0.0006	5.81	9238.35
0.0007	6.89	9210.96
0.0009	8.19	9094.02
0.0011	9.71	9235.81
0.0013	11.52	9030.22
0.0015	13.66	8971.16
0.0019	16.18	8691.93
0.0023	19.17	8455.98
0.0028	22.68	8143.16
0.0035	26.84	7659.26
0.0044	31.73	7216.86
0.0058	37.49	6492.29
0.0078	44.17	5664.04
0.0108	51.94	4806.05
0.0158	60.77	3858.12
0.0238	70.63	2966.31
0.0369	81.31	2201.20
0.0583	92.36	1583.75
0.0912	102.93	1128.26
0.1370	111.23	811.88
0.1879	116.11	617.95
0.2370	119.12	502.63
0.2857	121.93	426.77
0.3414	124.61	365.00
0.4057	127.41	314.05
0.4822	130.41	270.44
0.5730	134.00	233.86
0.6804	137.21	201.66
0.8075	141.31	174.99
0.9582	145.70	152.06
1.1400	150.30	131.84
1.3470	155.31	115.30
1.6000	160.80	100.50
1.8930	166.30	87.85
2.2470	172.39	76.72
2.6600	178.60	67.14
3.1500	185.80	58.98
3.7380	193.10	51.66
4.4300	200.60	45.28
5.2510	208.50	39.71
6.2210	216.70	34.83
7.3710	225.70	30.62
8.7340	234.80	26.88
10.3600	244.87	23.64
12.3000	255.30	20.76
14.5100	266.30	18.35
17.2100	278.10	16.16
20.4000	290.30	14.23
24.2000	302.90	12.52
28.7100	315.40	10.99
34.0000	328.50	9.66
40.2800	341.80	8.49
47.7300	354.50	7.43
56.6000	367.51	6.49
67.0300	381.31	5.69
79.4300	399.29	5.03
94.1500	411.70	4.37
111.8000	429.27	3.84
132.0000	449.00	3.40
157.0000	471.10	3.00
186.0000	494.00	2.66
220.0000	520.80	2.37

## APPENDIX I

Typical approximation of pumping conditions (system curves, i.e.  $Q$ - $\Delta P$  relations) from Herschel-Bulkley and Power Law models for the test pipe diameter of 48.1 mm):

Appendix I1:  $\Delta P$  vs.  $Q$  from Herschel-Bulkley model.



Appendix I2:  $\Delta P$  vs.  $Q$  from Power Law model.

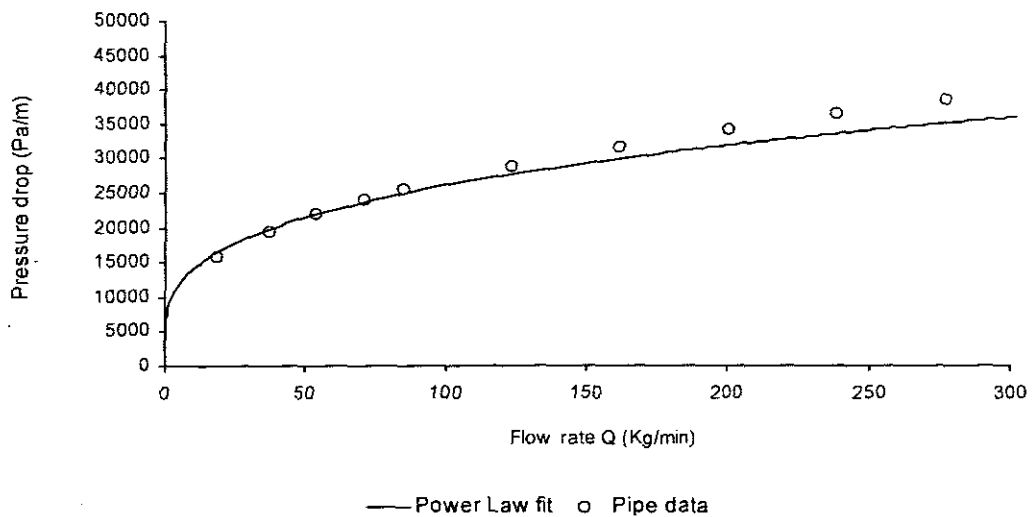


Table II list of possible errors for high internal phase ratio emulsion explosives for Herschel-Bulkley and Power Law models

Rheological Models	Mean Square Relative Error, $E_{rel}$	Maximum Possible Error
Herschel-Bulkley	0.149	$1.71 \times 10^{-2}$
Power Law	0.134	$4.46 \times 10^{-3}$

It is seen that these two fitting approaches are reasonably accurate. The maximum error for any of the approximations did not exceed 1.71 % which is reasonable for pumping predictions.

Due to the simplicity of the Power Law model with only two empirical coefficients, the Maximum Possible Error associated with the use of this model in prediction of  $\frac{8V}{D}$  was found to be the least, and thus, indicating a high degree of accuracy in the calculations (equation 2.57). The expressions for both the Herschel-Bulkley and the Power Law models are similar, except for the extra coefficient, which is associated with yielding ( $\tau_y$ ) in the case of the Herschel-Bulkley model (equation 2.56). Thus, the Maximum Possible Error associated with the use of Herschel-Bulkley model in prediction of  $\frac{8V}{D}$  was found to be the second least value.

## APPENDIX J

This appendix lists the Metzner and Reed Reynolds numbers (or simply  $Re_{MR}$ ) for the pipeline data calculated from equation 2.56 using the Power Law coefficients obtained from rheological characterization and emulsion density of  $1437 \text{ kg.m}^{-3}$ :

Appendix J1:  $Re_{MR}$  for Pipe diameter of 35.9mm:

M (kg/min)	V ( $\text{m.s}^{-1}$ )	K	n	$Re_{MR}$
3.55	0.041	134.34	0.24	0.072
4.83	0.055	132.86	0.24	0.126
6.22	0.071	132.68	0.24	0.197
8.90	0.102	136.51	0.23	0.371
12.20	0.140	136.29	0.23	0.649
20.20	0.231	135.10	0.24	1.537
42.40	0.486	145.15	0.23	5.530
49.20	0.564	148.12	0.23	7.051

Appendix J2:  $Re_{MR}$  for Pipe diameter of 48.1mm:

M (kg/min)	V ( $\text{m.s}^{-1}$ )	K	n	$Re_{MR}$
10.90	0.070	135.63	0.23	0.203
21.40	0.137	143.22	0.23	0.634
32.20	0.205	148.78	0.23	1.259
40.70	0.260	140.11	0.25	1.876
50.20	0.320	149.22	0.25	2.543

Appendix J3:  $Re_{MR}$  for Pipe diameter of 55.9mm:

M (kg/min)	V ( $\text{m.s}^{-1}$ )	K	n	$Re_{MR}$
11.10	0.052	149.83	0.25	0.111
21.70	0.103	149.50	0.25	0.359
31.50	0.149	149.50	0.25	0.689
41.50	0.196	141.49	0.22	1.304
50.50	0.239	142.83	0.23	1.768

Appendix J4:  $Re_{MR}$  for Pipe diameter of 65.9mm:

M (kg/min)	V (m.s <sup>-1</sup> )	K	n	$Re_{MR}$
11.60	0.039	149.83	0.25	0.070
20.90	0.071	149.50	0.25	0.197
32.50	0.110	149.50	0.22	0.461
41.80	0.142	141.49	0.23	0.741
48.80	0.166	142.83	0.23	0.965

Appendix J5:  $Re_{MR}$  for Pipe diameter of 77.6mm:

M (kg/min)	V (m.s <sup>-1</sup> )	K	n	$Re_{MR}$
12.30	0.0302	149.83	0.25	0.046
23.80	0.0583	149.50	0.25	0.145
34.80	0.0853	149.50	0.25	0.283
45.00	0.1103	141.49	0.22	0.504
55.50	0.1360	142.83	0.23	0.706

**APPENDIX K**

Graphical representation of the findings on the effect of pumping rate on the rheological properties of emulsion explosives.

